MICRODEST - MICRO-COMPUTER ANALYSES AND DESIGN OF PLANAR STEEL FRAMES

by

Henry Frank Herring

Submitted to the University of Cape Town
in partial fulfilment of the requirements
for the degree of Master of Science in
Engineering.

Department of Civil Engineering
University of Cape Town

April 1986

DECLARATION OF CANDIDATE

I hereby declare that this thesis is my own work and that it has not been submitted for a degree at any other University.

Signed

H F Herring

April 1986

DEDICATION

I would like to dedicate this thesis to my parents.

ACKNOWLEDGEMENTS

I would like to extend my appreciation to the following:-

Prof W S Doyle, under whose supervision this thesis was conducted.

Cheryl Wright for her patience and efficient typing of this thesis.

Mr Kevin Peterson for assisting with the Figures.

The Council of Scientific and Industrial Research and the South African Institute of Steel Construction for their financial assistance.

ABSTRACT

A two noded curved linear-cubic beam element is incorporated in a micro-computer frame analysis and steel design package. The spurious response involved by membrane locking in curved finite elements is eliminated by adopting mode decomposition projection methods in the element formulation.

A special finite element mesh refinement technique, Satellite Element Refinement, is developed to yield sufficient analysis results pertinent to the design procedure. To decrease the extra computational effort involved by Satellite Element Refinement, static condensation is used to condense out the uncoupled degrees of freedom.

The design procedure is based on a Direct Iteration technique guided by the recommendations of the SABS 0162-1984 Structural Steel code.

A preprocessor is also developed to assist in data generation and collection. Preprocessing techniques and strategies are discussed.

CONTENTS

NOMENCLATURE

This is a list of symbols used in the main text of this thesis.

Upper Case Characters

A	cross-sectional area
$[A]$	prescribed matrix of position
A_i	required cross-sectional area
B	strain matrix
$\underset{\sim}{B}_b$	bending strain matrix
$\underset{\sim}{B}_m$	membrane strain matrix
C_s	stress ratio
$C^{(m)}$	order of formulation
D	material matrix
D_B	bending constant
D_M	membrane constant
E	Young's modulus
$\underset{\sim}{F}$	global load vector
$\underset{\sim}{F}_c$	condensed global load vector
$\underset{\sim}{I}$	identity matrix
I_{xx}	second moment of area
K	global system stiffness matrix
K_c	condensed global system stiffness matrix
K_e	element stiffness matrix
K_{ei}	element stiffness matrix of Ω_e^i
K_e^{sat}	satellite assemblage element stiffness matrix of Ω_e^i
L	self-adjoint linear operator
L_e	length of the element

Lower Case Characters (continued)

n	iteration number or counter
p	body forces per unit volume
q	applied surface tractions
r	radius of gyration
u	longitudinal displacement
$\underset{\sim}{u}$	unknown degrees of freedom
$\underset{\sim}{u}_b$	bending nodal displacement
$\underset{\sim}{u}_c$	condensed global displacement vector
$\underset{\sim}{u}_2$	recovered degrees of freedom
v	transverse displacement
w	deformed shape of element
w^o	initial shape of element

Greek Characters

α_i	initial rotation of the nodal cross-section
β	ratio of end moments
δ	general unknown
ε	axial strain
$\bar{\varepsilon}$	average axial strain
$\dot{\varepsilon}$	total strain
ε_b	membrane strain in the bending mode
ε_t	total axial strain
κ	bending strain
Π	total potential energy
ϕ_i	deformational rotation of nodal cross-section

CHAPTER 1

INTRODUCTION

Micro-computers are providing structural engineers with the necessary numerical tools for investigating ordinary and complicated structural systems in a rapid and thorough manner. The prophetic words of Irons and Ahmad [31], aptly illustrate the numerical and computational revolution the engineering industry is experiencing.

> 'The greatest impact of computation will be in engineering. Experimentation will be restricted to those things that cannot be calculated ... Exotic objects will appear overnight, manufactured straight from the drawing board ...'

Up to a few years ago, the mainframe computer completely dominated this computational revolution. In the midst of this revolution, however, the giant machines are facing healthy competition from the micro-computers, which are gaining more than just a foothold to satisfy the requirements of FEM analysis. It is in this atmosphere that PREPRO and MICRODEST have been developed.

PREPRO is a simple preprocessor designed to provide the basic preprocessing capabilities to rapidly set up data and then to store it on an external mass storage device. The data is then used by MICRODEST (Micro-computer Design and Analysis of Steel Structures) for analysis and design purposes.

MICRODEST aims to be a general purpose frame analysis and steel design package. The processor MICRODEST incorporates a two noded curved beam element based on a one dimensional version of the Marguerre shallow shell equations. This element successfully copes with membrane locking by employing mode decomposition projection techniques to remedy this numerical problem. The element is fully described and derived in Chapter 2.

The Collins bandwidth reduction scheme is incorporated in the processor to ensure the minimum bandwidth for any model.

To extract results relevant to the design procedure a special mesh refinement technique, termed Satellite Element Refinement, has been developed.

As a consequence of Satellite Element Refinement, more than half the degrees of freedom in the Satellite Element Refined mesh are uncoupled. These uncoupled degrees of freedom are then statically condensed at the element level.

This represents a substantial decrease in computational effort involved by Satellite Element Refinement.

Satellite Element Refinement is a new and novel technique which is fully investigated in the main text of this document.

A Direct Iteration design procedure is adopted in the design of the frames or trusses in MICRODEST. The design procedure is governed by the recommendations of SABS 0162 : 1984, The Structural Use of Steel [35].

Several examples of the performance of two-noded curved beam elements are included together with some design examples.

CHAPTER 2

BASIC FINITE ELEMENT THEORY

2.1 Basic Equations for Linear Problems

When the potential energy of a structure achieves a minimum value it is said to be in equilibrium [1]. The Total Potential Energy, Π, can be expressed in general terms as

$$\Pi = \frac{1}{2}\int_V [\dot{\sigma}]^T \dot{\varepsilon}\, dV - \int_V [\delta]^T p\, dV - \int_S [\delta]^T q\, dS \qquad (2.1)$$

where σ and ε are the stress and strain vectors respectively, δ the displacements at any point, p the body forces per unit volume and q the applied surface tractions. The integrations are taken over the whole volume V of the structure and over the loaded surface S.

The first term on the righthand side of Equation (2.1) is referred to as the strain energy term, U. The second and third terms account for the work contributions from the body forces and surface loads respectively.

Since the displacements are the primary unknowns, the appropriate functional is that of Total Potential Energy. Total Potential Energy is expressed in terms of nodal degrees of freedom. Then, as required by the Principle of Stationary Potential Energy, the nodal degrees of freedom must assume such values that Π is stationary [2] which will yield a set of simultaneous algebraic equations in the nodal degrees of freedom. These equations can then be arranged into the classical Finite Element formulation of

$$\underset{\sim}{K}\underset{\sim}{u} = \underset{\sim}{F} \qquad (2.2)$$

where

$\underset{\sim}{K}$ is termed the stiffness matrix

$\underset{\sim}{u}$ the unknown degrees of freedom to be solved

$\underset{\sim}{F}$ the load vector.

2.2 Kinematic Relationships

A theory of shallow structures is used in the kinematic relationships. The curved beam is described by a one-dimensional version of the Marguerre shallow shell equations [3].

The kinematic relations for the Marguerre beam are given by

$$\varepsilon = u_{,x} + w^{o}_{,x} w_{,x} \tag{2.3}$$

$$\kappa = - w_{,xx} \tag{2.4}$$

Here u and w are the x and z components of the displacement of the midline. The initial shape of the element is also described by w^{o}. The rotation of the cross-section is given by $w_{,x}$. See Figure 2.1. The commas denote differentiation

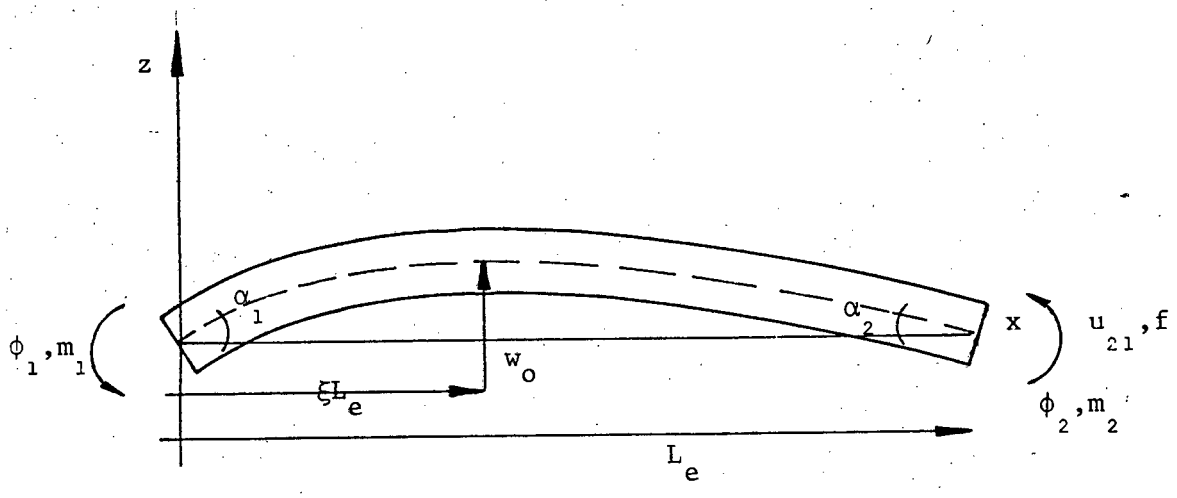

Figure 2.1 Curved Beam

To account properly for rigid body motion, consider the element in a co-rotating frame whose x-axis passes through both of its ends. The rigid body motion is removed from w, so that w is the displacement relative to the chord.

The deformational degrees of freedom are

$$\underset{\sim}{u}^T = [u_{21} , \phi_1 , \phi_2] \tag{2.5}$$

where $u_{21} = u_2 - u_1$

$$\phi_1 = \phi_1^{tot} - \frac{1}{L_e}(w_2 - w_1) \tag{2.6}$$

$$\phi_2 = \phi_2^{tot} - \frac{1}{L_e}(w_2 - w_1) \tag{2.7}$$

where u_{21} is the relative longitudinal displacement of the right end with respect to the left end of the element, ϕ_i are the deformational rotations and ϕ_i^{tot} the total rotations of the node.

The following interpolations are used for u, w and w^o :

$$u = u_{21}\,\xi \tag{2.8}$$

$$w = L_e(\phi_1 N_1 + \phi_2 N_2) \tag{2.9}$$

$$w^o = L_e(\alpha_1 N_1 + \alpha_2 N_2) \tag{2.10}$$

where α_1 and α_2 are the rotations associated with the initial shape of the element, L_e its length and N_1 and N_2 are cubic Hermite interpolants.

$$N_1 = \xi - 2\,\xi^2 + \xi^3 \tag{2.11}$$

$$N_2 = \xi^3 - \xi^2 \tag{2.12}$$

$$\xi = \frac{x}{L_e} \tag{2.13}$$

Appendix I schematically illustrates the shape functions.

For an elastic beam of thickness d, unit width and Young's modulus E, these constants are given by

$$D_B = \frac{1}{12} Ed^3 \tag{2.16}$$

$$D_M = Ed \tag{2.17}$$

The energies associated with the constants D_B and D_M are called the bending and membrane energies respectively. For a thin beam $d/L_e \ll 1$, and the ratios of bending to membrane energy will similarly be small if the strains are of equal order.

$$\frac{D_B}{L_e^2 D_M} \ll 1 \tag{2.18}$$

Membrane locking occurs in curved elements due to the inability of most finite elements to achieve deformed states in which the membrane strain vanishes throughout the element. Modes of deformation in which membrane stresses vanish are vital to the mechanics of shells. When a cylindrical shell is subjected to a state of pure bending, the membrane strains will completely vanish. This mode of deformation is referred to as an inextensible mode of deformation. When the membrane strain vanishes, all the lines in the middle surface of the shell remain constant in length. This is also referred to as inextensible bending. See Figure 2.2.

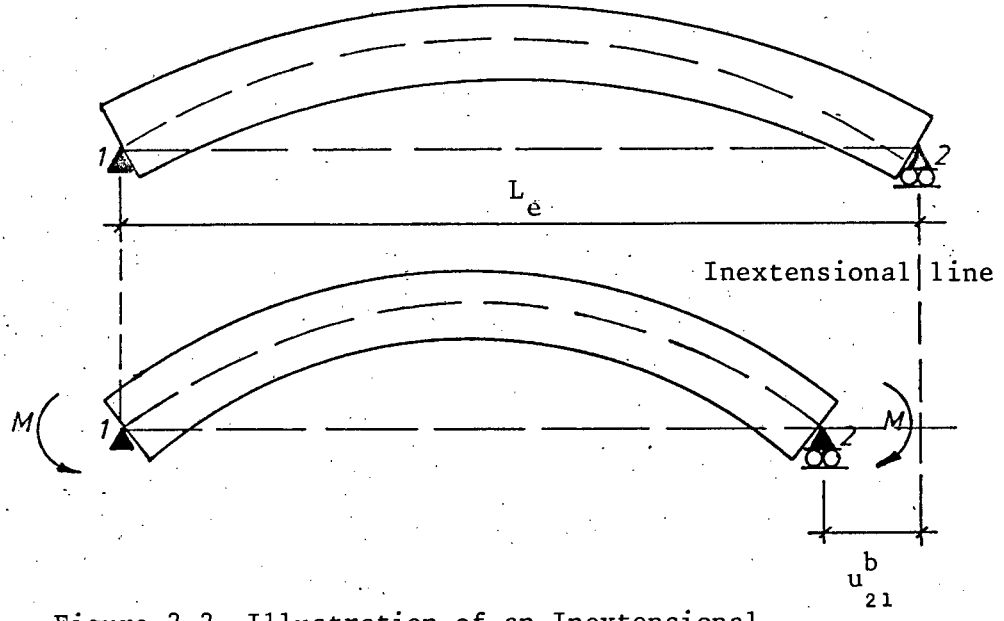

Figure 2.2 Illustration of an Inextensional Bending Mode of Deformation

In curved finite elements, inextensible states of deformation are often not possible. This has obvious shortcomings when models undergoing inextensible bending are used. Due to the regularity which holds for thin beams (2.18), small membrane strains will cause the membrane energy to overshadow the bending energy. It is important that if pure bending is applied to a model (using shallow shell theory), it must be capable of representing the deformation so that only the bending energy is non-zero.

If any membrane strains are developed, they will absorb a substantial amount of energy and the element will then behave too stiffly. This phenomenon is referred to as "membrane locking".

The stresses associated with these spurious energies are called membrane stresses. Eliminating the membrane stresses will eliminate locking.

Methods used to remedy membrane locking are

- Use high order polynomials to describe the inplane displacement field
- reduced integration and selective reduced integration [6]
- and more recently, mode decomposition projection methods [7]

Mode decomposition projection methods are used in this particular formulation.

2.4 Mode-Decomposition Projection Methods

The purpose of the mode-decomposition methods is to project the nodal displacements so that the parasitic membrane stresses are eliminated. This will then eliminate membrane locking.

The basic idea of mode-decomposition projection methods is to define the bending mode component of any deformation and to ignore the membrane energies associated with the bending modes. The strain energy expression becomes

$$U = \frac{1}{2} \int_{\Omega} [D_B \kappa^2 + D_M (\epsilon - \epsilon_b)^2] \, d\Omega \tag{2.19}$$

where κ - is the bending strain

ϵ - membrane strain

ϵ_b - the membrane strain in the bending mode.

The aim is to find the membrane strain ϵ_b so that in an inextensional mode deformation, the membrane energy vanishes in Equation (2.19). The projection for the curved linear-cubic beam element has been developed by Stolarski, et al [29], [17] and related to a mixed method by Belytschko, et al [7].

In a constant-moment state, the bending mode constitutes the total deformation, so the membrane energy will vanish. In that case $\epsilon = \epsilon_b$ in Equation (2.19).

To implement mode decomposition, the bending nodal displacements are defined through a projection.

$$\underset{\sim}{u}_b = P_b \underset{\sim}{u} \tag{2.20}$$

so that

$$\epsilon_b = B P_b \underset{\sim}{u} \tag{2.21}$$

The requirement that the bending part of the membrane strain, ϵ_b, be the strain that occurs in a constant moment state, is not sufficient to identify the projection operator P_b, Equation (2.20) as it is not the only bending mode. B is the strain matrix.

The displacement fields and initial deflection in this element are given by

$$u = u_1 (1 - \xi) + u_2 \xi \tag{2.22a}$$

$$w = \phi_1 L_e(\xi^3 - 2\xi^2 + \xi) + \phi_2 L_e(\xi^3 - \xi^2) \tag{2.22b}$$

$$w^o = \phi_1^o L_e(\xi^3 - 2\xi^2 + \xi) + \phi_2 L_e(\xi^3 - \xi^2) \tag{2.22c}$$

where

$$N_1 = \xi^3 - 2\xi^3 + \xi \; ; \quad N_2 = \xi^3 - \xi^2$$

as before.

A co-rotational coordinate system is used again so that the local x-axis always connects node 1 to node 2.

The stiffness matrix for this element is obtained by manipulating (2.19), (2.20) and (2.14). The derivation of the element stiffness matrix is covered in Section 2.5. The general form of the equation will be

$$\underset{\sim}{K}_e = \int_{\Omega_e} \underset{\sim}{B}_b^T \underset{\sim}{D}_B \underset{\sim}{B}_b \, d\Omega + \underset{\sim}{P}_m^T \int_{\Omega_e} \underset{\sim}{B}_m \underset{\sim}{D}_M \underset{\sim}{B}_m \, d\Omega \, \underset{\sim}{P}_m \tag{2.23}$$

where

$$\underset{\sim}{B}_b = [0 \; , \; - N_{1,xx} \; , \; - N_{2,xx}] \tag{2.24a}$$

$$\underset{\sim}{B}_m = [\frac{1}{L_e} \; , \; w^o_{,}(x) \; N_{1,x} \; , \; w^o_{,}(x) \; N_{2,x}] \tag{2.24b}$$

$$\underset{\sim}{u}^T = [u_2 - u_1 \; , \; \phi_1 \; , \; \phi_2] \tag{2.24c}$$

If no projection is used, i.e. $\underset{\sim}{P}_m = \underset{\sim}{I}$, then this element will lock. By considering B_m the mechanism of membrane locking can be understood. If the moment on an element is constant, then $\phi_1 = \phi_2$, so if $w^o(x) \neq 0$, then the constant term $\frac{1}{L_e}$ cannot negate the terms $w^o(x)\, N_{i,x}$, hence parasitic strains will arise. If $w^o(x) = 0$, the beam is straight and no coupling exists between flexural and membrane effects. The coupling is an important attribute of curved elements.

The projection operator is obtained by noting that the change in the chord length $u^b_{21} \equiv u^b_2 - u^b_1$ in a pure bending mode is given by

$$u^b_{21} = - \int_o^{L_e} w^o_{,x}\, w_{,x}\, dx \tag{2.25a}$$

Using Equation (2.22) and Equation (2.13) then

$$w^o_{,x} = L_e^2 \left[\alpha_1 \left(\frac{3}{L_e^2} x^2 - \frac{4}{L_e} x + 1\right) + \alpha_2 \left(\frac{3}{L_e^2} x^2 - \frac{2}{L_e} x\right)\right] \tag{2.25b}$$

$$w_{,x} = L_e^2 \left[\phi_1 \left(\frac{3}{L_e^2} x^2 - \frac{4}{L_e} x + 1\right) + \phi_2 \left(\frac{3}{L_e^2} x^2 - \frac{2}{L_e} x\right)\right] \tag{2.25c}$$

multiplying Equation (2.25b) and Equation (2.25c) and grouping yields

$$\begin{aligned} u^b_{21} = - L_e^2 \int_o^{L_e} & \alpha_1\, \phi_1 \left(\frac{9}{L_e^4} x^4 - \frac{24}{L_e^3} x^3 + \frac{22}{L_e^2} x^2 - \frac{8}{L_e} x + 1\right) \\ & + \alpha_1\, \phi_2 \left(\frac{9}{L_e^4} x^4 - \frac{18}{L_e^3} x^3 + \frac{11}{L_e^2} x^2 - \frac{2}{L_e} x\right) \\ & + \phi_1\, \alpha_2 \left(\frac{9}{L_e^4} x^4 - \frac{18}{L_e^3} x^3 + \frac{11}{L_e^2} x^2 - \frac{2}{L_e} x\right) \\ & + \phi_2\, \alpha_2 \left(\frac{9}{L_e^4} x^4 - \frac{12}{L_e^3} x^3 + \frac{4}{L_e^2} x^2\right) dx \end{aligned} \tag{2.25d}$$

integrating and grouping

$$u^b_{21} = \frac{L_e}{30} (-4\alpha_1 + \alpha_2)\, \phi_1 + \frac{L_e}{30} (\alpha_1 - 4\alpha_2)\, \phi_2 \tag{2.25e}$$

The projection operator becomes

$$\underset{\sim}{P}_m = \begin{bmatrix} 1 & \frac{L_e}{30}(-4\alpha_1 + \alpha_2) & \frac{L_e}{30}(\alpha_1 - 4\alpha_2) \\ 0 & 0 & 0 \\ 0 & 0 & 0 \end{bmatrix} \tag{2.26}$$

As can be seen from Figure 2.2, the change in chord length is required to maintain an inextensible midline during the bending of a curved element. If an element is straight then $\alpha_1 = \alpha_2 = 0$, then no change in chord length occurs during bending.

From Equation (2.25e) it can be seen that the bending part of the elongation couples the membrane response with the rotations and hence adds membrane/flexural coupling to the element.

2.5 Formulating the Stiffness Matrix

The Potential Energy of the continuum is given by Equation (2.1). From Equation (2.1) the Strain Energy is described as

$$U = \frac{1}{2}\int_{\Omega} \underset{\sim}{\sigma}^T \underset{\sim}{\varepsilon}_t \, d\Omega \tag{2.27}$$

where $\underset{\sim}{\varepsilon}_t$ is the total strain.

Discretize the continuum and write U as a sum over the elements.

$$U = \sum_e U^e = \sum_e \left[\frac{1}{2}\int_{\Omega^e} \underset{\sim}{\sigma}^T \underset{\sim}{\varepsilon}_t d\Omega^e\right] \tag{2.28}$$

The strain displacement relation and the stress strain relationships

$$\underset{\sim}{\varepsilon}_t = B\,\underset{\sim}{u} \tag{2.29a}$$

$$\underset{\sim}{\sigma} = D\underset{\sim}{\varepsilon} = DB\,\underset{\sim}{u} \tag{2.29b}$$

where B is the strain matrix

$\underset{\sim}{u}$ the displacement vector

D the material matrix.

Then

$$U = \sum_e \left[\frac{1}{2}\int_{\Omega_e} B^T\,\underset{\sim}{u}\,DB\,\underset{\sim}{u}\,d\Omega_e\right] \tag{2.30}$$

Interpolate $\underset{\sim}{u}$ in terms of nodal deformations $\underset{\sim}{u}_t$

$$\underset{\sim}{u} = N_i\underset{\sim}{u}_t \tag{2.31a}$$

where $N_1 = \xi - 2\xi^2 + \xi^3$ (2.31b)

$N_2 = \xi^3 - \xi^2$ (2.31c)

$\underset{\sim}{u}_t$ = total deformational degrees of freedom.

The Strain Energy is made up with contributions from the flexural and membrane modes. Equation (2.30) changes to

$$U = \sum_e \left[\frac{1}{2}\int_{\Omega_e} [D_B\kappa^2 + D_M(\varepsilon)^2]\,d\Omega\right] \tag{2.32}$$

$D_B = EIxx$

$D_M = EA$

where E = Young's modulus

Ixx = Second moment of area

A = Cross-sectional area

where $D_B\kappa^2$ is the contribution from flexure

$D_M\varepsilon^2$ is the contribution from membrane action.

The deformations associated with the bending mode, $\underset{\sim}{u}_b$

$$\underset{\sim}{u}_b^T = [u^b_{21} , \phi_1 , \phi_2] \tag{2.33a}$$

and the membrane mode, $\underset{\sim}{u}_m$

$$\underset{\sim}{u}_m^T = [u_{21} - u^b_{21} , 0 , 0] \tag{2.33b}$$

The total deformations per element is expressed as

$$\underset{\sim}{u}_t^T = \underset{\sim}{u}_b^T + \underset{\sim}{u}_m^T$$

$$\underset{\sim}{u}_t^T = [u_{21} , \phi_1 , \phi_2] \tag{2.33c}$$

The strain matrix B also separates to form a bending strain matrix B_b and a membrane strain matrix B_m.

$$\kappa = - \phi_{,x} = - \frac{d^2w}{dx^2} \tag{2.34}$$

From Equations (2.31a), (2.31b), (2.31c) and Equation (2.29a)

$$\kappa = B_b \underset{\sim}{u}_b$$

where B_b is the bending mode strain matrix

$\underset{\sim}{u}_b$ is the bending deformational degrees of freedom.

$$B_b = - \frac{d^2}{dx^2} N_i$$

Note that the bending strain mode exhibits no membrane action. No flexural/membrane mode coupling exists at this level. Using Equation (2.33a)

$$B_b = [0 \ , \ - N_{1,xx} \ , \ - N_{2,xx}]$$

$$B_b = [0 \ , \ 4 - 6\xi \ , \ 2 - 6\xi] \tag{2.35}$$

The membrane strain matrix B_m is derived in the same manner from the kinematic relationship

$$\varepsilon = u_{,x} + w^o_{,x} \, w_{,x}$$

If the element is initially straight, i.e. $w^o(x) = 0$, then no flexural/membrane coupling exists. However, for curved members flexural/membrane coupling is vitally important. To take into account the presence of curvature, i.e. $w^o(x) \neq 0$, the projection operator, P_m , is applied to the membrane strain energy.

$$\varepsilon = \frac{d}{dx}(u) + w^o_{,x} \frac{dN_i}{dx} \underset{\sim}{u}_m \tag{2.36a}$$

Also

$$\varepsilon = B_m \underset{\sim}{u}_m \tag{2.36b}$$

Taking into account the deformational degrees of freedom for the membrane mode, $\underset{\sim}{u}_m$, the membrane strain matrix can be easily constructed.

$$B_m = [\frac{1}{L_e} \ , \ w^o_{,x} \, N_{1,x} \ , \ w^o_{,x} \, N_{2,x}]$$

$$B_m = [\frac{1}{L_e} \ , \ w^o_{,x} \, (1 - 4\xi + 3\xi^2) \ , \ w^o_{,x} \, (3\xi^2 - 2\xi)] \tag{2.37}$$

From Equations (2.30), (2.31a) and (2.32) the Strain Energy becomes

$$U = \sum_e \underset{\sim}{u}_t^e \left(\frac{1}{2} \int_{\Omega_e} B_b^T D_B B_b \, d\Omega_e + P_m^T \int_{\Omega_e} B_m^T D_M B_m \, d\Omega_e \, P_m \right) \underset{\sim}{u}_t^e$$

Now $\delta U = 0 \equiv \dfrac{\partial U}{\partial \underset{\sim}{u}_t^e} = 0$

$$\therefore \sum_e \left(\int_{\Omega_e} B_b^T D_B B_b \, d\Omega_e + P_m^T \int_{\Omega_e} B_m^T D_M B_m \, d\Omega_e \, P_m \right) \underset{\sim}{u}_t^e = 0 \qquad (2.38)$$

This can be written as

$$\sum_e [K_e] \underset{\sim}{u}_t^e$$

where K_e is the element stiffness matrix. The sum is the assembly process of linking elements with common nodes and of including all the nodes in the continuum and not just those of a single element.

The Global stiffness matrix is obtained after the assembly process and the classical finite element equation can be written

$$\underset{\sim}{K}\underset{\sim}{u} = \underset{\sim}{F} \qquad (2.39)$$

Performing the integration Equation (2.38) for an element, see Figure 2.3, will yield K_e .

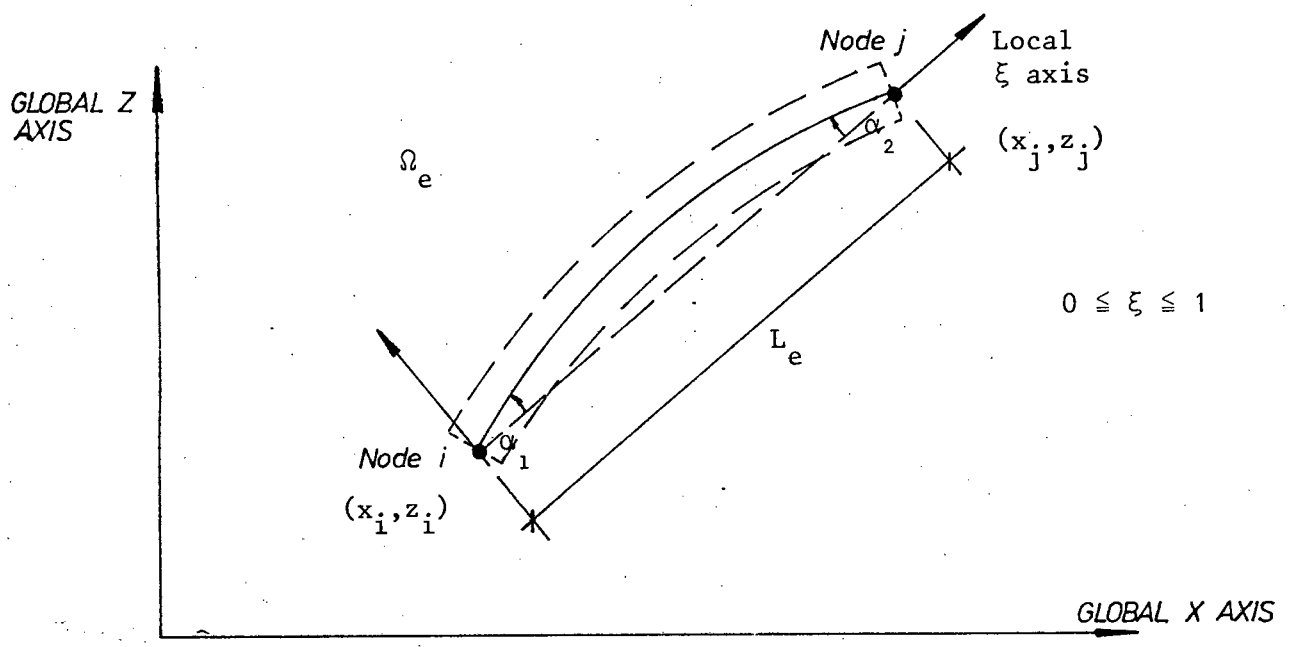

Figure 2.3 Element in Global Coordinate System

$$K_e = \frac{EI}{L_e} \begin{bmatrix} \frac{R}{L_e^2} & \frac{Rc_1}{L_e} & \frac{Rc_2}{L_e} \\ \frac{Rc_1}{L_e} & 4+Rc_1^2 & 2+Rc_1c_2 \\ \frac{Rc_2}{L_e} & 2+Rc_1c_2 & 4+Rc_2^2 \end{bmatrix} \qquad (2.40)$$

where $R = \frac{AL_e^2}{Ixx}$ and A = Cross-sectional area of element

Ixx = Second moment of area of element

$$c_1 = \frac{2}{15}\alpha_1 - \frac{1}{30}\alpha_2$$

$$c_2 = \frac{2}{15}\alpha_2 - \frac{1}{30}\alpha_1$$

To transform the element stiffness matrices to the global system, the transformation T is defined.

$$T = \begin{bmatrix} -c & -s & 0 & c & s & 0 \\ \frac{s}{L_e} & -\frac{c}{L_e} & 1 & -\frac{s}{L_e} & \frac{c}{L_e} & 0 \\ \frac{s}{L_e} & -\frac{c}{L_e} & 0 & -\frac{s}{L_e} & \frac{c}{L_e} & 1 \end{bmatrix}$$

where L_e = is the length of the element

$c = (Z_j - Z_i)/L_e$

$s = (X_j - X_i)/L_e$

The Global stiffness matrix becomes

$$K = T^T K_e T \tag{2.41}$$

The deformational degrees of freedom are also effectively transformed to the global sense. This yields 6 degrees of freedom per element or 3 degrees of freedom per node, then

$$u_t^{eT} = [u_i , v_i , \phi_i , u_j , v_j , \phi_j] \tag{2.42}$$

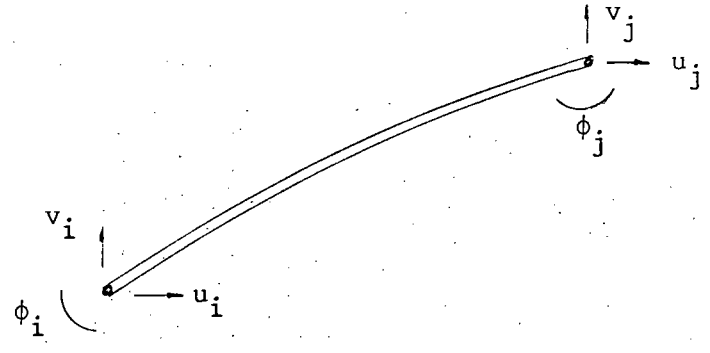

Figure 2.4 Global Deformational Degrees of Freedom

2.6 Optimum Sampling Point

In the potential energy functional, Π , the integrants contain derivatives of the 2nd order. If the order of the derivatives is called $(m+n)$ then to ensure convergence as the element size decreases, the shape functions must satisfy the following requirements.

i) The compatibility requirement - at element interfaces, there must be $C^{(m)}$ continuity. In this case C^1 continuity is implied, i.e. continuity of the slope (first derivative).

ii) The completeness requirement - within an element there must be $C^{(m+1)}$ continuity.

The curved linear-cubic beam element does not fulfill the above requirements. The shape functions of the curved linear-cubic beam element only ensures continuity of the main variable i.e. C^o continuity.

Note that the minimum value of an energy functional Π is defined as

$$\Pi = \frac{1}{2} \int_{\Omega} (Lu)^T A (Lu) \, d\Omega + \int_{\Omega} u^T b \, d\Omega$$

which gives the exact solution $u = \bar{u}$ is equivalent to minimum value of another functional Π^* defined as

$$\Pi^* = \frac{1}{2} \int_{\Omega} [L (u - \bar{u})]^T AL (u - \bar{u}) \, d\Omega$$

where L is a self adjoint linear operator
A prescribed matrix of position
b prescribed matrix of position.

With a finite element approximation of order p the Lu derivatives can at best be approximated by local polynomials of the order (p-m), where m is the differentiation order implied in the operator L, as before. Incomplete polynomials or other terms often add a spurious variation.

As the continuity of derivatives is not imposed, the approximation at element level can be considered. In general and certainly in this case, the A matrix is constant. The best fit available in the finite element approximation will be a complete polynomial of order (p-m). In Figure 2.6.1 a curve is shown which represents an assumed exact variation of the quantity $(L\bar{u})$ and a set of piecewise constant least square approximations to it (Lu).

At some points within each segment the approximate solution must equal the exact one.

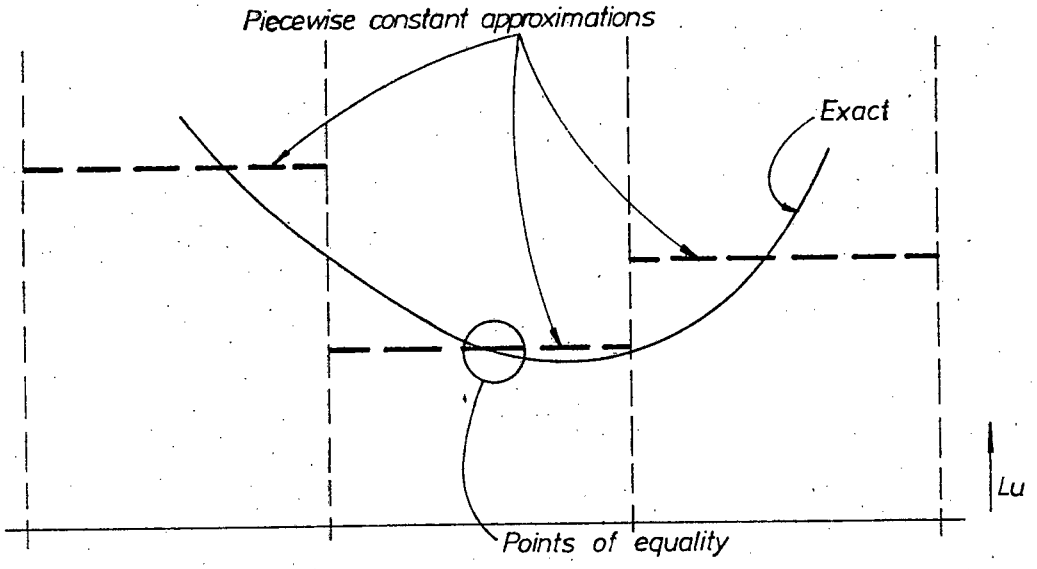

Figure 2.6.1 Piecewise Constant Least Square Fit to a Curve Lu

If the exact curve were a parabola, then two Gauss points would define uniquely a straight line which would be the least squares approximation to it. Conversely, if the approximation Lu were sampled at these points we would obtain an accuracy of one order greater than that available elsewhere by the approximation. These points are optimum for sampling the quantity Lu or the stresses in an elastic problem.

It can be stated that generally the approximation to Lu is always of order $0(h^{p-m+1})$, where p is the complete polynomial in the approximating shape function and in the order of the operator L. This means that at integration points which exactly integrate a polynomial of order $2(p-m)+1$, the approximation will be one order better.

It is, therefore, important to sample strains or stresses at integration points.

The curved linear-cubic beam element has a complete linear function but an incomplete cubic function in the shape functions. This implies $p = 1$. The differentiation order implied is, $m = 1$. This demonstrates that the curved linear-cubic beam element is a non-conforming element.

The curved linear-cubic beam element is classified as a C^o element. Zienkiewicz suggests that the "obvious" location of the optimum stress sample would be at the centroid of the element. Furthermore, Zienkiewicz states that in C^o elements, the stresses (or similar quantities) should never be calculated at nodes. See Figure 2.6.2 for the optimum sampling location. Figure 2.6.2 overleaf.

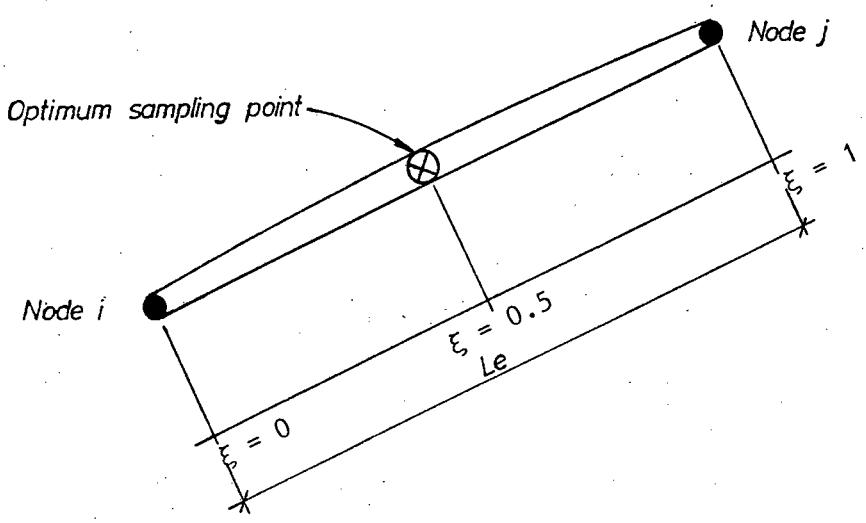

Figure 2.6.2 Location of Sampling Point

2.7 Calculating the Axial Forces and Bending Moments

As the results of the finite element analysis are used for design it is desirable to calculate forces and moments. The general stress-strain relationship can be written as

$$\begin{pmatrix} f \\ m \end{pmatrix} = D \begin{pmatrix} \bar{\varepsilon} \\ \kappa \end{pmatrix} \qquad (2.43a)$$

where f is the axial force in Ω_e

m is the moment in Ω_e

$$D = \begin{bmatrix} EA & 0 \\ 0 & EIxx \end{bmatrix}$$, is termed the material matrix. (2.43b)

$\bar{\varepsilon}$ is the average axial strain

κ is the bending strain

E is Young's modulus

A is the cross-sectional area

Ixx is the second moment of area.

Using Equation (2.42) the axial force in an Ω_e is written as

$$f = EA\bar{\epsilon} \tag{2.44}$$

where $\bar{\epsilon} = \frac{u_{21}}{L_e}$

u_{21} is the elongation of the Ω_e

L_e is the element length.

Therefore $\bar{f} = EA \frac{u_{21}}{L_e}$ (2.45)

From Equation (2.43a) again the expression for the bending moment can be written as

$$m = (EIxx)\kappa \tag{2.46a}$$

Recalling Equation (2.4) and Equations (2.9) to (2.13)

$$\kappa = \frac{d^2}{dx^2} L_e [\phi_1 (\frac{x}{L_e} - \frac{2x^2}{L_e^2} + \frac{x^3}{L_e^3}) + \phi_2 (\frac{x^3}{L_e^3} - \frac{x^2}{L_e^2})]$$

performing differentiation yields

$$\kappa = -\phi_1 (\frac{6x}{L_e^2} - \frac{4}{L_e}) - \phi_2 (\frac{6x}{L_e^2} - \frac{2}{L_e}) \tag{2.46b}$$

Section 2.6 clearly identifies the location of the optimum sampling point. The location of the sampling point is only of consequence when calculating the bending moment as it has the ability to vary in magnitude and direction over the element. The axial force is calculated using an average axial strain which, in effect, assumes the axial force distribution to be constant in the element.

The optimum sampling point in C^o elements is at the centroid of the element. Figure 2.7.1 illustrates the optimum sampling point.

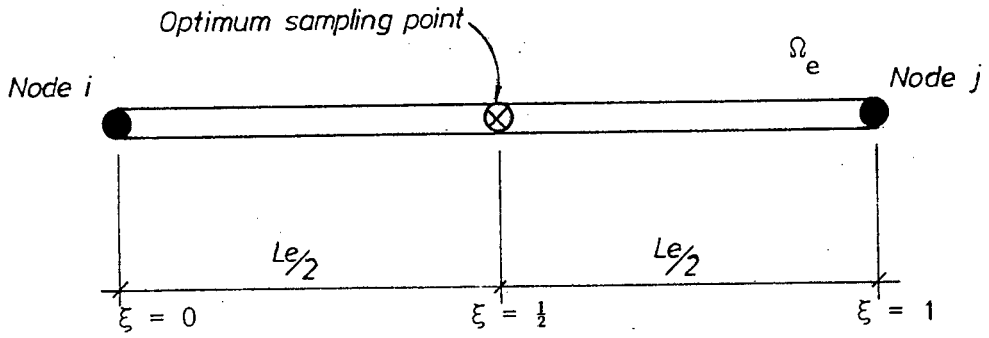

Figure 2.7.1 Optimal Sampling Point

The optimum sampling point is at $\xi = \frac{1}{2}$. From Equation (2.13) we can write $x = \frac{L_e}{2}$ as the sampling point. Substituting $x = \frac{L_e}{2}$ into Equation (2.46a) yields

$$m = EIxx \left(\frac{\phi_1}{L_e} - \frac{\phi_2}{L_e} \right) \tag{2.47}$$

Rewriting Equation (2.43) yields

$$\begin{pmatrix} \bar{f} \\ m \end{pmatrix} = \frac{1}{L_e} \begin{bmatrix} EA & 0 \\ 0 & EIxx \end{bmatrix} \begin{pmatrix} u_{21} \\ \phi_1 - \phi_2 \end{pmatrix} \tag{2.48}$$

where $\bar{f}$ = average axial force in Ω_e

m = mid element bending moment in Ω_e

2.8 Satellite Element Refinement

The curved linear-cubic beam element has one reliable stress sampling point, as discussed in Section 2.6.

For practical purposes it is fairly useless to have a stress result only at the centre of an element. Structural design demands knowledge of results (bending moments) at the extremes of the element, i.e. at the associated element nodes. The maximum stresses encountered in the element is also vital to the design operation.

Substitute shape functions can be used to interpolate the stresses in non-conforming elements. Another remedy is to refine the finite element mesh so that a reasonable stress distribution can be obtained. MICRODEST uses a variation on mesh refinement which is termed "Satellite Element Refinement" (SER).

In SER a typical element of length L_e is replaced by a satellite assemblage of the same length L_e. The satellite element is based on tests that very small elements will interact correctly with larger elements. See Figure 2.8.1 and accompanying Table 2.8.1 for verification examples and results. The elements referred to here being specifically the curved linear-cubic beam element.

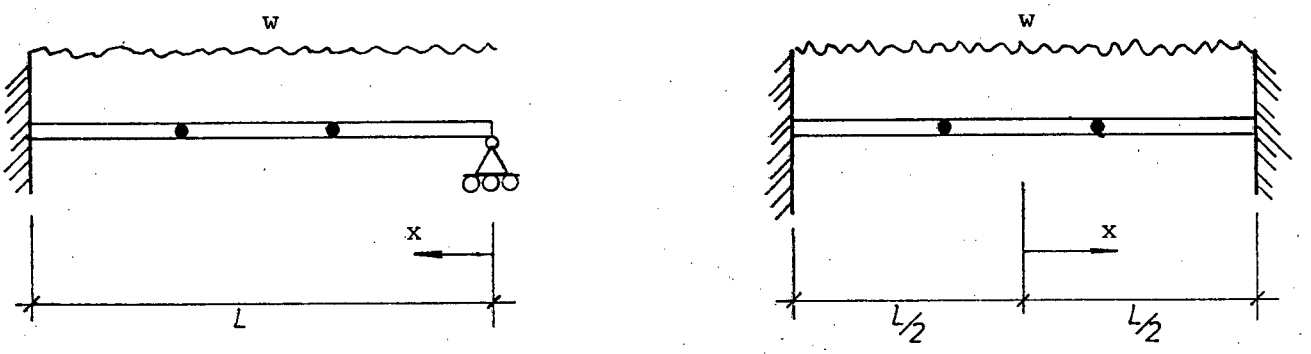

Example 1 Using 3 Satellite Refined Elements

Example 2 Using 3 Satellite Refined Elements

Figure 2.8.1 Examples Used for Verification

Aside

It is possible to execute the operation stated by $Ku = F$, after all the unknowns have been solved to yield F which can then be reduced to yield global nodal forces and moments. This is done by multiplying the stiffness matrix K, by the solution, u.

This will solve half the problem as it will eventually yield two sets of nodal results. This will indeed furnish nodal moments but it would not yield sufficient information to fit a quadratic curve and then to monitor quadratic variations along the element. If this approach is adopted then a maximum moment can not be predicted along the length of the element.

To obtain a third set of results, the stresses could be calculated at the centre of the element. This will provide the third set of results required for a quadratic curve fit.

The author feels it is more consistent to adopt a single strategy (SER) for finding nodal results and the maxima, than to mix these strategies. The method of finding F by multiplication is well used and researched. The method proposed by SER is indeed novel and requires investigation.

The manner of combining three elements in a satellite assemblage yields superior results than a single element would for a curved element.

Example	x	SER	Theory	Difference
1	L/2	1.915mm	1.915mm	** exact
	L/4	1.735mm	1.735mm	** exact
2	0	0.957mm	0.957mm	** exact
	L/3	0.295mm	0.295mm	** exact
	L/4	0.539mm	0.539mm	** exact

Table 2.8.1 Verification Examples on Satellite Element Refinement

The strategy of satellite elements is to fit a very small element in near the nodes of the parent element to yield a reliable result as close to the nodes as possible. This is best illustrated in Figure 2.8.2.

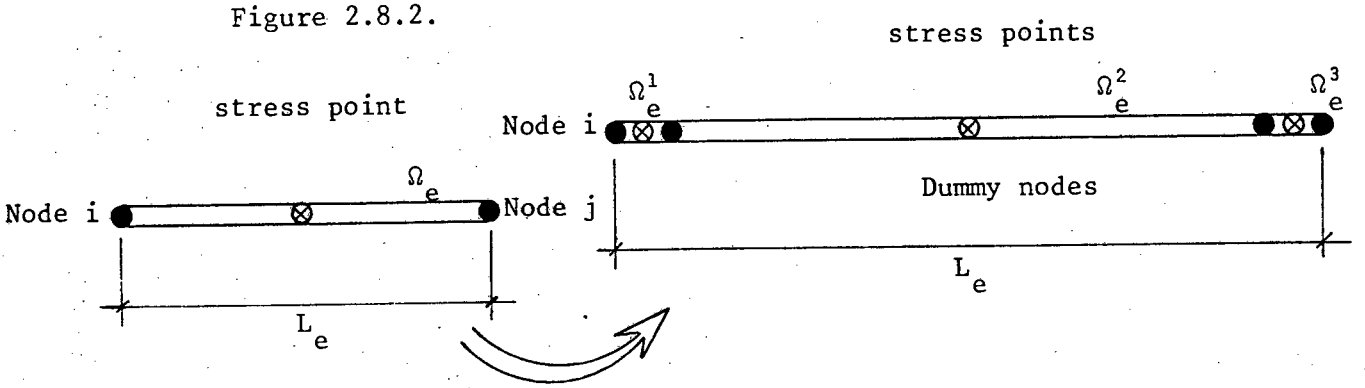

Figure 2.8.2 Illustration of Satellite Element

where Ω_e a typical element in the mesh

Ω_e^{sat} the associated satellite element

Ω_e^i the element topology of Ω_e^{sat}

$$\Omega_e^{sat} = \sum_{i=1}^{3} \Omega_e^i$$

The length of the outer small elements in the satellite formulation is $0.01\ L_e$. This means that the stresses sampled at the end elements are located $0.005\ L_e$ from the nodes in the original element.

In a normal element, Ω_e, there are six degrees of freedom. The associated satellite element, Ω_e^{sat}, however, will now possess 12 degrees of freedom per "element". See Figure 2.8.3.

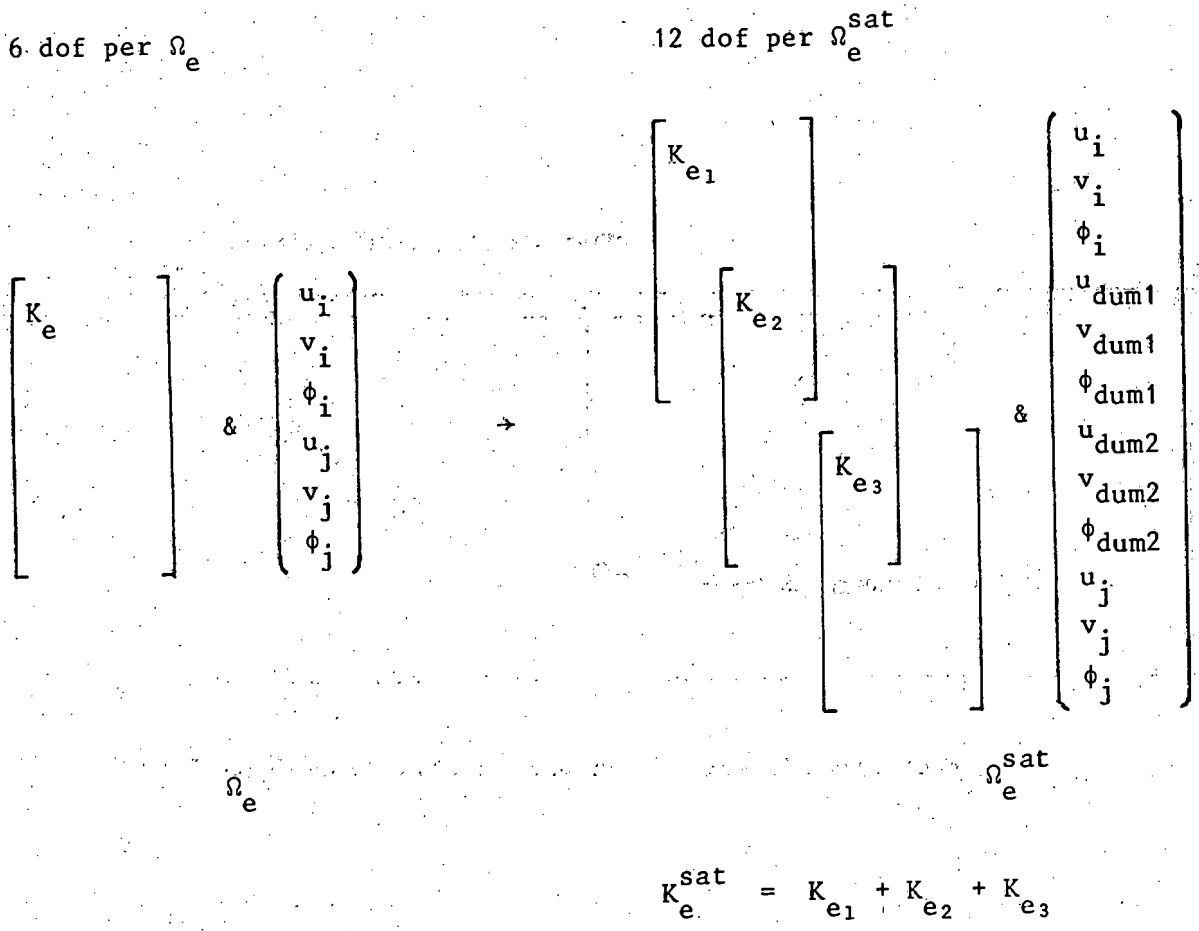

Figure 2.8.3 Associated Degrees of Freedom of Satellite Element

where K_{e_i} is the element stiffness of Ω_e^i

$K_e^{sat} = \sum_{i=1}^{3} K_{e_i}$ which is the "element" stiffness matrix of Ω_e^{sat}

A verification example demonstrates the curve fitting and extrapolation of results. See Table 2.8.2. and Figure 2.8.5.

	Mid Element Moment
Ω_1	4.902
Ω_2	- 14.803
Ω_3	8.115

Table 2.8.2 Results of Satellite Refined Element Ω_e^{sat}

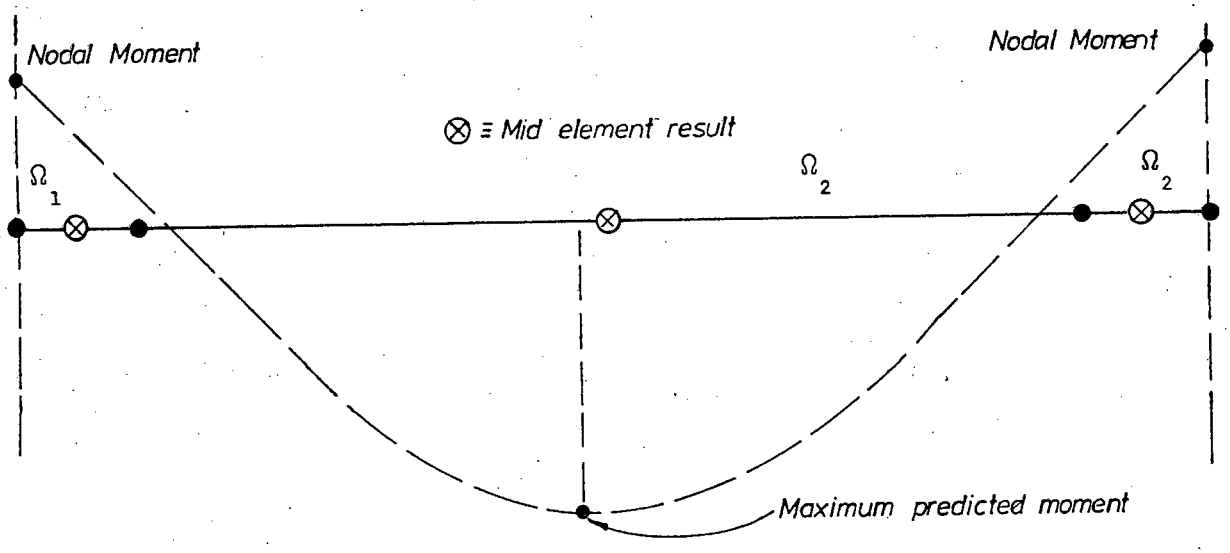

Figure 2.8.5 Curve Fitting and Extrapolation Element Results

The predicted nodal moments and maximum predicted moment are then used in the design routine.

2.8.1 Implementing SER

Construction of the satellite elements is transparent to the prospective user of MICRODEST. The finite element model is conceived in the normal manner and run on MICRODEST.

The subroutine SATELLITE constructs the satellite elements and sets up the necessary data structures.

Due to SER the total number of elements and nodes analysed in the model will be

Total nodes = Nodes + (2xLments)

Total elements = 3xLments

where Nodes = No of nodes in original model
Lments = No of elements in original model.

Section 4.6 sets out the mechanics of SER and the data storage.

2.9 Static Condensation

Static condensation is an algorithm that can be used effectively in the solution of the equilibrium equations. The name "static condensation" was coined in dynamic analysis for which this solution technique is often employed.

Static condensation is employed to reduce the number of element degrees of freedom and thus, in effect, to perform the part of the solution of the total finite element system equilibrium equations prior to assembling the structure matrices.

2.9.1 Static Condensation in the Satellite Element

The satellite element is described in Section 2.8. Figure 2.9.1 illustrates the satellite element.

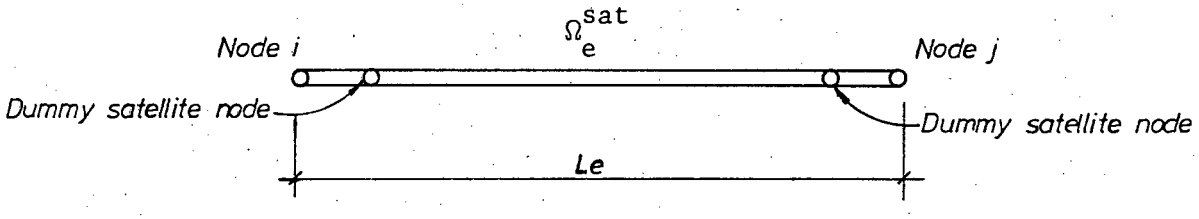

Figure 2.9.1 Associated Nodes of a Satellite Element

The element stiffness matrix, K_e^{sat}, of a typical element, Ω_e^{sat}, can be assembled using the original element topology, Node i and Node j. The dummy satellite nodes are transparent as they are always straddled by the original element topology. This provides an implied topology for Ω_e^{sat}, which is deduced from $\Omega_e^{sat} = \sum_{i=1}^{3} \Omega_e^i$.

The associated degrees of freedom of the satellite element are illustrated in Figure 2.8.3.

All nodal loads and equivalent nodal loads are applied to the nodes in the original mesh i.e. Node i and Node j on an element level. This means that the dummy satellite nodes are never loaded. The corresponding locations in the load vector f_e^{sat} will then be zero.

$$[K_e^{sat}] \ (u_e^{sat}) = (f_e^{sat}) \tag{2.49a}$$

where $[K_e^{sat}]$ previously defined in Section 2.8 (2.49b)

$$(u_e^{sat})^T = (u_i, v_i, \phi_i, u_{d1}, v_{d1}, \phi_{d1}, u_{d2}, v_{d2}, \phi_{d2}, u_j, v_j, \phi_j) \tag{2.49c}$$

$$(f_e^{sat})^T = (f_{xi}, f_{zi}, m_i, 0, 0, 0, 0, 0, 0, f_{xj}, f_{zj}, m_j) \tag{2.49d}$$

Reordering Equation (2.49c) so that

$$(u_e^{sat}) = \begin{pmatrix} u_1^{sat} \\ \hline u_2^{sat} \end{pmatrix} \tag{2.50a}$$

$$(f_e^{sat}) = \begin{pmatrix} f^{sat} \\ \hline 0 \end{pmatrix} \tag{2.50b}$$

where $(u_{\sim 1}^{sat})^T = (u_i, v_i, \phi_i, u_j, v_j, \phi_j)$ (2.50c)

$(u_{\sim 2}^{sat})^T = (u_{d1}, v_{d1}, \phi_{d1}, u_{d2}, v_{d2}, \phi_{d2})$ (2.50d)

$(f_{\sim 1}^{sat})^T = (f_{xi}, f_{zi}, m_i, f_{xj}, f_{zj}, m_j)$ (2.50e)

and partitioning K_e^{sat}, then

$$\left[\begin{array}{c|c} K_{11}^{sat} & K_{12}^{sat} \\ \hline K_{21}^{sat} & K_{22}^{sat} \end{array}\right] \left(\begin{array}{c} u_1^{sat} \\ \hline u_2^{sat} \end{array}\right) = \left(\begin{array}{c} f_1^{sat} \\ \hline 0 \end{array}\right) \qquad (2.51)$$

The partitioned equations can be written in the form

$$[K_{11}^{sat}] (u_{\sim 1}^{sat}) + [K_{12}^{sat}] (u_{\sim 2}^{sat}) = (f_{\sim 1}^{sat}) \qquad (2.52a)$$

$$[K_{21}^{sat}] (u_{\sim 1}^{sat}) + [K_{22}^{sat}] (u_{\sim 2}^{sat}) = (0) \qquad (2.52b)$$

The second of these equations can be used to write $(u_{\sim 2}^{sat})$ in terms of $(u_{\sim 1}^{sat})$

$$(u_{\sim 2}^{sat}) = [K_{22}^{sat}]^{-1} [K_{21}^{sat}] (u_{\sim 1}^{sat}) \qquad (2.53a)$$

let $[K^*] = [K_{22}^{sat}]^{-1} [K_{21}^{sat}]$ (2.53b)

then $(u_{\sim 2}^{sat}) = [K^*] (u_{\sim 1}^{sat})$ (2.53c)

We now substitute Equation (2.53a) into Equation (2.52a) and obtain

$$([K_{11}^{sat}] - [K_{12}^{sat}] [K^*]) (u_{\sim 1}^{sat}) = (f_{\sim 1}^{sat}) \qquad (2.54)$$

Writing Equation (2.54) in the shortened form

$$[K_c^{sat}]\ (\underset{\sim 1}{u}^{sat}) = (\underset{\sim 1}{f}^{sat}) \tag{2.55a}$$

where $[K_c^{sat}] = [K_{11}^{sat}] - [K_{12}^{sat}]\ [K^*]$. (2.55b)

Equation (2.55a) represents a new system of equations with fewer displacement parameters than the original system.

Static condensation and the solution of equations by a direct method are basically the same process. In both processes the unknowns are eliminated by substitution into the remaining equations.

If, instead of using condensation, the internal degrees of freedom associated with the dummy satellite nodes were included, practically the same results would be obtained. A verification example is provided in Table 2.9.1. The discrepancy due to round-off error is negligible.

	Solving all the dof	Using Static Condensation	% Difference
Tip displacement	$-666.66665 \times 10^{-1}$	$-666.6668543 \times 10^{-1}$	0.000031 %
Tip rotation	$499.9999885 \times 10^{-1}$	$500.0001399 \times 10^{-1}$	0.000030 %
Moment reaction	$199.999994057 \times 10^{2}$	$200.000055862 \times 10^{2}$	0.000031 %

Table 2.9.1 Verification Example - Cantilever under a Tip Load

If static condensation is not utilized, the system of equations becomes longer and has a larger bandwidth. The computational effort also increases.

2.9.2 Global Assembly of the Condensed Stiffness Matrix

The equations modified in K_e^{sat} by static condensation pertain only to the nodes of Ω_e^{sat}, the element being condensed. Adjacent elements are not affected so the dummy satellite nodes, whose associated degrees of freedom are condensed out, interact on an element level only.

The condensed element stiffness matrix, $[K_c^{sat}]$ can then be assembled into the global system stiffness matrix using the original mesh topology (Node i and Node j). At this stage, as in the classical finite element algorithm, the element interaction is defined.

$$K_c = \sum_{e=1}^{Lments} [K_c^{sat}]_e \tag{2.56a}$$

where K_c = Global system stiffness matrix

Lments = the total number of elements in the original mesh

e = the element being assembled.

Then $K_c \, u_{\sim c} = F_{\sim c}$ (2.56b)

where $u_{\sim c} = \sum_{e=1}^{Lments} (u_{\sim 1}^{sat})_e$, condensed global displacement vector (2.56c)

$$F_{\sim c} = \sum_{e=1}^{Lments} (f_{\sim 1}^{sat})_e \text{ , condensed global load vector} \tag{2.56d}$$

2.9.3 Recovering the Condensed Degrees of Freedom

The fundamental purpose of SER and hence static condensation is to obtain three sets of results per "element". See Section 2.8. Solving Equation (2.56b) will yield $u_{\sim c}$. In order to obtain the three sets of results, the degrees of freedom that have been condensed out must be recovered.

Recalling Equation (2.53c) and defining all the degrees of freedom that have been condensed out in the mesh as

$$u_{\sim 2} = \sum_{e=1}^{Lments} (u_{\sim 2}^{sat})_e \tag{2.57a}$$

the degrees of freedom condensed out can then be recovered at the element level.

$$(\underset{\sim}{u}_2^{sat}) = K^* \ (\underset{\sim}{u}_1^{sat}) \tag{2.57b}$$

The complete global displacement vector is then known

$$\underset{\sim}{u} = \begin{bmatrix} \underset{\sim}{u}_c \\ \hline \underset{\sim}{u}_2 \end{bmatrix}. \tag{2.57c}$$

CHAPTER 3

PREPROCESSING

3.1 The Purpose of the Preprocessor

The fundamental purpose of any preprocessor is to streamline the data preparation stage in a finite element analysis. The finite element method has gained tremendous popularity in the engineering industry. Attempts to reduce the time consuming data preparation phase of the method evolved naturally. Any self-respecting Finite Element package currently available, will provide preprocessing facilities. Data for the processor MICRODEST is prepared by PREPRO, the preprocessor, developed as part of this project.

3.2 Preprocessor Design Philosophy

The preprocessor PREPRO, developed here, operates in the inquiry/response mode, i.e. interactively. As the potential user interacts with the preprocessor, it is important that a consistent software design philosophy is maintained.

This software design philosophy must impart the following characteristics to the preprocessor

- when collecting data the preprocessor must perform its task in a logical and sequential manner
- the preprocessor must be absolutely clear when prompting for data from the user
- errors should be trapped and diagnosed
- visual monitoring should be available throughout the preparation stage
- overall data logic check

- the program should be general so that it can be easily adapted.

PREPRO is a menu driven preprocessor. Figure 3.1 illustrates these menus as well as the layout of the preprocessor.

3.3 Data Sets

Nodes or elements can be grouped into sets. This allows the user to define the following types of data in terms of sets:

- Nodal loads
- Element loads
- Material section data
- Design groups.

The above data types can also be defined individually. Using data sets avoids a great deal of repetitive data definition.

3.4 Mesh Generation

Mesh generation is a painless method to generate nodal coordinates and the accompanying element topology. PREPRO provides a Super-element mesh generation technique together with the more primitive incremental node generator, and incremental element generator. The Super-element concept is discussed in Section 3.4.1.

3.4.1 Mesh Generation by Super-elements

A Super-element is defined here as the set of identical elements generated between two points. The node and element numbering is arbitrary and need not be incremental.

3.4.1.1 Straight Super-element

Data required to generate a straight Super-element are

- the nodal coordinates of the two end points
- and the number of identical elements to be generated.

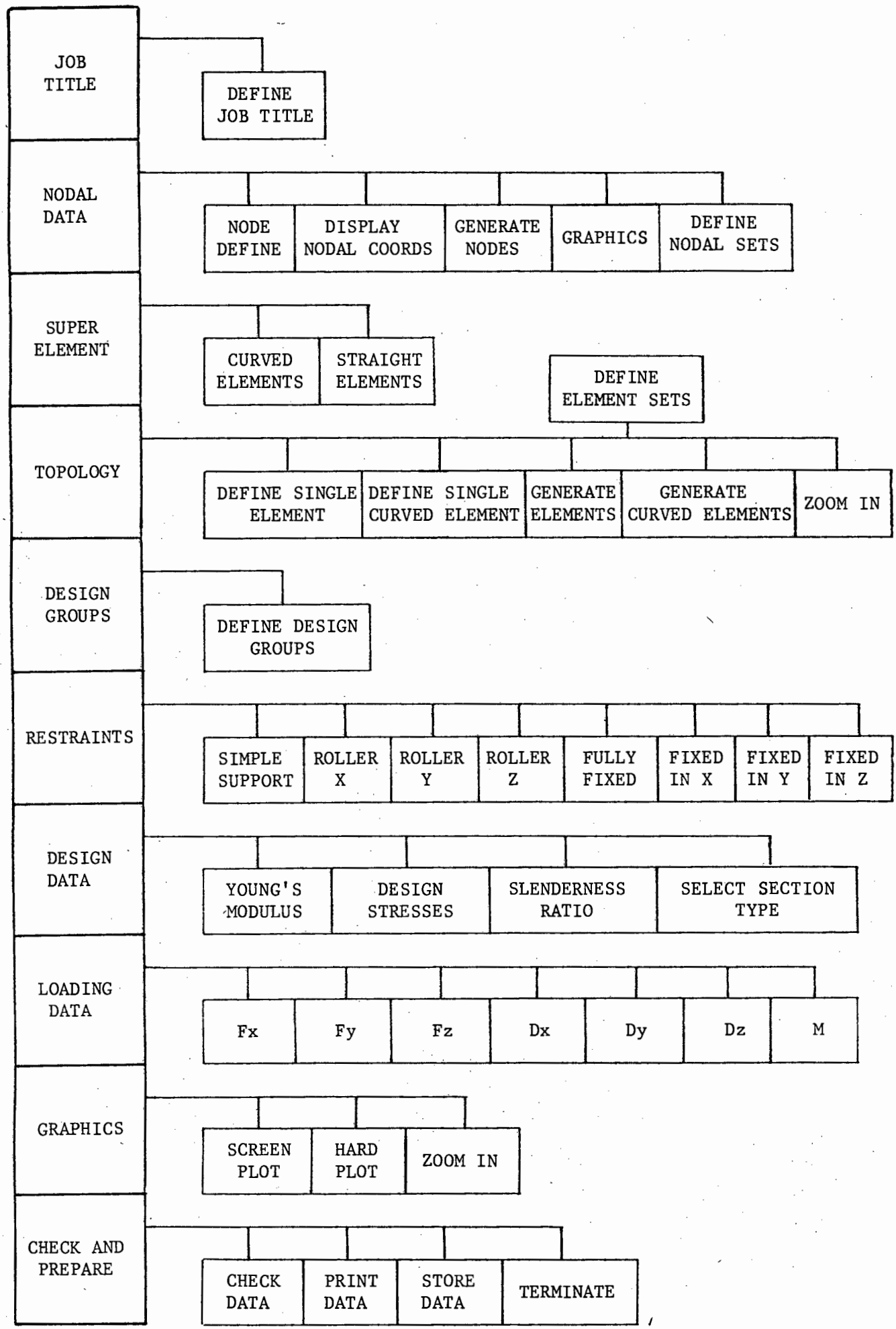

Figure 3.1 Menu overview of PREPRO

Figure 3.4.1 is an illustration of the method of generating a Super-element.

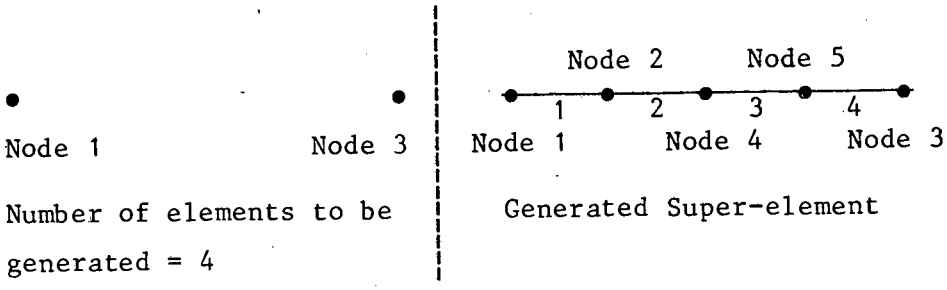

Figure 3.4.1 Illustrating the Super-Element

The data given in Figure 3.4.1 for the Super-element are the coordinates for nodes 1 and 3 and the number of elements to be generated.

The coordinates within the Super-element are generated incrementally. The node numbers of these coordinates are allocated on a first come - first served basis. The coordinates of the first generated node are allocated in Figure 3.4.1. Nodes 1 and 3 are defined and the lowest available node number is node 2, which represents the first generated node. The following generated node, i.e. node 4, is allocated the next lowest node number in the same way.

Element numbering is also performed in this manner. The first generated element is allocated the lowest available element number and the element numbering is then automatically incremented for each generated element thereafter.

The indiscriminate and random numbering of the generated nodes has no ultimate effect upon the bandwidth of the stiffness matrix. Before the stiffness matrix is assembled, an optimum node numbering configuration is obtained, using the Collins bandwidth reduction technique [14] , hence a minimum semi-bandwidth is used in storage and solution.

3.4.1.2 Curved Super-element

The node and element number allocation in this case is identical to the straight Super-element (Section 3.4.1.1).

Elements generated by the curved Super-element option can only be circular. The origin coordinates of the circular arc described by the Super-element have to be furnished in addition to the data required in Section 3.4.1.1.

The initial curvature of the element is calculated and stored along with the element data. Appendix B outlines the method used to calculate the nodal co-ordinates on a circular arc.

3.4.2 Nodal Generation

To provide an alternative to the Super-element concept, a simple incremental node generator can be requested when using PREPRO. This is useful if the user requires to generate nodal coordinates with specific node numbers.

The start and end node must be specified together with the node number increment and the number of nodes to be generated. See Figure 3.4.2 for an example.

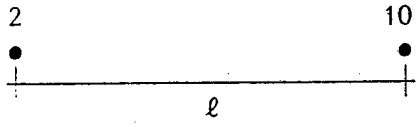

Start node = 2

End node = 10

Node increment = 3

Number of generated nodes = 3 , then

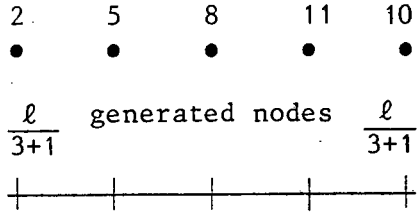

Figure 3.4.2 Illustration of Nodal Generation

3.4.3 Element Generation

The element generator uses a defined master element to generate other elements. The increment in the node numbers is calculated from the master element topology.

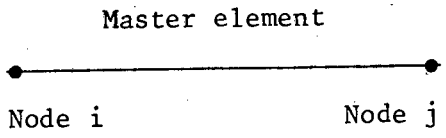

Figure 3.4.3 Master Element

The increment is taken to be

$$\text{increment} = \text{Node } j - \text{Node } i \qquad \text{where } j > i$$

where node i and node j is the master element topology.

This is useful when nodes are defined in a particular order and elements can be generated incrementally.

3.5 Data Check

The following checks are made on the data before a data file for the use on MICRODEST can be set up.

Check

- if all the nodes exist
- if any two nodes have the same coordinates
- if all the elements exist
- if the element topology is unique
- if a node in a node set is not repeated
- if an element in an element set is not repeated
- if boundary conditions are present
- if all design data is specified
- if all the load cases are present.

Diagnostic messages appear if any of the above checks fail.

3.6 Graphics

At any stage of the data preparation the current defined data can be plotted on the computer screen or on a plotter. A magnification facility is provided to view the more densely populated areas of the mesh.

3.7 Default Data

If certain data is not specifically defined, PREPRO then provides default values. The users manual in Appendix I lists the default values.

3.8 Collating the Data

Provided the data has passed the checks mentioned in Section 3.5 it is collated and stored in a two dimensional array. The array is called "Base" and has

Length + 1 rows and
3 columns.

Length depends on the volume of data to be stored.

When the data has been collated and located in its correct position in array "Base", it is stored on a floppy or a hard disc for use by MICRODEST.

Appendix A shows the assemblage of data in "Base".

CHAPTER 4

PROCESSOR

4.1 Preamble

The processor, MICRODEST, is specifically designed for use on micro-computers. Micro-computers are easily accessible and readily available. A reasonable balance is sought between the size of problem and the solution time.

The speed of the solution is considered to be of secondary importance. More attention is given to the size of the problem that can be processed and solved in a reasonable time. This implies a direct in-core solution technique.

MICRODEST incorporates the theory and ideas expounded in Chapter 2. In this chapter attention is given to the micro-computer application of these ideas and the algorithms developed to incorporate them.

4.2 Computer Programming Strategies

The Top-Down Design [25, 26, 27] method of programming has been incorporated in designing MICRODEST. The reasons for this software design approach are

- the program can be easily implemented and tested
- program logic can be easily followed
- changes can be made easily
- additions and improvements to the program are relatively straightforward
- translation of the program for use on other micro-computers is facilitated.

A Hewlett Packard 9816 micro-computer was used to develop MICRODEST. Some of the special intrinsic commands of the HP9816 are utilized.

The mathematical matrix operations are used extensively as they usually require no more than one programming line and are time efficient.

Dynamic memory allocation is possible using the ALLOCATE and DE-ALLOCATE commands.

MICRODEST operates in an overlay mode. Besides the control program, there are only relevant sub-programs resident in memory. New sections, or sub-programs, are annexed to the control program with LOADSUB according to the program advance. Once a sub-program has been called by the control program and is no longer necessary, it is removed from memory using DELSUB. This makes available the previously occupied memory which can be used by following sub-programs or be utilized by ALLOCATE.

The sub-programs are grouped into libraries to enable them to perform general tasks. MICRODEST uses a total of seven sub-program libraries. To minimise time-consuming disc input operations the libraries are annexed to the control program. As the sub-programs of the annexed libraries are executed, they are deleted from memory if they have no immediate use.

Data arrays are used to store different data or results as the program advances. To minimise input-output disc operations, MICRODEST stores internally generated data and intermediate results internally.

The unmodified global stiffness matrix is written to disc for calculating reactions and solving subsequent load cases.

4.3 General Layout of MICRODEST

The general layout of MICRODEST is shown schematically in Figure 4.3.1 to demonstrate the general tasks of the sub-program libraries. The complete MICRODEST sub-program library comprises LIBRARY-1 through to LIBRARY-7.

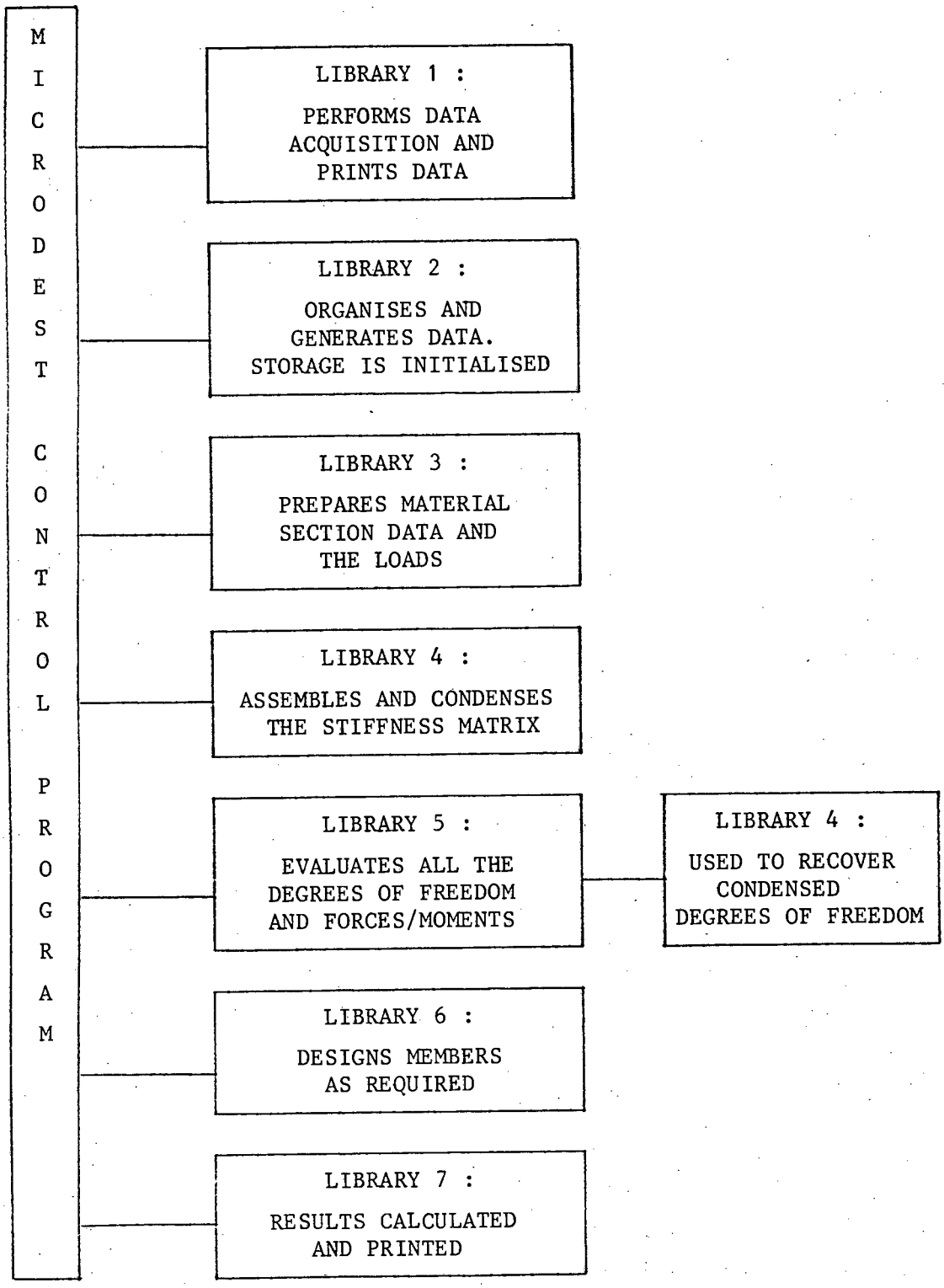

Figure 4.3.1 General Tasks of the Sub-Program Libraries

4.4 MICRODEST as a Structural Analysis Program

Resident in MICRODEST is a comprehensive material section list. See Appendix H. Material data is normally obtained from this internal section list which is used in the design process.

However, by using the Interactive data input routine, MICRODEST can be used as a pure structural analysis program. Material data is either used from the internal section list or extraneous material data is specified. This lends flexibility to MICRODEST as any material section properties can be considered in an analysis.

4.5 Bandwidth Reduction

To reduce computational effort and to increase the solving capacity of MICRODEST the Collins renumbering scheme [14] is used to find the minimum bandwidth. This is done by automatically renumbering the mesh which will yield N different node numbering schemes if there are N nodes in the mesh. This algorithm is incorporated in the sub-program OPTNUM.

The maximum nodal difference (minmax), on an element level, measures the feasibility of the renumbered scheme. When minmax has reached a minimum the associated renumbered scheme is adopted, which yields the optimum bandwidth.

Figure 4.5.1 demonstrates the optimum node numbering of an arbitrary mesh using the Collins renumbering scheme.

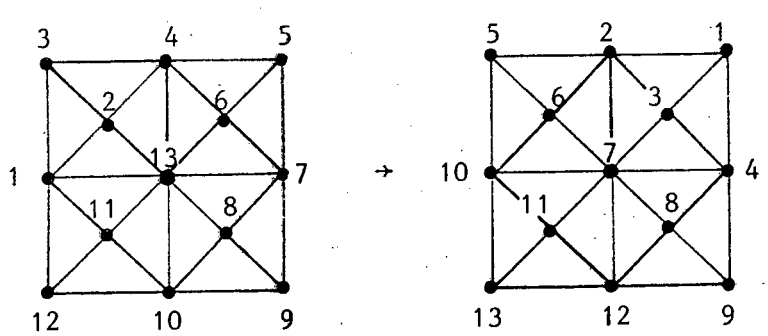

Original Scheme
minmax = 12

Optimum Scheme
minmax = 5

Figure 4.5.1 Optimum Node Renumbering of an Arbitrary Mesh

The optimum node numbering scheme is performed on the original mesh before SER is considered. As the generated nodes associated with SER are condensed from the satellite element, the node numbering of the original mesh need only be considered in reducing the bandwidth and hence in assembling the condensed stiffness matrix.

4.5.1 Renumbering Nodal Data and Results

Once the optimum node numbering scheme has been obtained the following nodal data has to be re-organised accordingly.

- topology (connectivities)
- nodal loads
- boundary conditions
- nodal coordinates
- nodal sets.

For nodal renumbering to remain transparent to the user, nodal results are presented for the original mesh. This affects

- the solution and
- the reactions.

The nodal re-organisation is performed by sub-programs NEW_NUMBERS and OLD_NUMBERS respectively.

4.6 Implementing Satellite Element Refinement

Lments and Nodes are the number of elements and the number of nodes in the original mesh respectively. Then due to SER

Total nodes = Nodes + (2 x Lments)
Total elements = 3 x Lments.

Generated data is annexed to existing data structures and adjustments are made where necessary.

An element from the original mesh is considered to be the parent element. The satellite element adopts the parent element number.

The topology of the parent element is reflected in the satellite element. See Figure 4.6.1.

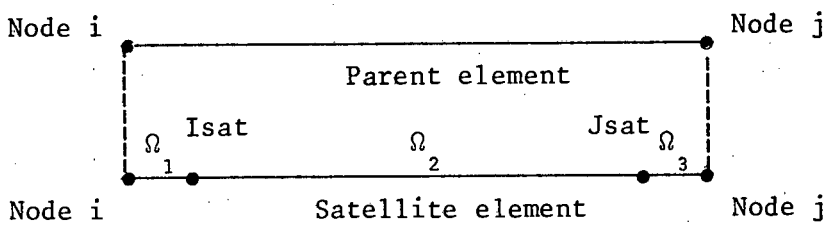

Figure 4.6.1 Parent and Satellite Element

The control element, Ω_2, in the satellite element also adopts the parent element number and hence the number of the satellite element it resides in.

Element numbering for the generated elements will be in the range

$$\text{Lments} < \Omega_1 \leqq \text{Total elements}$$
$$\text{Lments} < \Omega_2 \leqq \text{Total elements}$$

where $\Omega_1 \neq \Omega_3 \neq \Omega_2$.

Likewise, the generated nodes are assigned numbers in the following range

$$\text{Nodes} < \text{Isat} \leqq \text{Total nodes}$$
$$\text{Nodes} < \text{Jsat} \leqq \text{Total nodes}$$

where Isat $\neq$ Jsat.

To manage the administration of SER, satellite topology is introduced. Sat-topol(*) is a Lments x 3 array that stores the assemblage of the satellite elements. Figure 4.6.2 illustrates Sat-topol(*).

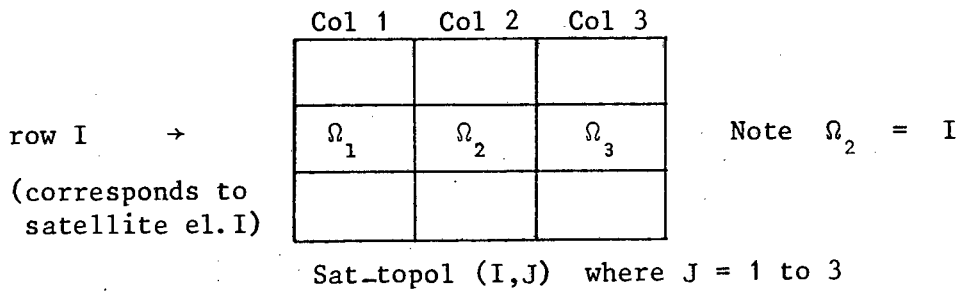

Figure 4.6.2 Sat_topol(*)

Figure 4.6.3 illustrates the algorithm to generate satellite elements.

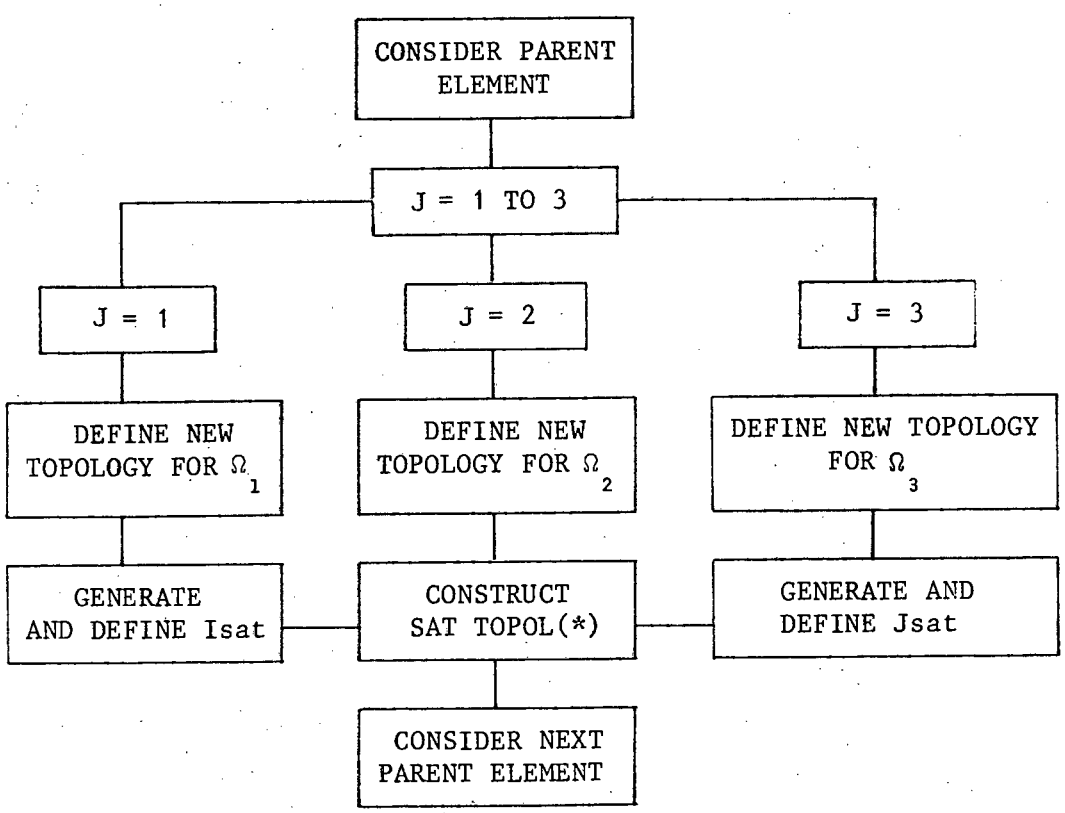

Figure 4.6.3 Algorithm to Generate Satellite Elements

Sub-programs SATELLITE, STRAIGHT-SAT and CURVED-SAT perform this task.

4.6.1 Generating Coordinates for Straight SER

The coordinates for Isat and Jsat are interpolated linearly using the coordinates of Node i and Node j.

4.6.2 Generating Coordinates for Circular SER

The coordinates of Isat and Jsat are generated using polar coordinates and then converting to rectangular coordinates. See Appendix B.

4.7 Equivalent Loads

Distributed and dead loads are approximated as equivalent nodal loads. Consider a typical element, Figure 4.7.1, subjected to a uniformly distributed load, w.

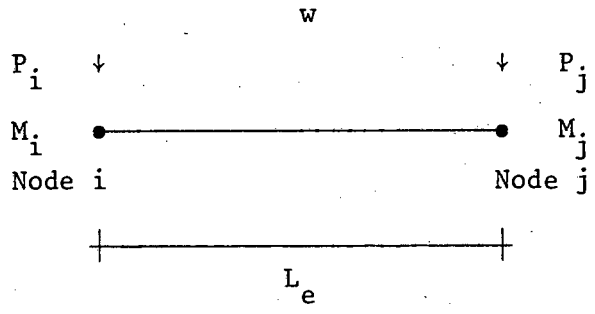

Figure 4.7.1 Typical Element Subjected to a udℓ.

The equivalent nodal loads due to w are

$$P_i = \frac{wL_e}{2}$$

$$M_i = +\frac{wL_e^2}{12}$$

$$P_j = \frac{wL_e}{2}$$

$$M_j = -\frac{wL_e^2}{12}$$

Loading is calculated and applied in the sub-programs DEAD-LOAD and LOAD_BEAM.

4.8 Implementing Static Condensation

The rudiments of static condensation in MICRODEST are clearly laid out in Section 2.9. In this section the algorithm is placed in a computing context. Figure 4.8.1 illustrates the basic steps of static condensation in MICRODEST.

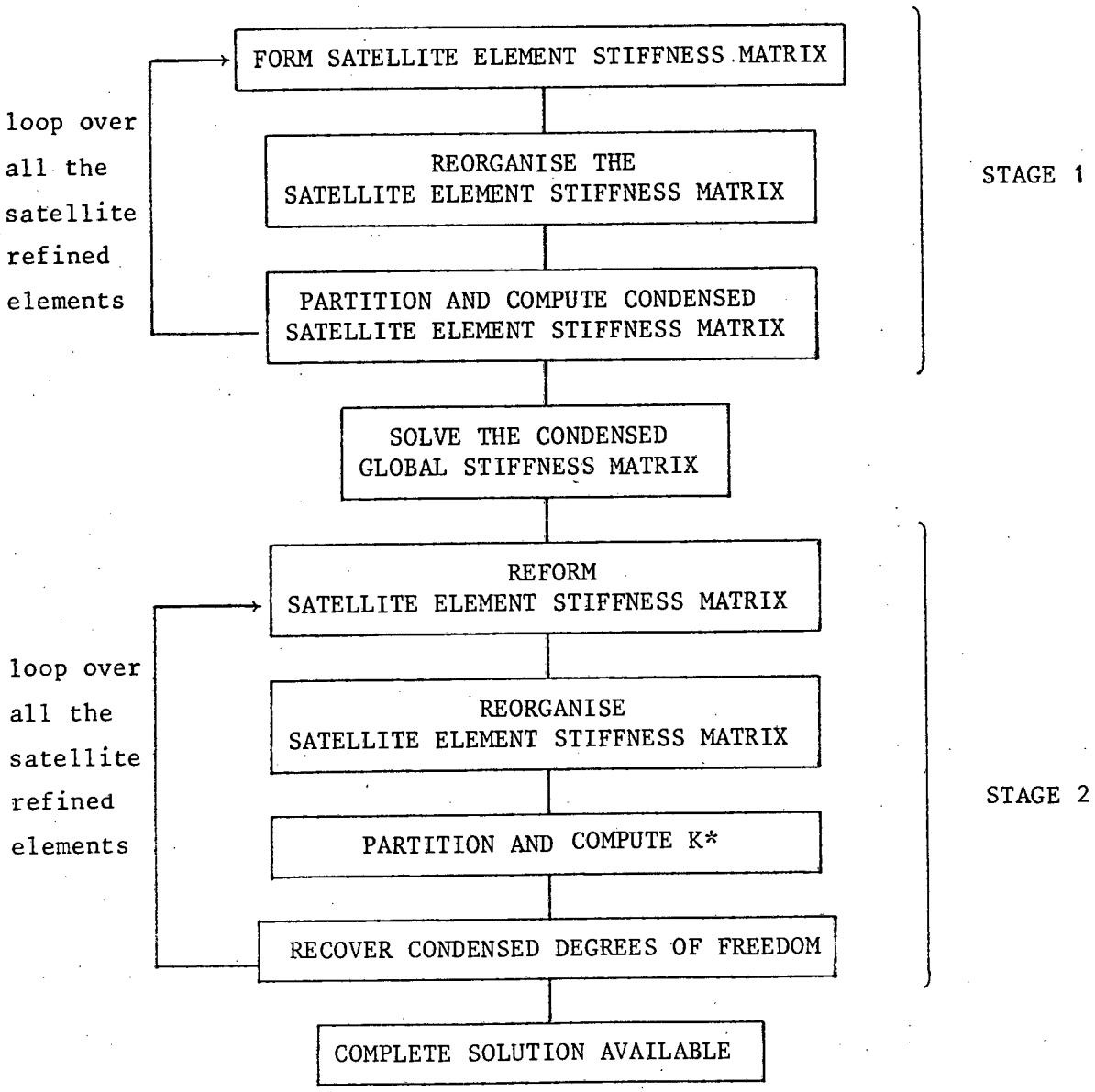

Figure 4.8.1 Static Condensation in MICRODEST

It is possible to store K* at Stage 1 either in memory or on external storage. If K* is stored on disc, the overall execution time will increase rapidly due to the input-output disc operations. Storing K* in memory occupies a fair size of core. It is more desirable to utilize internal storage to analyse larger problems than to store intermediate results.

In this case reforming K* at Stage 2 is more satisfactory and time efficient than the methods mentioned above.

Static condensation and the recovery of the degrees of freedom are performed by the following sub-programs in MICRODEST.

- CONDENSE
- REORGANISE
- KE-CONDENSE
- BEAM-ELEMENT
- RECOVER-DOF

4.9 External Storage

The unmodified stiffness matrix and load vector are stored externally for subsequent use. This is performed in a single operation after the data file has been created.

4.10 Predicting the Maximum Moment

Fitting a quadratic curve to a set of three moments per element as discussed in Section 2.7 yields the equation (see Appendix F)

$$M = a\xi^2 + b\xi + c$$

where M is the moment at ξ ; $0 \leq \xi \leq 1$

There is a maximum or minimum value if $\frac{dM}{d\xi} = 0$

$$\therefore \quad \xi_1 = \frac{-b}{2a}$$

If $0 < \xi_1 < 1$ then a maximum or minimum moment exists on the element with a value of $M = a\xi_1^2 + b\xi_1 + c$.

If $0 > \xi_1 > 1$ then the maximum or minimum moments are located at $\xi = 0$ or $\xi = 1$. i.e. at the nodes of the element.

The maximum predicted moment is the absolute maximum moment calculated.

4.11 Calculating Reactions

Reactions due to the boundary conditions are calculated using the unmodified stiffness matrix. The reaction equations are constructed from the semi-band stiffness vector. See Appendix E.

Figure 4.11.1 sets out the basic steps in calculating reactions.

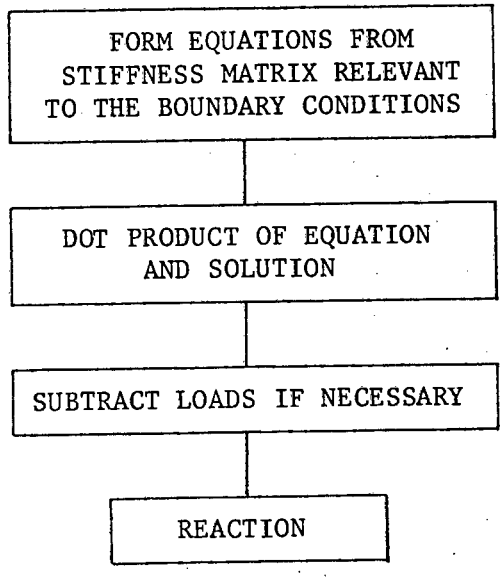

Figure 4.11.1 Calculating reactions

The above routine is performed by the sub-program REACTIONS.

4.12 Overall Layout of MICRODEST

Figure 4.12.1 provides a macro-flowchart of MICRODEST. The design routines are treated as a blackbox at this stage as they are discussed in detail in Chapter 6.

The various sub-programs are listed and introduced below.

LOAD_DATA	:	loads prepared data from either floppy or hard disc
PRINT_DATA	:	echos data on printing device
LOGO	:	draws out a logo for MICRODEST
INTERACTIVE	:	interactive options can be set
OPTNUM	:	automatically renumbers the nodes and finds the optimum node numbering configuration (Section 4.5)
NEW_NUMBER	:	renumbers all nodal data and related data (Section 4.5.1)
SATELLITE	:	co-ordinates the generation of a SER mesh (Section 4.6)
STRAIGHT_SAT	:	generates a straight satellite element
CURVED_SAT	:	generates a curved satellite element
ANULL	:	initializes and curtails storage
LOAD_SECTIONS	:	initializes storage for the on-board design sections
SECTIONS	:	loads sections into storage

DEAD_LOAD	:	calculates and forms the dead load vector (Section 4.7)
LOAD_BEAM	:	calculates and forms the applied load vector (Section 4.7)
BEAM_ELEMENT	:	co-ordinates the calculation, assembly and external storage of the stiffness matrix
MATPROP	:	returns the area and radius of gyration of a particular section
SECOND_MOM_AREA	:	returns Ixx of a section
CONDENSE	:	co-ordinates the static condensation on an element load (Sections 4.8 and 2.9.1)
REORGANISE	:	reorganises the element stiffness matrix (Sections 4.8 and 2.9.1)
KE_CONDENSE	:	performs the static condensation on the element stiffness matrix (Sections 4.8 and 2.9.1)
BEAM_BCS	:	applies the boundary conditions to the system stiffness matrix
SOLVE	:	direct solution of stiffness matrix by Crout reduction - Appendix D
RECOVER_DOF	:	co-ordinates the recovery of the condensed degrees of freedom (Sections 2.9.3 and 4.11)
BEAM_FORCES	:	calculates axial forces and bending moments (Section 2.7)
QUADRATIC	:	extrapolates to find nodal moments and maximum bending moment - see Section 4.10 and Appendix F

DESIGN ROUTINES : refer to Chapter 6

REACTIONS : calculates the reactions due to the boundary conditions - see Appendix E and Section 4.11

OLD_NUMBERS : renumbers nodal results in original configuration for output (Section 4.5.1)

RESULTS : co-ordinates the printing of results

BEAM_OUT : prints the nodal results and reactions

DES_OUT : prints the design results.

A users manual for MICRODEST is provided in Appendix J.

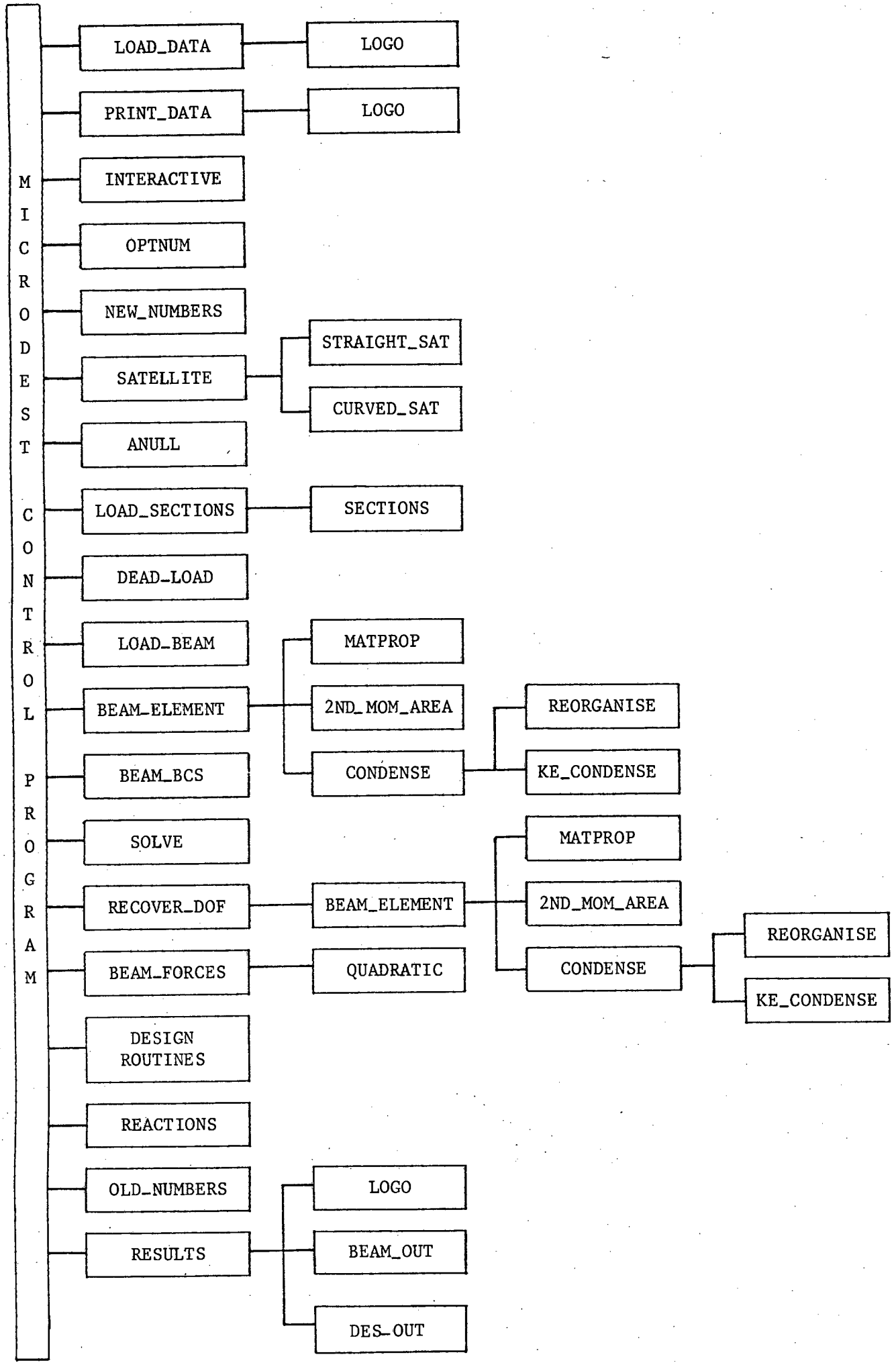

Figure 4.12.1 Macro Flowchart of MICRODEST

CHAPTER 5

VERIFICATION EXAMPLES

5.1 Preamble

Various examples are presented in this chapter to demonstrate the versatility of MICRODEST as a frame analysis program and to verify the results obtained. To check accuracy, deflections and bending moments are compared. Mesh convergence studies are also performed.

To obtain realistic results, different modelling techniques are employed in the frame examples. In this chapter, CLC refers to "Curved Linear-Cubic" to describe the beam element discussed in Chapter 2 and incorporated in MICRODEST.

5.2 Square Cantilever Under Tip Load

The problem illustrated in Figure 5.2.1 is solved using different finite element models and compared to the analytical solution in Table 5.2.1.

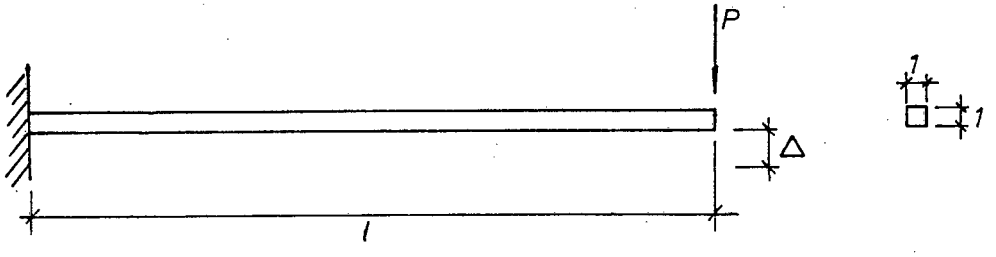

Data

EIxx = 10^5 A = 1

ℓ = 24 Δ = vertical tip deflection

P = 20

Figure 5.2.1 Square Cantilever Problem

The various models considered are listed below:-

MODEL A : One 2-noded Hermitian Beam Element
MODEL B : Two 3-noded Isoparametric Beam Elements
MODEL C : One 4-noded Isoparametric Beam Element
MODEL D : One 2-noded CLC Beam Element.

Shear deformation is excluded from all the models. The analytical solution for this problem is $\Delta = 0.9216$.

Model	Deflection Δ	% Difference
A	0.9216	exact
B	0.8685	5.762
C	0.9224	0.087
D	0.9216	exact

Table 5.2.1 Comparison of Cantilever Model Deflections

Models A and D provide the exact solution. The Hermitian element in Model A, however, does not possess the capacity to be curved, whereas the CLC element in Model D does. The Isoparametric cubic element in Model B does not perform well when compared to the other models.

The 4-noded Isoparametric element provides a very close solution, but it is not exact. As the CLC beam element, it has the capacity to be curved, but does not furnish the exact solution.

In bending it appears that the CLC beam element performs as well as the Hermitian beam element and in this case furnishes the exact result.

Models A, B and C were computed using the ADINA [32] Finite Element package. Model D was computed on MICRODEST.

5.3 Shallow Elastic Arch

A shallow elastic arch is considered (Figure 5.3.1). The midspan deflection, v , is compared to the analytical solution [28] for various mesh configurations. Results are tabulated in Table 5.3.1.

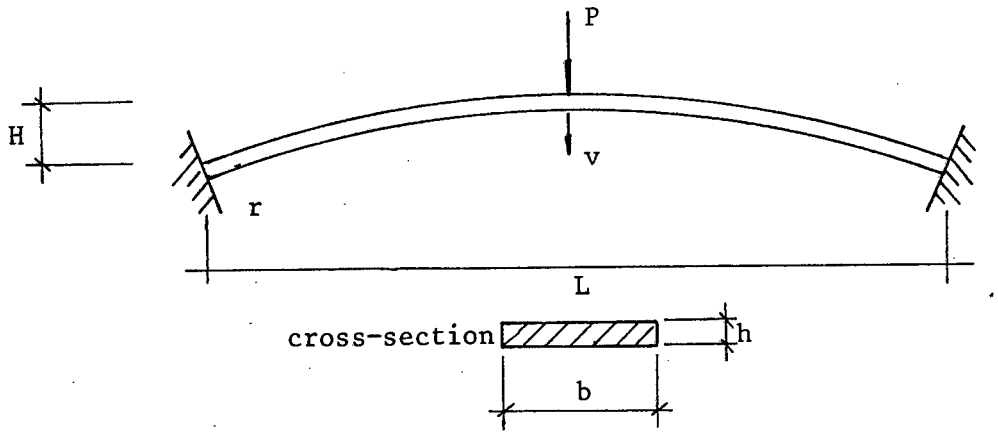

Data

Young's modulus	E	=	2×10^7
Depth of section	h	=	0.2
Width of section	b	=	1.0
Area		=	0.2
Second moment of area		=	6.6667×10^{-4}
Radius	r	=	200.5
	L	=	40
	H	=	1.0
	P	=	20

Figure 5.3.1 Shallow Elastic Arch Data

The analytical solution for this problem is $v = 0.0483357$.

Model	Initial Rotations α_i in Radians
A	0.049958×10^{-2}
B	0.024979×10^{-2}
C	0.016653×10^{-2}
D	0.012490×10^{-2}
E	0.009992×10^{-2}
F	0.004996×10^{-2}
G	0.002498×10^{-2}

Table 5.3.2 Initial Rotations

In this case the most reliable results are obtained for Models C and D. This implies that any model with initial rotations in the range,

$$0.016653 \times 10^{-2} \leqq \alpha_i \leqq 0.00992 \times 10^{-2} \quad (\alpha_i \text{ in radians})$$

will yield reliable results. A rule of thumb check can be used to pre-empt this problem.

$$\frac{3}{r} \lesssim \alpha_i \lesssim \frac{2}{r}$$

where r is the radius of the arch.

The upper bound of $\frac{2}{r}$ radians limits the initial rotation and this, in turn, the length of the element. The lower bound value of $\frac{3}{r}$ for α_i is less serious, as this is dependant on the word length and hence the round-off error of a particular micro-computer.

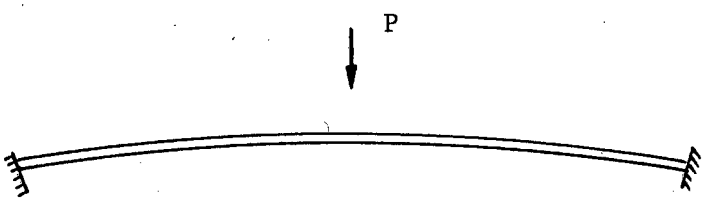

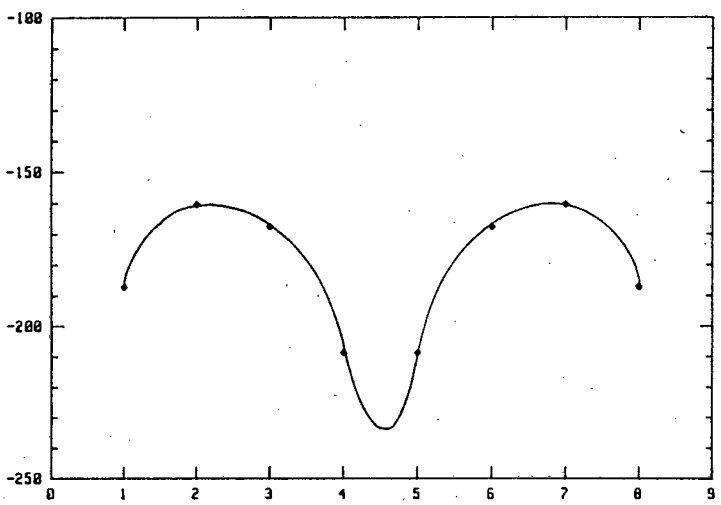

Figure 5.3.2a Axial Force in Shallow Arch

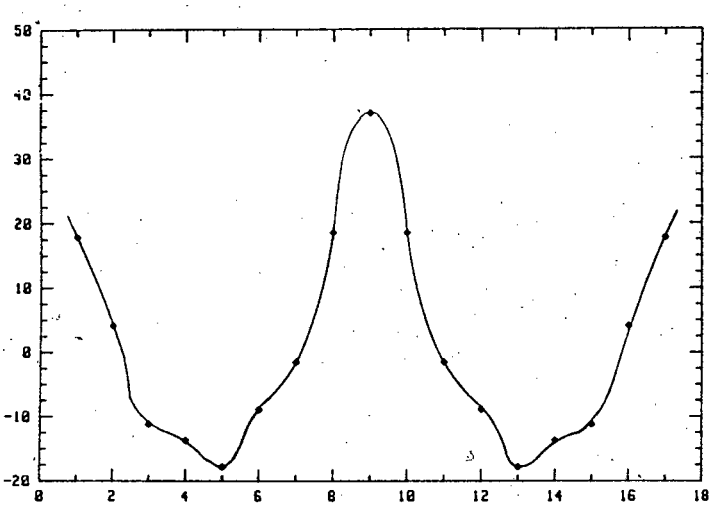

Figure 5.3.2b Bending Moments in Shallow Arch

Figure 5.3.2 a and b provide plots of the axial force and bending moment diagrams respectively.

Similar results can be obtained using straight offset elements (28). The CLC beam element is inherently superior as it requires no special modelling techniques and furnishes the correct result.

5.4 Deep Elastic Arch

An elastic ring (arch), Figure 5.4.1, is used in this example. A unit control deflection, v , is sought. The convergence of the load P for various mesh configurations are considered. Results are tabulated in Table 5.4.1 and compare well with (6, 28, 29). The analytical solution (6) for this problem is, P = 942.2 .

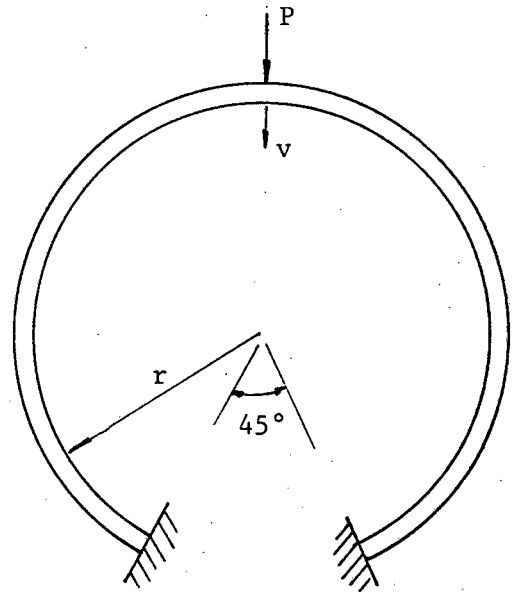

Data

Young's modulus	E	=	1.05×10^{7}
Depth of section		=	0.125
Width of section		=	1.2
Area		=	0.15
Second moment of area		=	0.195313×10^{-3}
Radius	r	=	2.935

Figure 5.4.1 Deep Elastic Arch Data

Model	Elements in Mesh	Deflection v	% Difference Compared to Analytical Result
A	2	0.01992053	41.213%
B	4	0.04674116	3.299%
C	6	0.04809194	0.504%
D	8	0.04832010	0.0322%
E	10	0.04838332	0.0985%
F	20	0.04825565	0.1657%
G	40	0.04842865	0.1923%

Table 5.3.1 Convergence Study of a Shallow Arch

The horrendous result of Model A is due to the crude mesh. This mesh yields initial rotations, α_i , (Equation 2.10), which are too large for the initial shape and hence for Marguerre shallow shell theory [3,28] to perform accurately.

As the mesh is refined the accuracy increases dramatically (Models A to D). The slight increase in percentage difference in Models F and G are due to round-off error. As the mesh becomes finer, the initial rotations, α_i , become much smaller. Round-off error and truncation does have an effect in this case. Table 5.3.2 presents the initial rotations of the various models.

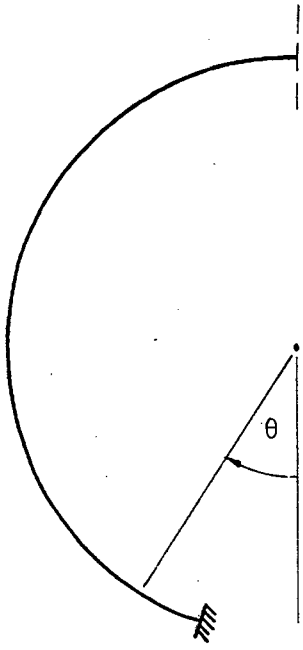

Half of deep arch results plotted due to symmetry

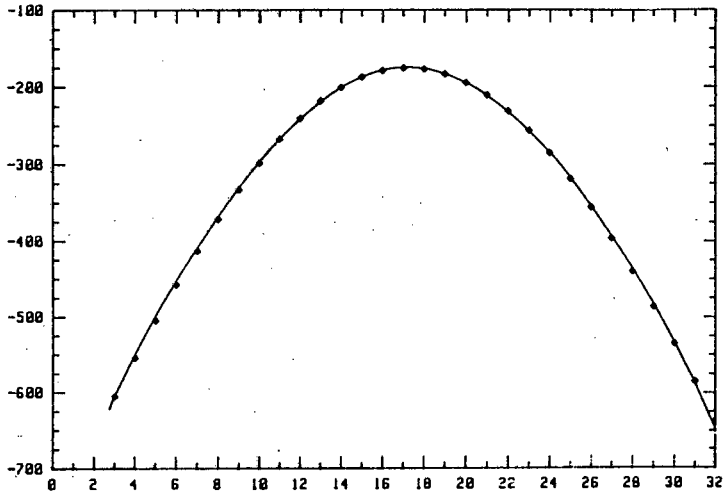

x $\frac{\Pi}{32}$ θ in rad

Figure 5.4.2a Axial Force Plot on Half of Deep Arch

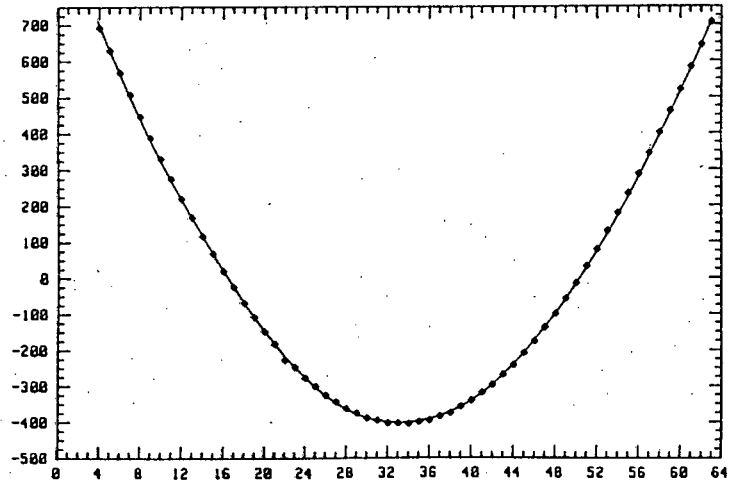

x $\frac{\Pi}{64}$ θ in rad

Figure 5.4.2b Bending Moment Plot on Half of Deep Arch

Model	Elements in Mesh	Load P	% Difference Compared to Analytical Result
A	24	957.4	1.613%
B	36	950.0	0.828%
C	60	946.1	0.414%
D	100	944.0	0.191%

Table 5.4.1 Convergence Study of a Deep Arch

A reasonably fine mesh is necessary to get the load P within 1% of the analytical solution.

The fine mesh is necessary to get the initial rotations, α_i , into acceptable bounds (see Section 5.3). Using a SER mesh also yields sufficient results to plot a detailed bending moment diagram and axial force diagram for this problem. Figures 5.4.2 a and b illustrates the bending moment and axial force diagrams. This also demonstrates the success of SER for curved members.

Frey and de Ville de Goyet [28] also obtain good results using straight elements for this problem. The CLC element with SER provides very good answers as well as sufficient axial force and bending moment results.

5.5 Frame Analysis

The frame in Figure 5.5.1 is analysed using various modelling techniques and compared to the plane stress solution. The deflections and the bending moments are compared.

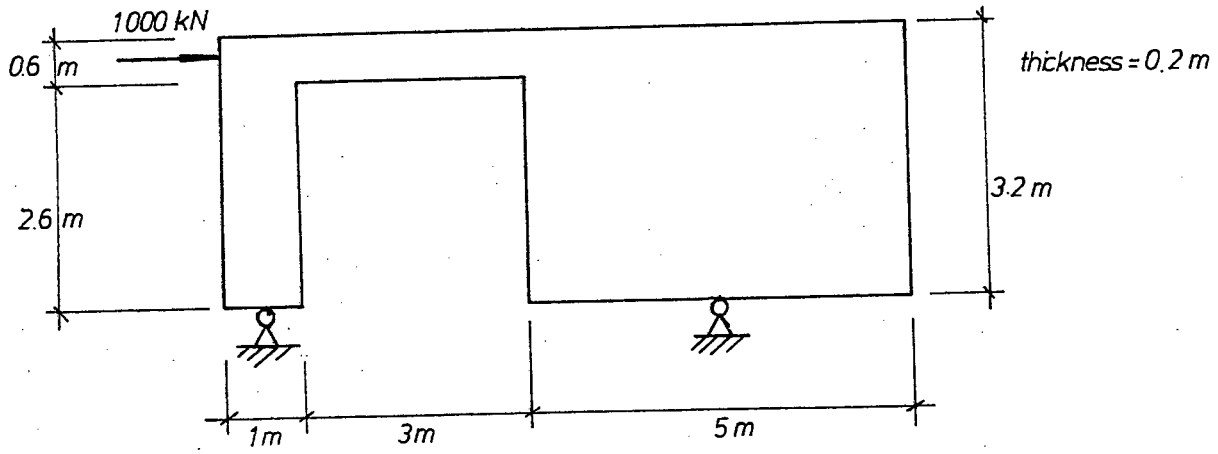

Figure 5.5.1 Shear Wall Type Frame

The various models considered are illustrated in Figure 5.5.2 (a, b, c).

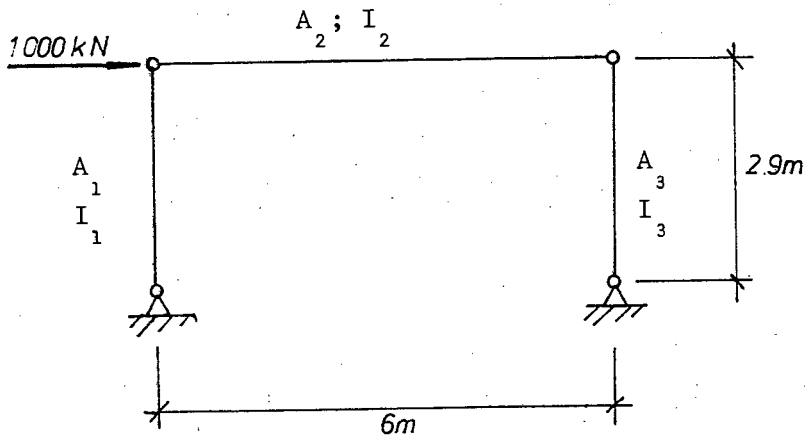

Figure 5.5.2a MODEL 1 (stick model)

Data

E	=	28 GPa
A_1	=	0.2 m^2
I_1	=	0.0167 m^4
A_2	=	0.12 m^2
I_2	=	0.0036 m^4
A_3	=	1.0 m^2
I_3	=	2.083 m^4

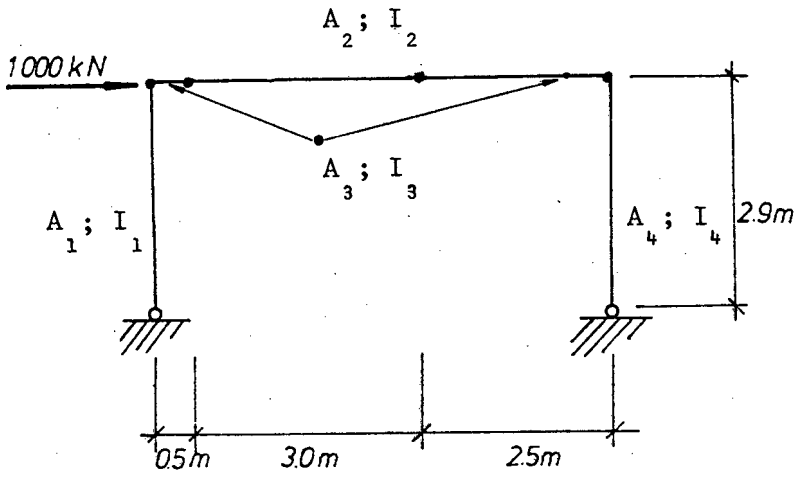

Data

E	=	28 GPa
A_1	=	0.2 m^2
I_1	=	0.0167 m^4
A_2	=	0.12 m^2
I_2	=	0.0036 m^4
A_3	=	12 m^2
I_3	=	3.6 m^4
A_4	=	1.0 m^2
I_4	=	2.083 m^4

Figure 5.5.2b MODEL 2 (rigid arm model)

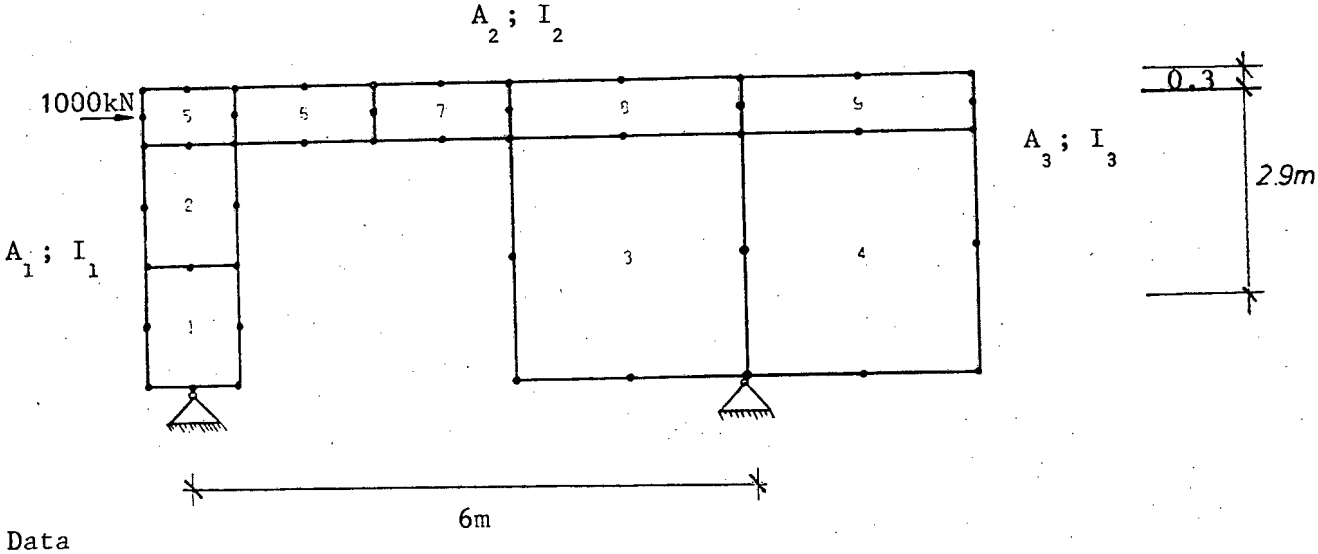

Data

E = 28 GPa

v = 0.2 m

thickness = 0.2 m

Figure 5.5.2c MODEL 3 (plane stress model)

Figure 5.5.3 illustrates where deflections and bending moments are sampled.

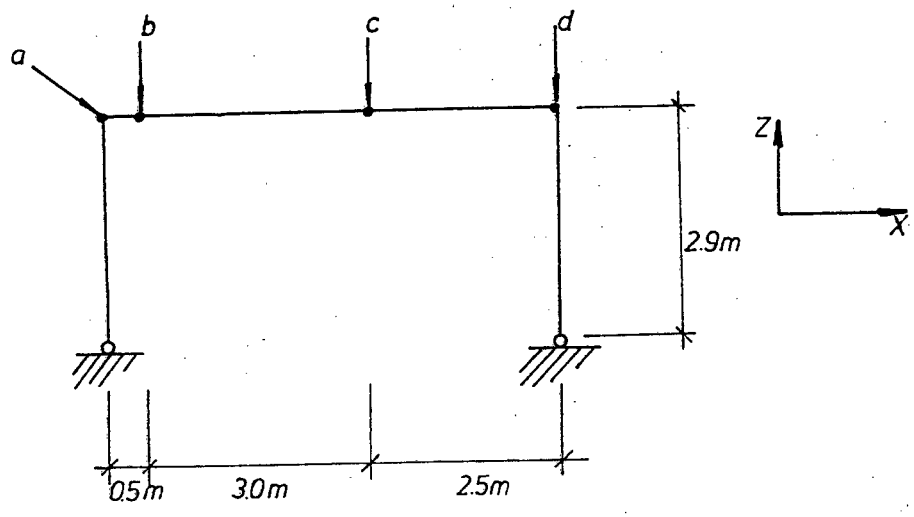

Figure 5.5.3 Sampling Points, Locations on Model Centre-Line

The various models considered in this study are listed below:-

MODEL 1a : Stick model using 3 SER CLC beam elements

MODEL 1b : Stick model using 3 Hermitian beam elements

MODEL 2a : Rigid arm model with 5 SER CLC beam elements

MODEL 2b : Rigid arm model with 5 Hermitian beam elements

MODEL 2c : Rigid arm model with 5 Hermitian beam elements including shear deformation

MODEL 3 : Plane stress model with nine 8-noded rectangular elements (3 integration points).

In the stick model (Model 1) the centre line of the frame is idealised to be the structure. This is a crude representation of a frame and does not take into account the finite dimensions.

The Rigid arm model (Model 2) aims to take into account the finite dimensions. The centre line of the structure is still modelled. However, the beam-column connections at sampling points a, b and c, d are given "rigid" material properties as they are essentially still part of the columns. In Figure 5.5.2 b, A_3 and I_3 are the rigid material properties. Hence rigid arm modelling [33] .

The plane stress model (Model 3) is expected to yield the most realistic results. The geometry of the plane stress elements take into account the finite dimensions of the structure. See Figures 5.5.1 and 5.5.2 c.

Model	Sampling Point See Figure 5.5.3	Deflections (mm)		Bending Moment (kNm)
		x	z	
1a	a	46.7	0.25	1400
	d	45.6	-0.05	1486
1b	a	46.7	0.25	1407
	d	45.7	-0.05	1493
2a	a	7.71	0.25	911
	b	7.71	-0.13	672
	c	7.1	5.93	780
	d	7.1	-0.05	1987
2b	a	7.71	0.25	912
	b	7.71	-0.13	671
	c	7.1	5.93	779
	d	7.1	-0.05	1987
2c	a	8.5	0.25	910
	b	8.5	-0.20	669
	c	7.8	6.40	781
	d	7.8	-0.05	1990
3	a	10.4	0.01	920
	b	9.56	-0.04	679
	c	9.35	0.07	771
	d	9.96	-0.08	1979

Table 5.5.1 Frame Analysis Results

All the models except Model 2c exclude shear deformation.

MODEL 1a
MODEL 2a
} Solved using MICRODEST

MODEL 1b
MODEL 2b
MODEL 2c
MODEL 3
} Solved using ADINA [32]

The results are tabulated in Table 5.5.1.

Models 1a and 1b yield practically the same results except for a slight discrepancy in the bending moments. Models 2a and 2b yield identical results, which compare well with 2c which includes shear deformation. Shear deformation slightly affects the sidesway deflection but does not significantly change the bending moments. Although the members modelled are deep, the inclusion of shear deformation in this problem appears to be academic and offers no real practical advantage. When modelling a multi-storey frame, however, the shear contribution might well be substantial and ought to be considered.

Assuming that the plane stress model (Model 3) provides the most accurate approximation of the structural response, Model 2c offers the best deflection comparison.

Comparing bending moments, however, the bending moments of Models 2a and 2b tally well with those of Model 3. Models 2a and 2b provide a superior bending moment diagram than Model 2c which includes shear deformation.

It appears that the rigid arm models (Models 2a and 2b) yield reliable bending moment results. However, their current mesh configurations yield deflections that are too small. This suggests that a finer mesh be utilized in these models; say two elements in the "columns" instead of one to model the bending response of the pinned "columns" more accurately.

MICRODEST performs excellently when results of similar models are compared. The rigid arm model (Model 2a) run on MICRODEST compares favourably with the plane stress model as discussed earlier. This demonstrates that MICRODEST and, in general, beam elements, can be used effectively to gauge the response of coupled shear-walls [34].

5.6 Multi-Storey Frame Analysis

A 10-storey frame with the same geometry and material properties as the single storey frame described in Section 5.5 is modelled. Various models are considered.

MODEL 1 - 3 SER beam elements per floor. Analysis on MICRODEST

MODEL 2 - 5 Hermitian beam elements per floor with constraint equations. Analysis on ADINA

MODEL 3 - 5 SER beam elements per floor with rigid arms. Analysis on MICRODEST

MODEL 4 - 5 Hermitian beam elements per floor with rigid arms. Transverse shear deformation included. Analysis on ADINA

MODEL 5 - 6 Plane Stress elements per floor. Analysis on ADINA.

The beam element models are illustrated in Figure 5.6.1 and the plane stress model in Figure 5.6.2.

Forces of 100kN per floor are applied horizontally at mid-beam depth. See Figures 5.6.1 and 5.6.2. The extreme horizontal deflections at locations A and D as shown in Figure 5.5.3, are virtually identical. The bending moments in the beams at the centres of the verticals at floor levels 1, 4 and 10 are tabulated in Table 5.6.1. The maximum bending moments and their respective locations in the shear-wall and column are also provided.

The analysis with 3 CLC elements per floor is quite unacceptable as the deflections are too severe and the distribution of the bending moments in the structure is inaccurate.

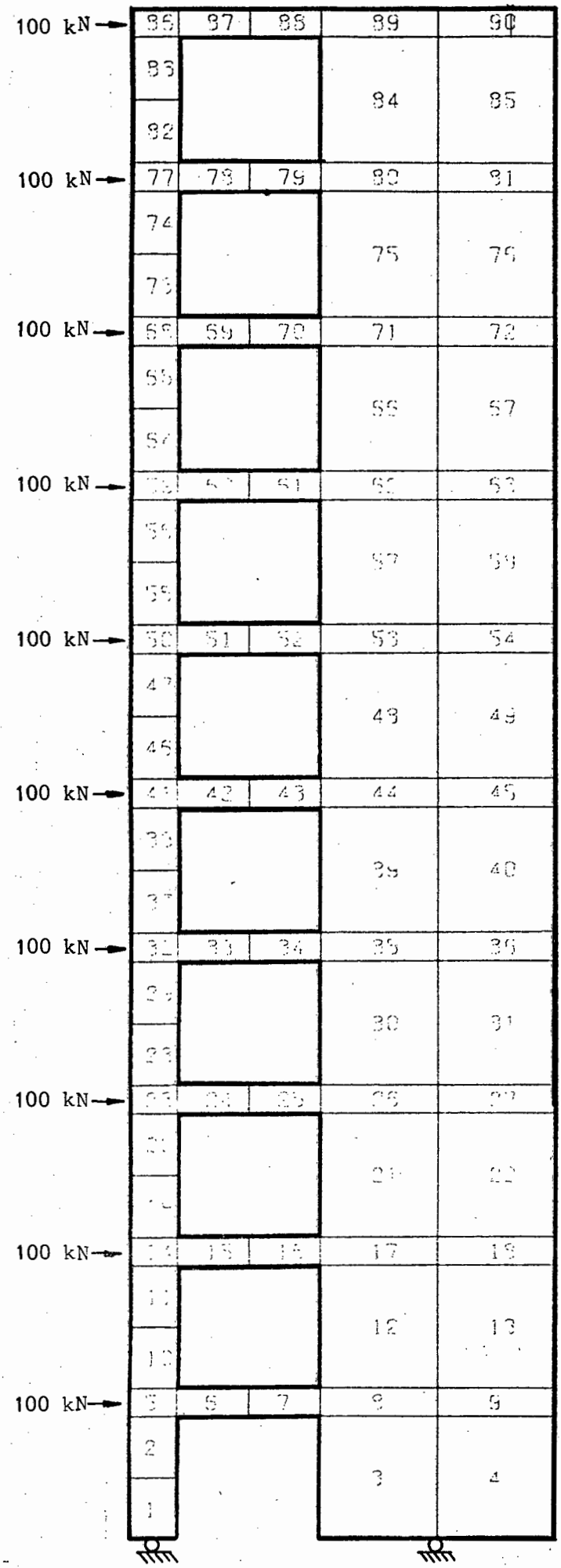

Figure 5.6.2 Ten Storey Plane Stress Model (Model 5)

Models 2 and 3 yield practically identical results. This verifies MICRODEST's ability to analyse multi-storey frames. Models 2 and 3 are comparable with Model 4 which includes transverse shear deformation. The sidesway deflections in Model 4 are slightly larger. However, the bending moments do not differ significantly when compared to Models 2 and 3.

Model 5 (Plane Stress model) yields the most reliable results. Models 2, 3 and 4 compare very favourably with the Plane Stress results. This demonstrates that a multi-storey shear-wall type frame can be adequately analysed using beam elements. Therefore MICRODEST can be used to model multi-storey shear-wall type frames provided the finite dimensions of the frame are accounted for. The Rigid-Arm modelling technique is used in this case [34].

5.7 Execution Time History

The solution time of various sized problems was monitored on MICRODEST. Certain factors have to be kept in mind when critically scrutinizing the execution time history.

- MICRODEST uses an Interpretive and not a Compiled language (HP9816 Micro-computer).

- The number of degrees of freedom (Ndof) quoted does not imply that all the degrees of freedom are coupled. Ndof refers to the ultimate size of the solution used to calculate forces and moments.

Table 5.7.1 lists a breakdown of the execution time history.

Due to automatic node renumbering [14] (Section 4.5) all the matrices solved are well banded and will represent the optimum semi-bandwidth. Hence the solution time on MICRODEST will represent the minimum.

Ndof	Assembly and Static Conden. (Seconds)	Crout Reduction (Seconds)	Recover Condensed dof (Seconds)	Total Time (Seconds)	Total Time (Minutes)
21	2.94	1.39	2.60	6.93	0.115
30	3.68	1.41	3.23	8.23	0.137
48	6.13	2.73	5.37	14.23	0.237
147	23.46	25.05	21.05	69.56	1.16
219	35.14	31.83	31.69	98.66	1.64
327	52.71	65.46	47.90	166.07	2.77
363	58.72	79.21	58.21	191.44	3.19
543	88.03	168.75	81.22	338.03	5.63
726	110.37	173.42	96.93	380.72	6.35
1266	187.66	645.04	164.56	996.66	16.61

Table 5.7.1 Breakdown of Execution Time History

As the problem size gets larger the time taken to recover the condensed degrees of freedom become consistently less than the time taken to perform the Crout reduction. This reinforces the policy of reforming K* (see Section 4.10).

The time taken to solve these problems are considered to be reasonable. See Figure 5.7.1. These results will probably improve over the next year as new software and hardware developments become available.

CHAPTER 6

STRUCTURAL DESIGN

6.1 Direct Iteration Method of Design

6.1.1 Basis of the Procedure

The linear elastic analysis described in Chapters 2 and 4 is used in conjunction with elastic structural design procedure to proportion the member sizes for plane frame structures in MICRODEST.

An initial set of section properties is chosen. The set of section material properties is then cyclically revised in accordance with a design procedure. The design variables in each cycle relate to the member properties, viz

cross-sectional area,
radius of gyration and
second moment of area.

The technique involves a series of structural (material section) modifications, each of which undergoes a linear-elastic displacement analysis. Subsequent modifications are then based on the stress levels associated with the displacement analysis.

The cyclical re-proportioning of section sizes ultimately leads to the optimum set of design variables being obtained.

A lower limit can be set for the section sizes by selecting initial sections. If the chosen sections are close to the optimum, the computational effort is substantially reduced since the number of iterations required for convergence is reduced.

The structural design is carried out in accordance with the recommendations set out in South African Bureau of Standards (SABS) 0162-1984.

The structural response analysis is performed for specific values of the design variables (cross-sectional area and second moment of area). A set of bending moments and axial forces is then computed for the design procedure. These design forces and moments are then temporarily stored, for each cycle, in the stiffness vector (Appendix C).

The ratio of member stress to permissible stress limits gives an indication of the efficiency of a particular member. Let the ratio of actual to permissible stress be C_s .

$$C_s = \frac{\sigma_a}{P} \tag{6.1}$$

where σ_a = total actual stress in a member
P = permissible stress.

For an ideal design $C_s = 1.0$ for all members in the structure.

The effect on the forces/moments in each member is assumed to remain constant for small changes in the cross-sectional dimensions of the member.

Equation 6.1 represents a simplification for calculating C_s . In a structure that is idealized to be pin jointed Equation 6.1 would be perfectly feasible [37]. In frame structures, however, there is a stress interaction between axial and flexural forces. If Equation 6.1 is used in predicting cross-sectional areas in the following design cycle, the areas will always be underestimated as flexure is not accounted for. The required area, A_i , to produce a unit value of C_s is

$$A_i = \frac{f_i}{P} \tag{6.2}$$

where f_i = axial force.

Let the force obtained from iteration n be $f_i^{(n)}$ and the design variable to calculate the force, $A_i^{(n)}$. Consequently, an improved prediction of the required area for iteration n+1 is

$$A_i^{(n+1)} = \frac{f_i^{(n)}}{P} \qquad (6.3)$$

which is used in the analysis. The improved area prediction also yields an improved second moment of area, Ixx and radius of gyration, r . Using the area as a predictor leads to a stable convergence for the optimum set of design variables.

For compression, the permissible stress value P depends upon the slenderness ratio (ℓ_e/r) and the permissible stress of the material used. This is covered in detail in Section 6.5.

A cyclical re-analysis and design calculation is carried out until no further improvements in the value of C_s , and hence design variables, can be found for any member. In this way an optimum stressed design is attained.

6.1.2 Overview and Design Routines

Data preparation and analysis is covered in Chapters 3 and 4 respectively. In Section 4.12 the design procedure is given the black box treatment. This section aims to demonstrate how the design associated routines assemble into the overall flowchart in Figure 4.12.1.

Figure 6.1.2.1 provides a macro flowchart of the overall procedure.

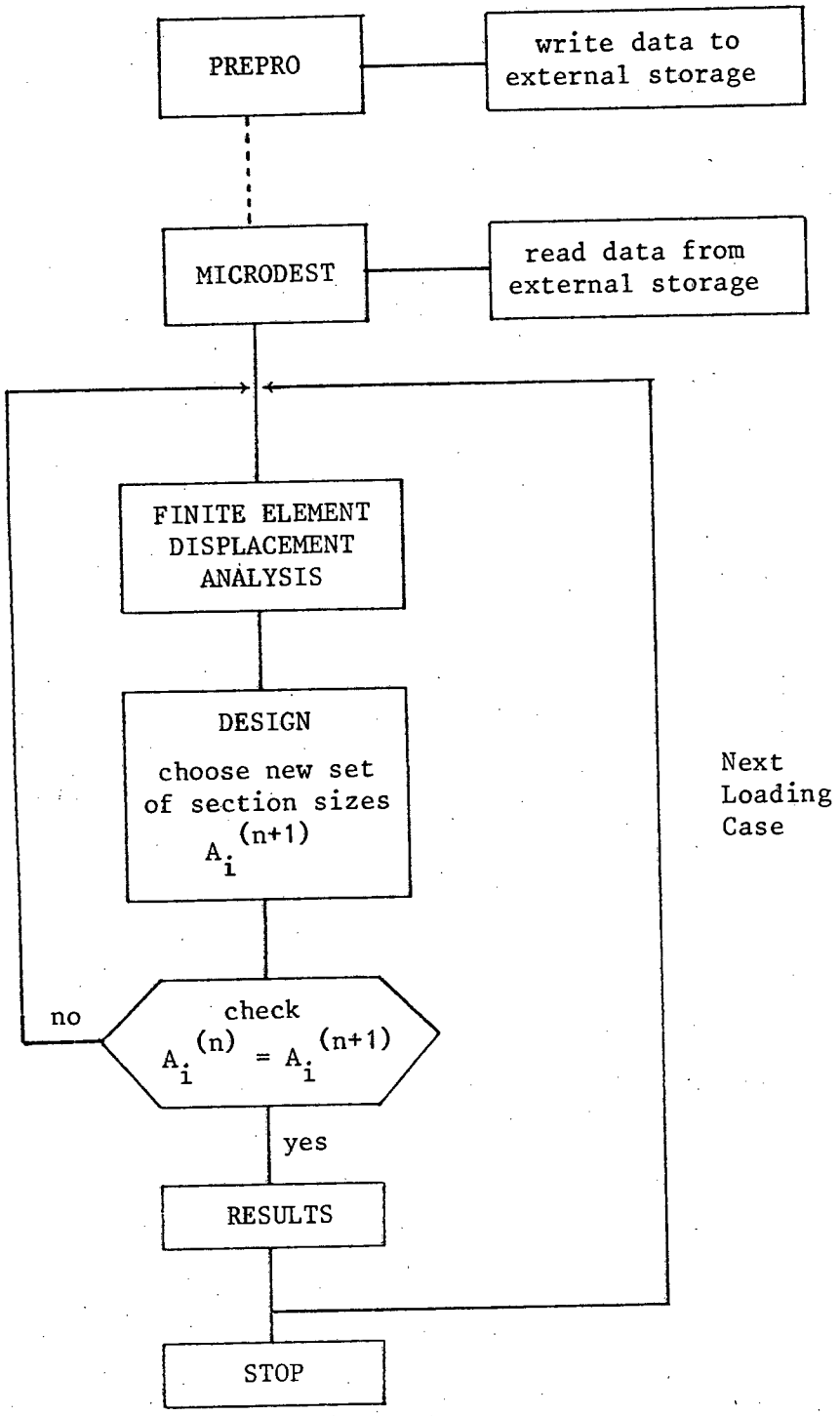

Figure 6.1.2.1 Macro Flowchart of Major Events in the Overall Procedure

The sub-programs involved in design are introduced and described below.

DESIGN : checks and adapts the structural design for each member in accordance with SABS 0162-1984 [35].

SEARCH : chooses an acceptable section from a list of sections provided (Section 6.6)

PERMST : calculates the permissable compressive stress and slenderness ratios for compression members (Section 6.5)

PROP_ZE : chooses the elastic section modulus for a section.

Figure 6.1.2.2 illustrates how the above sub-programs fit in with the overall flowchart of MICRODEST presented in Figure 4.12.1.

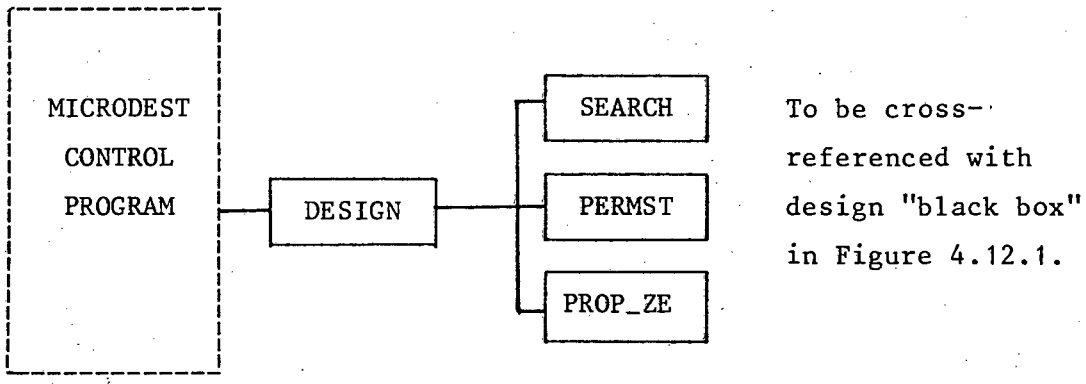

Figure 6.1.2.2 Design Routines in Overall Context

6.2 Lists of Sections

In order to produce a practical, usable computer-aided design a comprehensive list of sections is provided. The most suitable members are chosen by the program from this list. The analysis and design is performed with those actual listed sections.

Initial sections can be prescribed using the interactive mode on MICRODEST. The complete section lists appear in Appendix H.

6.2.1 Types of Sections

Seven different section classes have been specified representing a total of 206 different sections. The following sub-programs store and furnish the material properties.

MATPROP : area and radius of gyration
PROP-ZE : elastic section modulus
SECOND-MOM-AREA : second moment of area, Ixx .

Members are arranged in ascending numerical order with respect to their cross-sectional areas. The lists of sections contain 7 classes which are identified by "Nsid". Table 6.2.1 lists these classes.

Nsid	Section Class
1	pipe section
2	single equal angle
3	single unequal angle
4	double equal angle back to back
5	double unequal angle back to back (long leg attached)
6	channel section
7	tee section

Table 6.2.1 Section Classes and Identifiers

6.3 Member Design

The DESIGN sub-program is used to check the design of the structural members and to re-proportion member sizes if required. The design is consistent with the recommendations of SABS 0162-1984 [35] and follows the steps discussed in Equations (5.1, 5.2 and 5.3) in the above reference. A macro flowchart illustrates the design procedure in Figure 6.3.1.

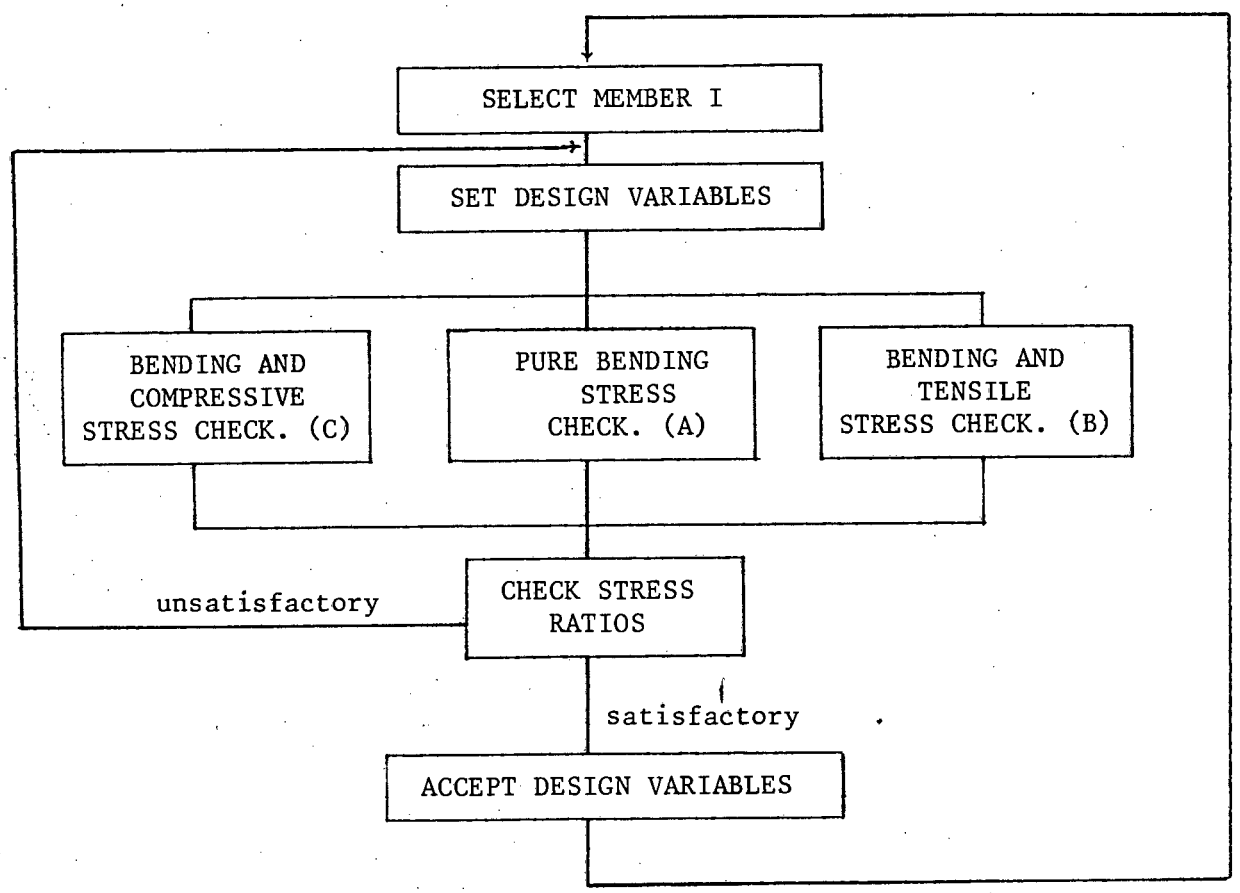

Figure 6.3.1 Macro Flowchart of Sub-Program DESIGN

If a member is not subjected to any axial force or bending moment then the design variables assume nominal values in this case.

6.3.1 Pure Bending Stress Check

A detailed description of pure bending design procedure mentioned in Figure 6.3.1 (A) is provided in this section. Pure bending implies that no axial forces are present.

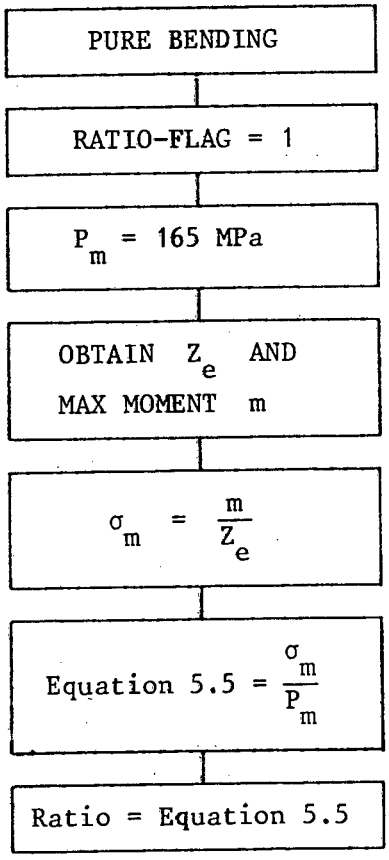

where P_m = allowable bending stress

Z_e = elastic section modulus

m = bending moment

σ_m = actual bending stress

Ratio = ratio to assess the structural efficiency of a member.

Figure 6.3.1 Design Procedure for Pure Bending

The equation to be satisfied for pure bending is

$$\frac{\sigma_m}{P_m} \leqq 1.0 \qquad (6.4)$$

6.3.2 Combined Bending and Tensile Stress Check

The equation to be satisfied for axial tension and bending is Equation 5.4 in SABS 0162-1984. Procedure (B) mentioned in Figure 6.3.1 is elaborated on in this section.

$$\frac{\sigma_t}{P_t} + \frac{\sigma_{mt}}{P_{mt}} \leqq 1.0 \qquad (6.5)$$

where σ_t = average axial tensile stress

P_t = allowable axial tensile stress

= 155 MPa (Grade 43 Steel) [35]

σ_{mt} = tensile stress for bending

P_{mt} = allowable tensile bending stress

= 165 MPa (Grade 43 Steel) [35]

Figure 6.3.2 lists the calculation steps involved.

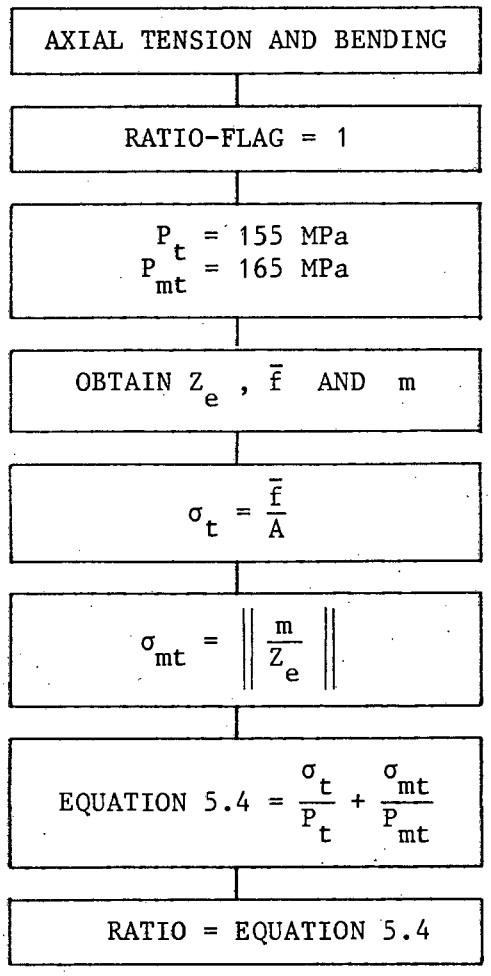

Figure 6.3.2 Axial Tension and Bending Calculation Steps

where f = average axial tensile force

m = maximum bending moment

A = associated cross-sectional area.

Nomenclature for Figure 6.3.2.

6.3.3 Combined Bending and Compressive Stress Check

A member subjected to axial compression and bending must be proportioned to satisfy the following requirements in MICRODEST at any point along the length of the member.

$$\frac{\sigma_c}{P_c} + \frac{\omega\ \sigma_{mc}}{(1 - \sigma_c/f'_{cr})P_{mc}} \leqq 1.0 \qquad (6.6)$$

and

$$\frac{\sigma_c}{P_{co}} + \frac{\sigma_{mc}}{P_{mco}} \leqq 1.0 \qquad (6.7)$$

When $\sigma_c/P_c \leqq 0.15$ then the following expression is used instead of Equation (6.6) and (6.7)

$$\frac{\sigma_c}{P_c} + \frac{\sigma_{mc}}{P_{mc}} \qquad (6.8)$$

Equations (6.6), (6.7) and (6.8) are Equations (5.1), (5.2) and (5.3) in SABS 0162-1984 [35] respectively.

Where f'_{cr} = 0.6 times the Euler buckling stress for the member

= $1.22 \times 10^6/(\ell_e/r)^2$ MPa

ℓ_e = effective length of member for buckling

P_c = allowable axial compressive stress (7.1 in SABS 0162 [35])

P_{co} = allowable axial compressive stress (7.1 in SABS 0162 [35])

P_{mc} = allowable compressive bending stress (Section 6.5)

P_{mco} = allowable bending stress from Table 6.1 in SABS 0162-1984 [35].

r = radius of gyration

σ_c = average axial compressive stress

σ_{mc} = calculated minimum compressive bending stress relating to bending

ω = coefficient relating to bending.

Figure 6.3.3 illustrates the calculation steps.

When a member is bent in single curvature (i.e. subjected to a uniform bending moment) it is most unstable, i.e. the worst case (Figure 6.3.4).

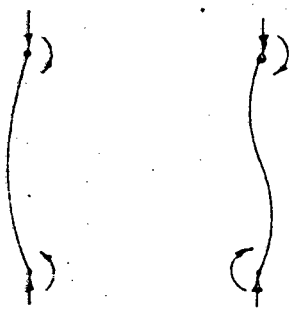

Figure 6.3.4 Single and Double Curvature

Members bent in double curvature as shown in Figure 6.3.4 (b) will be much more stable.

In the case of the double curvature member, the maximum moments occur near the ends, where the member is restrained against lateral movement. Furthermore, a member bent in double curvature is considerably stiffer than one bent in single curvature and hence the coefficient ω in Equation (6.6)

$$\omega = 0.6 + 0.4\beta \qquad (6.9)$$

where $$\beta = \frac{\text{Smaller end moment}}{\text{Larger end moment}} \qquad (6.10)$$

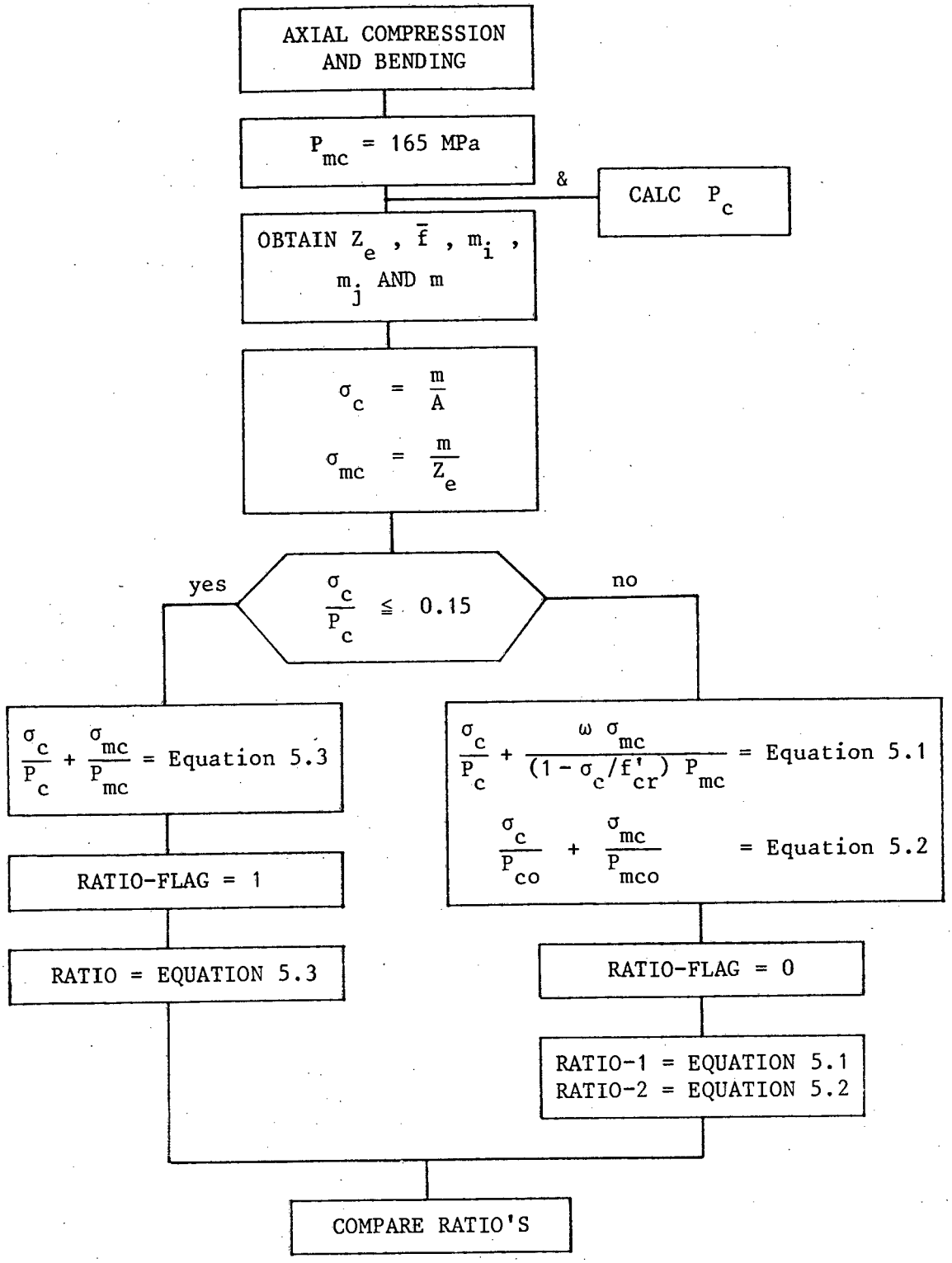

where m_i and m_j = end moments

The other variables are previously defined in this section.

Figure 6.3.3 Axial Compression and Bending Calculation Steps

β is positive when the member is bent in single curvature and negative when bent in double curvature. The signs of the moments in Equation (6.10) must be taken into account.

6.4 Permissible Slenderness Ratio (ℓ_e/r)

The maximum permissible slenderness ratio (ℓ_e/r) allowed for compressive members and tensile members undergoing stress reversal is 300.

6.5 Permissible Compressive Stresses

Permissible axial compressive stress, P_c, is dependant on the slenderness ratio of a member and the permissible elastic stress.

$$P_c = \frac{1}{1.7}\left[\frac{f_y + (\eta+1)f_{cr}}{2} - \sqrt{\left(\frac{f_y + (\eta+1)f_{cr}}{2}\right)^2 - f_y f_{cr}}\right] \qquad (6.11)$$

where f_{cr} = 0.6 times the Euler buckling stress

$$= \frac{1.22 \times 10^6}{(l_e/r)^2}$$

$$\eta = 0.3\left[\frac{\ell_e}{100r}\right]^2$$

f_y = minimum yield stress

ℓ_e/r = slenderness ratio

6.6 Choice of an Acceptable Section

Calculating the value C_s determines the efficiency of a member. The variables ratio, RATIO-1 and RATIO-2, keep track of these efficiencies. Acceptable limits of 1.05 and 0.92 are specified. Suitable member areas are checked against the size required by members of the same group and adjustments are made until the best value is selected.

Ratio values above 1.05 represent unacceptably large stresses and hence a larger section must be found. This is done by the sub-program SEARCH.

Over-design is indicated by a smaller ratio value than 0.92. A smaller target area is calculated by

$$\text{target area} = 0.75 \times \text{RATIO}^{-2} \times \text{Current area} \qquad (6.12)$$

The section size corresponding closest to the "target area" is then adopted by the sub-program SEARCH. This will probably yield an inadequate design (over-design), but this is dealt with as a matter of course.

This Direct Iteration Design procedure yields a lower bound convergence and appears to be stable.

6.6.1 Searching for a Section

The comprehensive list of sections provided by MICRODEST (Appendix H) serves as a reservoir of possible designs. The design routine predicts a cross-sectional area, i.e. a target area in numerical terms. A systematic search is then performed through the list to choose an actual section which is most suitable. Care is taken to ensure that both the area and the radius of gyration of the section chosen are acceptable. The corresponding elastic section modulus, Z_e is then simply located by index. Figure 6.6.1 shows the details of the sub-program SEARCH.

6.7 Design Acceptability

A final design is considered to be acceptable when the section sizes chosen from consecutive iterations are identical.

For an acceptable design, program control is transferred to a sub-program which then prints out the relevant results. Further load cases can then be analysed and designed.

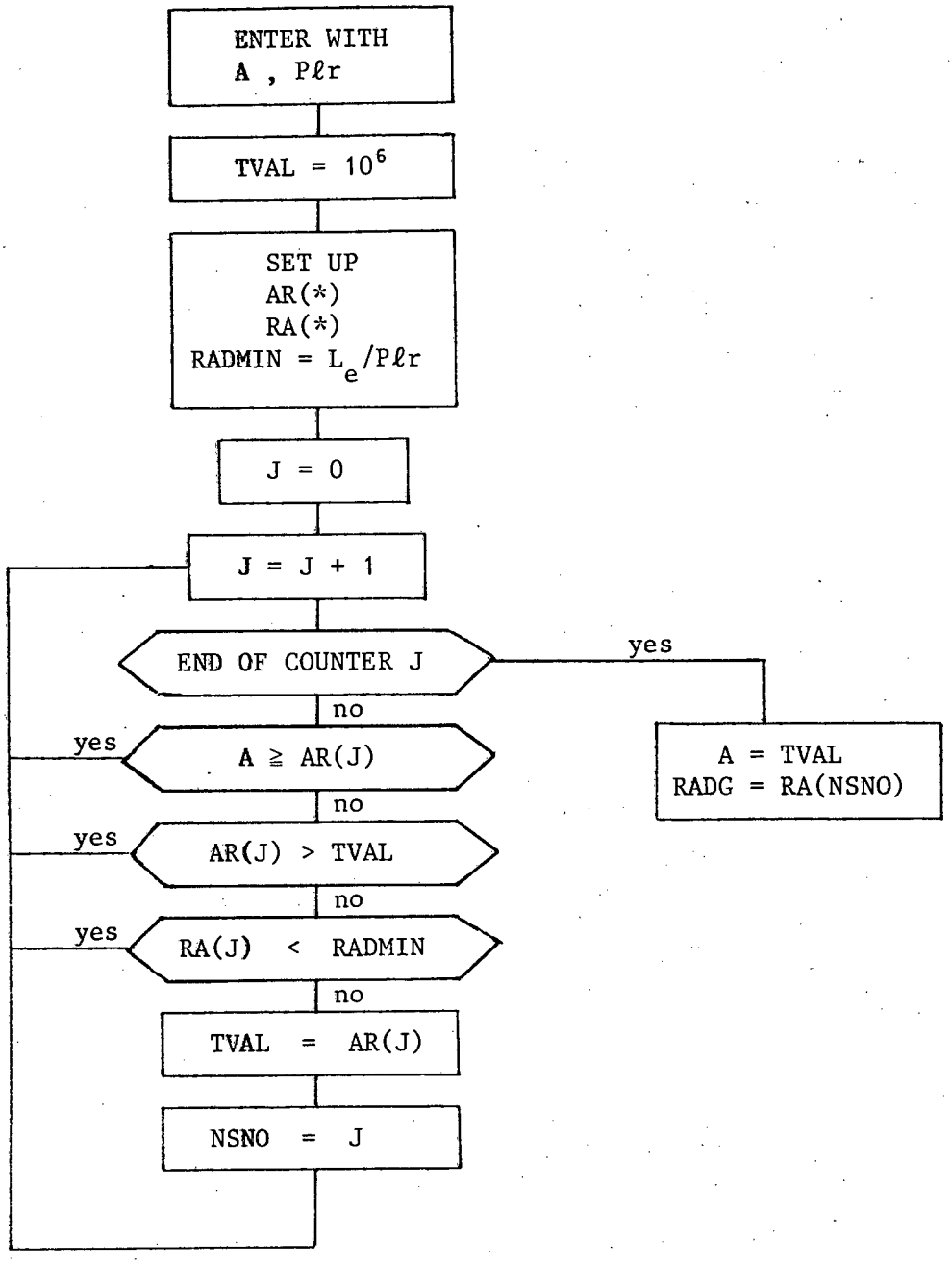

Nomenclature

A	=	area required to produce a value of $C_s = 1$
Pℓr	=	permissible ℓ_e/r ratio
TVAL	=	temporary value of area
I,J	=	counter within section list
AR(*)	=	required section areas
RA(*)	=	required section radii of gyration
RADMIN	=	minimum allowable radius of gyration
NSNO	=	new section size number.

Figure 6.6.1 Sub-Program SEARCH

6.8 Design Examples

Two design examples are presented to test the Direct Iteration design procedure. A truss and a Vierendeel girder are designed.

6.8.1 Truss

Figure 6.8.1 shows the geometry of the truss which is symmetrical. The purlin points are also shown.

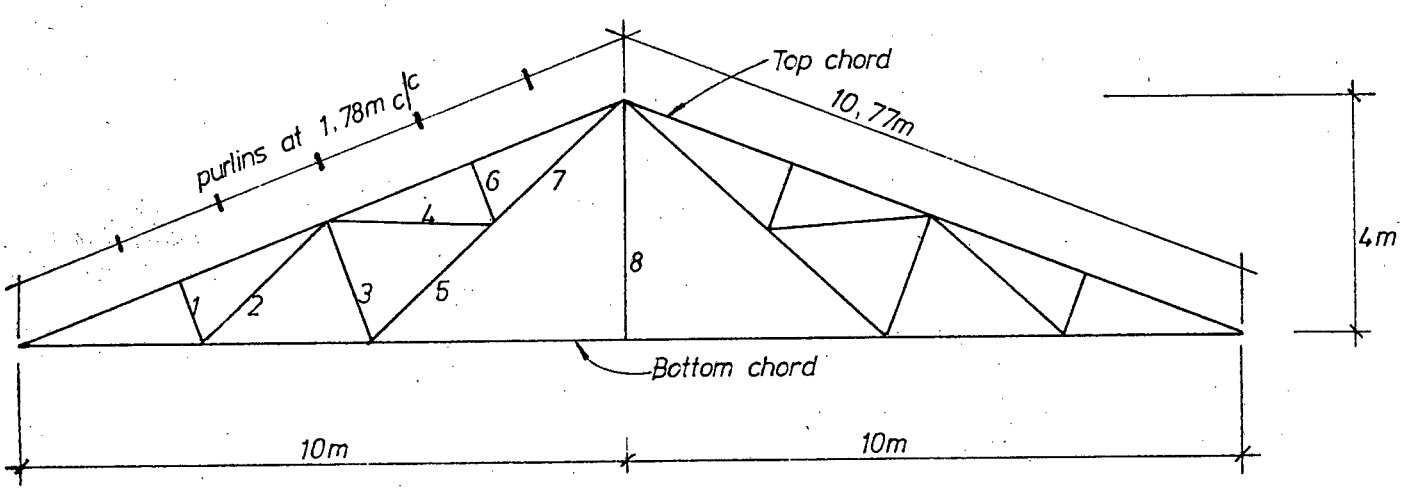

Figure 6.8.1 20m Truss

Top and bottom chords - T-sections
All internal sections - Equal angles.

Note that the purlin points are mostly off panel points thus inducing bending in the top chord. The design and comparison is presented in Table 6.8.1.

Member	Manual Design	MICRODEST
Top chord	165x152x23 kg/m Tee	165x152x23 kg/m Tee
Bottom chord	102x127x11 kg/m Tee	102x127x11 kg/m Tee
1	51x 51x6.3kg/m L	45x 45x 6 kg/m L
2	51x 51x6.3kg/m L	51x 51x6.3kg/m L
3	64x 64x6.2kg/m L	60x 60x 6 kg/m L
4	51x 51x6.3kg/m L	51x 51x6.3kg/m L
5	76x 76x6.2kg/m L	76x 76x6.2kg/m L
6	51x 51x6.3kg/m L	51x 51x6.3kg/m L
7	76x 76x6.2kg/m L	76x 76x6.2kg/m L
8	51x 51x6.3kg/m L	35x 35x 3 kg0m L

Table 6.8.1 Design Comparison

The designs are practically the same except that MICRODEST selected a smaller section for some internal members which might be regarded as impractical. If MICRODEST design is rationalised in terms of practicality the designs would be identical.

6.8.2 Vierendeel Girder

The girder is designed with channel sections. The same section size is used for the whole structure. The geometry and loading is shown in Figure 6.8.2.

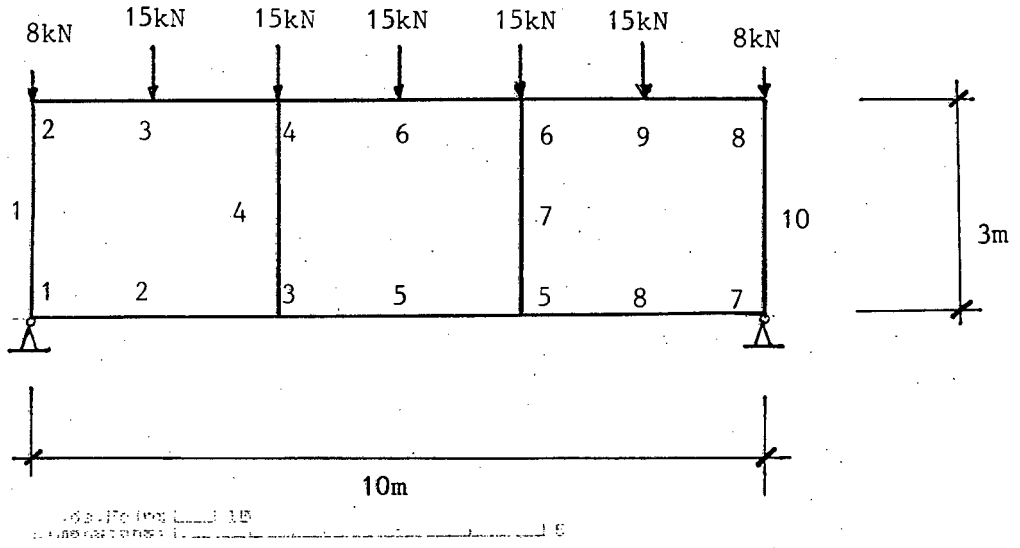

Figure 6.8.2 Vierendeel Girder and Loads

MICRODEST selected the 200x75x25 kg/m channel section. A manual check satisfied the design solution to be acceptable. Table 6.8.2 lists the design stresses.

Member	Axial Stress MPa	Bending Stress MPa at Nodal Points			
		Node		Node	
1	-9.242	1	135.274	2	-147.733
2	-1.381	1	-135.274	3	139.548
3	-5.602	2	-147.733	9	100.716
4	-4.896	3	106.286	4	-103.064
5	2.762	3	33.262	5	33.262
6	-9.746	4	-2.347	10	63.075
7	-4.896	5	-106.286	6	103.064
8	-1.381	5	139.548	7	-135.274
9	-5.602	6	100.716	11	-147.733
10	-9.242	7	-135.274	8	147.733

Table 6.8.2 Vierendeel Design Stresses

CHAPTER 7

CONCLUSIONS

7.1 Concluding Remarks

The preprocessor, PREPRO, performs a vital task in rapid data preparation. Data errors are usually made when this task is performed manually. Using a preprocessor minimizes the risk of making an obvious data error. The current version of PREPRO provides the basic preprocessing tools. Subsequent versions of PREPRO will present more refined preprocessing capabilities.

The CLC beam element displays remarkable versatility and accuracy in the examples listed in Chapter 5. The problem of "membrane locking" is cured by applying the stress projection method to the element. No spurious results were obtained except when an unreasonable mesh was analysed. Together with the correct modelling techniques, a large variety of problems can be reliably modelled using the CLC beam element in MICRODEST.

Satellite Element Refinement (SER) provides an excellent vehicle for investigating the variation of bending moments in a member, especially in the vicinity of the element nodes. Although SER and the accompanying process of static condensation is a complex method to predict bending moments at element nodes, it is totally transparent to the user of MICRODEST. Care should be taken to keep the initial rotations of curved members within certain limits. See Section 5.2. By fitting a quadratic curve to the bending moment results of a SER element, the nodal moments can easily be extrapolated. The magnitude and location of the maximum moment on a member is easily calculated for the structural design process.

Static condensation performs well with negligible disturbance from round-off error. The 16 bit word length of the HP9816 micro-computer is responsible for maintaining the numerical integrity of the process.

Care must be taken when installing MICRODEST on smaller 8 bit word length machines. Double precision should be used as a matter of course when using 8 bit machines. Static condensation also provides a great saving on computational effort. Together with the Collins bandwidth reduction technique, time and internal memory is saved. In considering FEM analysis on micro-computers the availability and utilization of internal memory is currently of primary concern. This consideration will soon become less important as micro-computers with 5 Megabyte of core are currently available.

The structural steel design procedure of MICRODEST can potentially require a great deal of computational effort to converge to the optimum solution. If, however, an initial design section were prescribed, the convergence time would decrease markedly. This provides an opportunity for the designer to interact with MICRODEST and to exercise his structural design experience by prescribing initial design sections. MICRODEST also facilitates the investigation of different section configurations of a structure. In this way a cost analysis can be performed.

7.2 Scope for Further Research and Development

Various developments can be considered to improve the performance of the preprocessor, PREPRO. These are listed below

- Three-dimensional and colour graphics will greatly enhance the graphics capabilities of PREPRO.

- A data editing facility that will take global and local data changes into account and adjust the data accordingly.

- A data file editing facility to edit completed data files and then to update them.

MICRODEST presents a great deal of scope for further research and development.

- Incorporate three-dimensional capabilities in the processor. This then implies that torsional effects should be taken into account. Torsional deformation has to be included in the Strain Energy. The CLC beam element has the ability to curve, therefore torsional effects in curved members have to be included.

- Include shear deformation in the Strain Energy. To avoid shear locking problems, apply the stress projection technique to the shear deformation energy in the same manner that membrane locking was remedied.

- To find the optimum geometric configuration within certain limits, Dynamic Programming can be used. To keep computational effort to a minimum, one geometric State Variable should be considered. By strategic positioning of the State Variable on successive analyses, an optimum geometric configuration can be obtained.

Virtually no postprocessing capability is currently available for MICRODEST. The basic postprocessing requirements of MICRODEST are

- Selective result output

- Obtain and present the extreme deflections, forces and moments

- Plot deflected shapes of models and selected bending moment diagrams.

The possibility of implementing the SER technique in two-dimensional C^0 elements in conjunction with static condensation should be investigated.

In order to model and analyse larger structures, the sub-structuring technique should be implemented. A direct solution technique should be utilized to ensure that the solution process is as rapid as possible. This should not represent a major increase in data preparation and the process should strive to be transparent to the potential user.

REFERENCES

1. RICHARDS, T.H., "Energy Methods in Stress Analysis", Ellis Horwood, Chichester, U.K., 1977.

2. COOK, R.D., "Concepts and Applications of Finite Element Analysis", John Wiley & Sons Inc., New York, 1974.

3. MARGUERRE, K., "Zur Theorie Der Gekrummten Platte Grosser Formanderung", Proc. 5th Int. Congress Appl. Mech., pp. 93-101, 1938.

4. AHMAD, S., IRONS, B.M., and ZIENKIEWICZ, O.C., "Analysis of Thick and Thin Shell Structures by Curved Finite Elements", Int. J. for Numerical Methods in Eng., Vol. 2, pp. 419-451, 1970.

5. ASHWELL, D.G., and GALLAGHER, R.H., eds., Finite Elements for Thin Shells and Curved Members, Wiley, London, 1976.

6. BELYTSCHKO, T., STOLARSKI, H., Membrane Locking and Reduced Integration for Curved Elements, Journal of Applied Mechanics, Vol. 49, March 1982.

7. BELYTSCHKO, T., STOLARSKI, H., LIU, W.K., CARPENTER, N., ONG, J. S-J., Stress Projection for Membrane and Shear Locking in Shell Finite Elements. Computer Methods in Applied Mechanics and Engineering. To appear.

8. ZIENKIEWICZ, O.C., "The Finite Element Method", Third Edition, McGraw Hill, 1983.

9. HINTON, E., and OWEN, D.R.J., "An Introduction to Finite Element Computations", Pineridge Press Limited, 1979.

10. HINTON, E., and OWEN, D.R.J., "Finite Element Programming", Academic Press, 1977.

11. OWEN, D.R.J., and HINTON, E., "A Simple Guide to Finite Elements", Pineridge Press Limited.

12. BECKER, E.B., CAREY, G.F., and ODEN, J.T., "Finite Elements - An Introduction", Volume 1, Prentice-Hall Inc.

13. ROBINSON, J., "New and Future Developments in Commercial Finite Element Methods", Third World Congress, J. Robinson, Ed., Robertson and Associates, 1981.

14. COLLINS, R.J., "Bandwidth Reduction by Automatic Renumbering", Int. J. for Numerical Methods in Engineering, Vol. 6, 345-356, 1973.

15. IRONS, B.M., "Structural Eigenvalue Problems: Elimination of Unwanted Variables", A.I.A.A. Journal, 3, 961-962, 1965.

16. GUYAN, R.J., "Reduction of Stiffness and Mass Matrices", A.I.A.A. Journal, 3, 380, 1965.

17. STOLARSKI, H., BELYTSCHKO, T., CARPENTER, N., and KENNEDY, J.M., "A Simple Triangular Curved Shell Element" - Engineering Computations, Vol. 1, September 1984.

18. BATHE, K.J., "Finite Element Procedures in Engineering Analysis", Prentice Hall, 1982.

19. HERRING, H.F., and DOYLE, W.S., "Micro Frame Analysis and Design", Proceedings of the FEMSA Symposium 1986, paper submitted.

20. FENVES, S.J., PERRONE, N., ROBINSON, A.R. and SCHNOBRICH, W.C., "Numerical and Computer Methods in Structural Mechanics", Academic Press, New York, 1973.

21. BETTES, J.A., "A Data Structure for Finite Element Analysis", Int. J. Num. Methods Eng., Vol. 11, 169-181, 1978.

22. LONINK, G., and BRINK, E., "A Universal Pre- and Post-processing System, Feasible or Fiction?", Nuclear Engineering and Design, 70, 117-123, 1982.

23. STELZER, J.F., "Consideration and Strategies in Developing Finite Element Software for Desktop Computers", Eng. Comput., Vol. 1, June 1984.

24. ADEY, R.A., "Engineering Software", Proceedings of the 1st International Conference held at Southampton University, September 1979, Pentech Press, London, 1979.

25. YOURDAN, E., "Techniques of Program Structure and Design", Prentice Hall, 1975.

26. DAHL, DIJKSTRA and HOARE, "Structured Programming", Academic Press, New York, 1972.

27. Basic Programming Techniques with extensions 2.0 - for the HP Series 200 Computers, Hewlett Packard, 1982.

28. DE VILLE, V., DE GOYET and FREY, F., "Use of Marguerre Theory in the Nonlinear Analysis of Beam and Plate Structures", Proc. 4th World Congress, Finite Element Methods, Interlaken, 1984.

29. STOLARSKI, H., BELYTSCHKO, T., Shear and Membrane Locking in C° elements. Comp. Meth. Appl. Mech. and Engineering, 41, 279-296, 1983.

30. SALMON, E.H., "Materials and Structures" - Vol. 1, Longmans, 1948.

31. IRONS, B., and AHMAD, S., Techniques of Finite Elements, Ellis Horwood, Chichester, 1980.

32. BATHE, K.-J., "ADINA - A Program for the Automatic, Dynamic, Integral, Nonlinear, Analysis", ADINA Eng. AB, Munkgaten 20D, S-72212, VÄSTERÅS, Sweden.

33. DOYLE, W.S., and RICHARDSON, B.W., "The Finite Element Analysis of a Reinforced Concrete Tower Block Structure". Proceedings of the International Conference on Computer Aided Analysis and Design of Concrete Structures, Part II, editors Damjanic F., Hinton E., Owen D.R.J., Bicanic N., Simovic V., Split-Yugoslavia, Pineridge Press, September 1984.

34. DOYLE, W.S.,"The Finite Element Modelling of Coupled Shear-Walls" Proceedings of FEMSA Symposium 1986, paper submitted.

35. SOUTH AFRICAN BUREAU OF STANDARDS, "The Code of Practice for the Design of Structural Steelwork - 0162", 1984.

36. SOUTH AFRICAN INSTITUTE OF STEEL CONSTRUCTION, "Commentary on the Code of Practice for the Design of Structural Steelwork - 0162", 1984.

37. HOWELL, G.C., "Dynamic Programming and Direct Iteration for the Optimum Design of Space Structures", M.Sc. Thesis, U.C.T. 1978.

38. MONDKAR, D.P., and POWELL, G.H., "Towards Optimal In-Core Equation Solving", Computers and Structures, Vol. 4, pp. 531-548, 1974.

APPENDIX A

DATA STORAGE

The preprocessor, PREPRO, collates the generated and specified data in a specific format to be written to external mass storage. In this case either flexible or hard disc. MICRODEST then reads the data from disc for processing. The bulk of the data is stored in a two-dimensional array called Base with dimensions

rows = Length
columns = 3 .

The variable Length and the Job-title for the specific data file are stored separately. This facilitates the identification of the stored data and also provides a method of determining the exact size of the variable Length and, therefore, of Base.

The construction of Base is illustrated in Figure A1.

The first row in Base(*) contains all control data.

Base

Col 1	Col 2	Col 3
No of Nodes	No of Elements & Curved Elements	No of Node Sets & Element Sets
X-coord ⋮	Y-coord ⋮	Z-coord ⋮
Element Number ⋮	Topology ⋮	Topology ⋮
Curved Element No ⋮	Initial Curvature ⋮	Initial Curvature ⋮
Node Set Number Nodes in Set	No of Nodes in Set Nodes in set →	..... etc
Element Set Number Elements in Set	No of Elements in Set Elements in Set →	..... etc
No of Restraints	Node and Restraint →	.....
Design, group data	.....	.....
Design Parameters	.....	.....
Element No	Effective Length	Cross-section Identifier
Number of load cases		
Load Case No	No of Element Loads	No of Node Loads
Loaded Element ⋮	Type of Load ⋮	Magnitude ⋮
Loaded Node ⋮	Type of Load ⋮	Magnitude ⋮

Figure A1 Construction of Base

APPENDIX B

GENERATING NODAL COORDINATES ON AN ARC

The method employed to generate nodal coordinates on an arc is set out here.

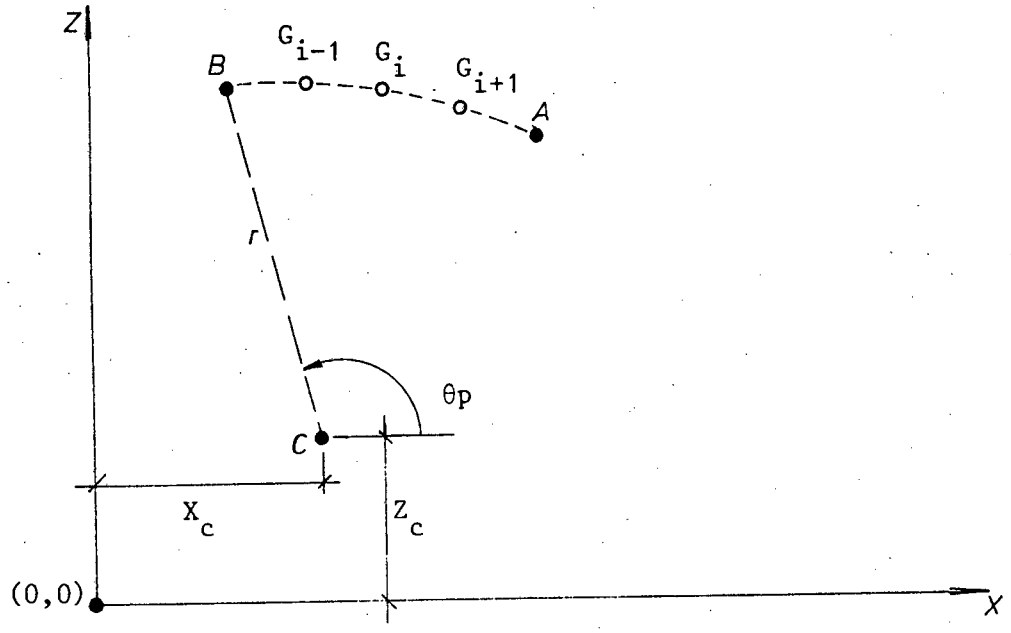

Figure B1 Graphical Representation

The following data needs to be furnished

- A (X_a , Z_a)
- B (X_b , Z_b)
- C (X_c , Z_c)
- and the number of equi-spaced nodes to be generated.

The radius, r , is easily calculated from the given data. Nodes G_i are generated in a clockwork sense, i.e. from B to A.

The new coordinates of G_i are calculated in polar coordinates in a local sense. All calculations are performed in radians. This is done by decrementing the angle θp by an appropriate amount. This depends solely on the amount of nodes to be generated.

Calculate $\theta' p$ from θp (decrement)

then $\Delta_x = r \cos \theta' p$ (local coords)

$\Delta_z = r \sin \theta' p$

Global coordinates.

$$G_i(X) = X_c + \Delta_x$$

$$G_i(Z) = Z_c + \Delta_z \ .$$

APPENDIX C

STORAGE TECHNIQUE OF THE GLOBAL STIFFNESS MATRIX AND AXIAL FORCES/BENDING MOMENTS

All stiffness matrices of the type required by the finite element displacement method are symmetric positive definite. If the node numbering of the mesh is considered so that the bandwidth of the matrix is a minimum, then the matrix will be well bonded (Figure C1). Well bonded implying that the terms in the matrix congregate around the leading diagonal and are not scattered to the extremes of the matrix. An automatic node renumbering scheme [14] ensures that the minimum bandwidth is obtained.

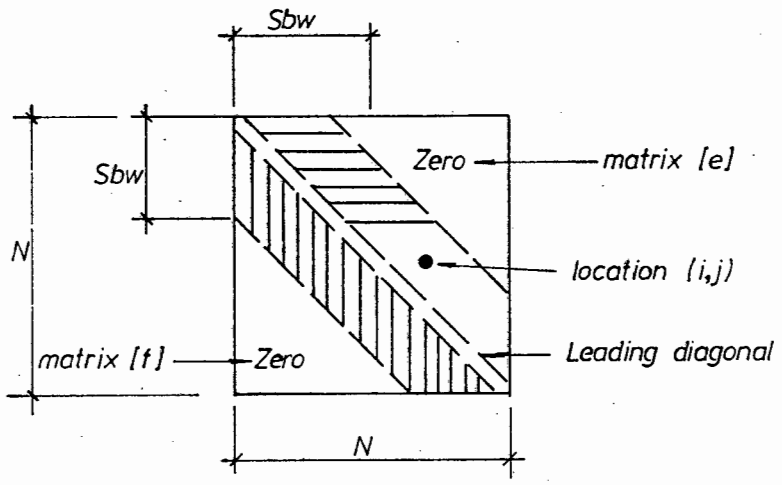

Figure C.1 Square Matrix A - Size NxN

where i = row number
j = column number
Sbw = semi-bandwidth
[e] = the upper triangular matrix
[f] = the lower triangular matrix.

For computer storage, especially on micro-computers, it is wasteful and often impossible to store the whole N x N matrix. Since matrix [e] is merely the mirror image of matrix [f] only one need be stored including the leading diagonal (Figure C2).

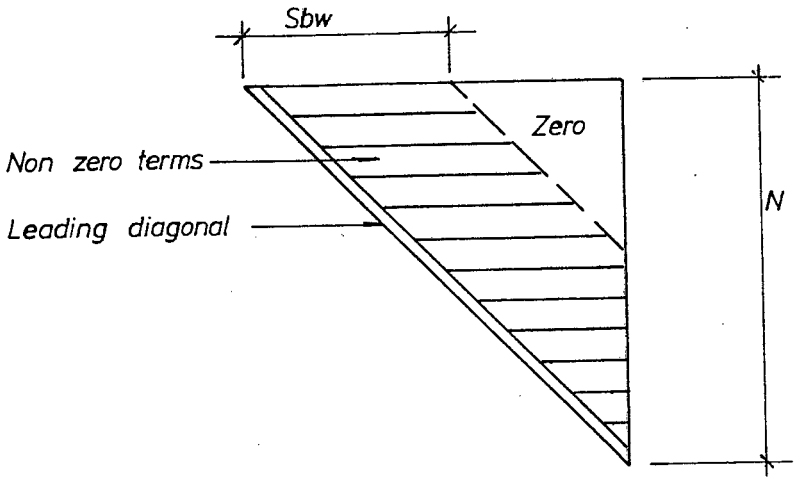

Figure C.2 Upper Triangular Matrix [e] of A

In considering the upper triangular matrix [e] only the portion that falls in the shadow of the Sbw need be stored. All the other terms in matrix [e] being zero. The portion that has to be stored has dimensions Sbw x N and this can be condensed into a rectangular matrix as shown in Figure C3.

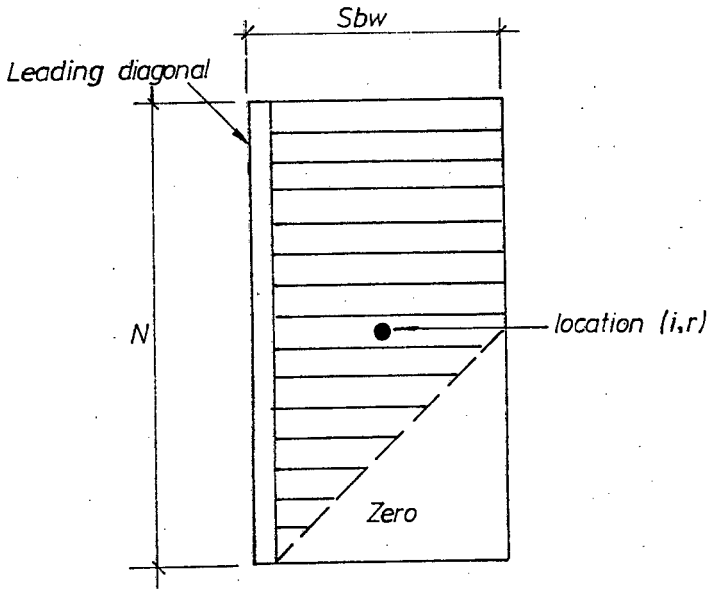

Figure C.3 Equivalent Rectangular Matrix Form of A

Let i and r be the row and column indices respectively in the rectangular matrix. The equivalent locations in the square matrix A and the rectangular matrix are given in Table C.1.

	Square Matrix	Rectangular Matrix
row number	i	i
column number	j	r = j - i + 1

Table C1 Equivalent Locations in Matrix A and a Rectangular Matrix Form of A.

An efficient method of storing the stiffness matrix A would be to assemble a one dimensional array to store the rectangular matrix form of A. See Figure C4.

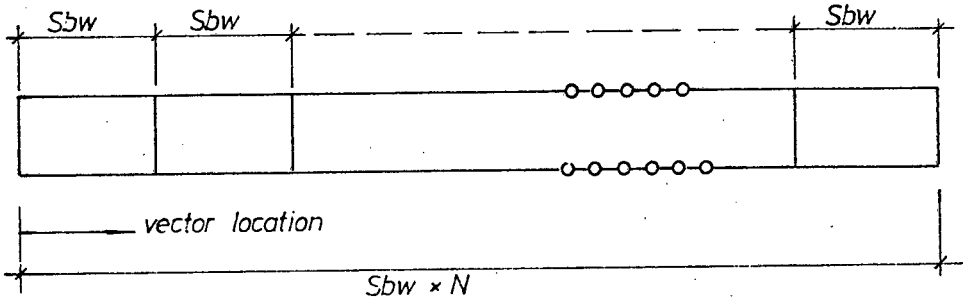

Figure C.4 Equivalent Single Dimension Array A

The equivalent location of A(i,j) in the single dimension array will be

$$\text{vector location} = j - i + 1 + (i-1)\ Sbw$$

where $1 \leq \text{vector location} \leq (Sbw \times N)$

After the system of equations represented by vector A have been solved it is then used to store axial forces and bending moments.

Consider SER member, I. There will be a total of 6 values to store per member. See Table C2 for the corresponding locations.

Forces and Moments in Member I	Index Location
Axial Force i	6 x I - 5
Axial Force	6 x I - 4
Axial Force j	6 x I - 3
Moment i	6 x I - 2
Moment	6 x I - 1
Moment j	6 x I

Table C2 Index Location for Forces/Moments in Member I

APPENDIX D

CROUT REDUCTION FOR THE SOLUTION OF LINEAR SIMULTANEOUS EQUATIONS

Crout reduction [38] is used in MICRODEST to solve a system of linear equations which is a consequence of the finite element displacement method of analysis.

$$[K]\ \underset{\sim}{u} = \underset{\sim}{F}$$

where [K] is the stiffness matrix

$\underset{\sim}{u}$ are the nodal displacements

$\underset{\sim}{F}$ are the equivalent nodal forces.

More generally $[A]\ \underset{\sim}{x} = \underset{\sim}{b}$

In Gauss elimination, a modification of each team of the reduced coefficient matrix is made every time an equation is eliminated.

By Gauss elimination, the algorithm is

$$a_{ij}^{(k)} = a_{ij}^{(k-i)} - \frac{a_{ik}^{(k-i)}\ a_{kj}^{(k-i)}}{a_{kk}^{(k-i)}}$$

for $i = k+i, \ldots, N$

$j = k, \ldots, N$

where N is the number of equations with back substitution

$$b_{i}^{(k)} = b_{i}^{(k-i)} - \frac{a_{ik}^{(k-i)}\ b_{k}^{(k-i)}}{a_{kk}^{(k-i)}}$$

for $i = k+i, \ldots, N$

where i is the row number

j is the column number in the matrix A

Aside

1. Symmetry has not been taken into account

2. a_{ik}/a_{kk} is a constant operator while j runs from k to N, and hence can be used as a common factor both in the forward elimination as well as in the back substitution.

3. Where $a_{ik} = a_{kj} = 0$, there is no change in a_{ij} which should be recognised.

Essential features of the Crout Reduction Process are:

1. Re-order the sequence in which the terms of the coefficient matrix A are modified.

2. Each term is directly changed from its initial value in the unreduced matrix to its final value in the upper triangular reduced matrix.

The procedure is a direct consequence of the fact that in the Gauss Elimination process, row i of the triangular matrix is obtained by a linear combination of rows 1 to i-1.

The Crout algorithm is then

$$a_{ij}^{(i-1)} = a_{ij} - \sum_{k=1}^{i-1} \frac{a_{ki}^{(k-1)} \; a_{kj}^{(k-i)}}{a_{kk}^{(k-i)}}$$

for $j = 2, \ldots, N$

$i = 2, \ldots, j$

and the back substitution will then be

$$b_{ij}^{(i-1)} = b_i - \sum_{k=1}^{i-1} \frac{a_{ki}^{(k-1)} \; b_k^{(k-1)}}{a_{kk}^{(k-1)}}$$

The Crout Reduction Algorithm is implemented by sub-routine "SOLVE" in the processor MICRODEST.

APPENDIX E

CONSTRUCTING EQUATIONS FROM SEMI-BAND VECTOR STORAGE

In Appendix C the method of storing the stiffness matrix is clearly set out. To assemble the full equation the symmetry of the stiffness matrix is used.

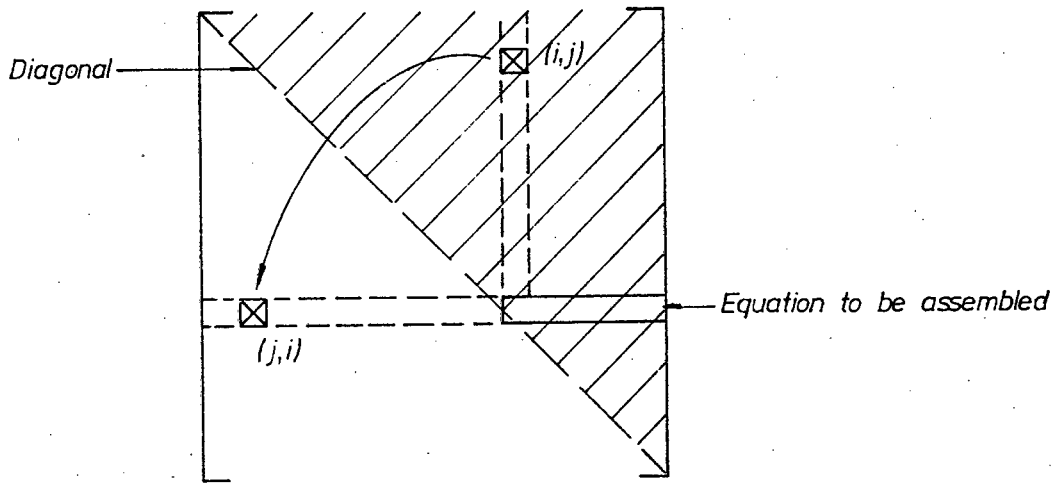

Figure E.1 Using Symmetry

Due to symmetry element (i,j) is the same as (j,i). As the upper diagonal section is stored in semi-band vector format any element can be located by index manipulation.

If i = row
j = column
ℓ = location of (i,j) in vector storage

then

$$\ell = j - i + 1 + (i - 1)\ Sbw$$

where Sbw = semi-band width of the square symmetric matrix.

This is performed by sub-routine REACTIONS in MICRODEST.

APPENDIX F

QUADRATIC CURVE FIT

A quadratic curve is fitted through three points on the interval [0,1]. The coefficients of the quadratic are worked out using formulae arising out of standard Lagrange interpolation theory.

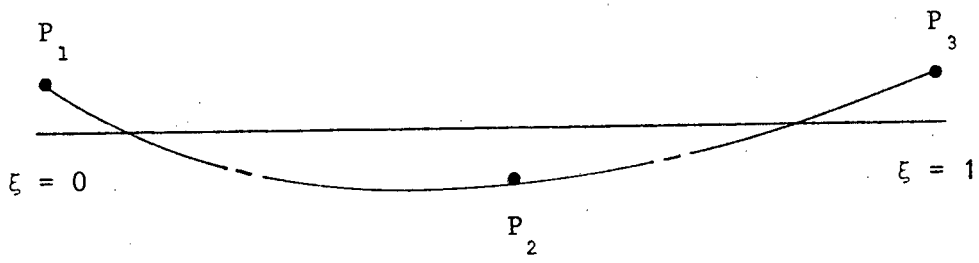

$P_1 = (0.05 , m_1)$

$P_2 = (0.5 , m_2)$

$P_3 = (0.995 , m_3)$

Figure F1 Points on Interval [0,1]

The Lagrange constants are

$$c_1 = m_1/((0.05 - 0.5) \times (0.05 - 0.995))$$
$$c_2 = m_2/((0.5 - 0.05) \times (0.5 - 0.995))$$
$$c_3 = m_3/((0.995 - 0.05) \times (0.995 - 0.5))$$

If the equation is

$$m(\xi) = a\xi^2 + b\xi + c$$

then the coefficients are

$$a = c_1 + c_2 + c_3$$

$$b = - [c_1(0.5 + 0.955) + c_2(0.05 + 0.955) + c_3(0.05 + 0.5)]$$

$$c = c_1(0.5 \times 0.955) + c_2(0.05 \times 0.955) + c_3(0.05 \times 0.5)$$

APPENDIX G

HERMITE SHAPE FUNCTIONS

The cubic Hermite Interpolants used in CLC beam element formulation are graphically represented below.

$$N_1 = \xi - 2\xi^2 + \xi^3$$

$$N_2 = \xi^3 - \xi^2$$

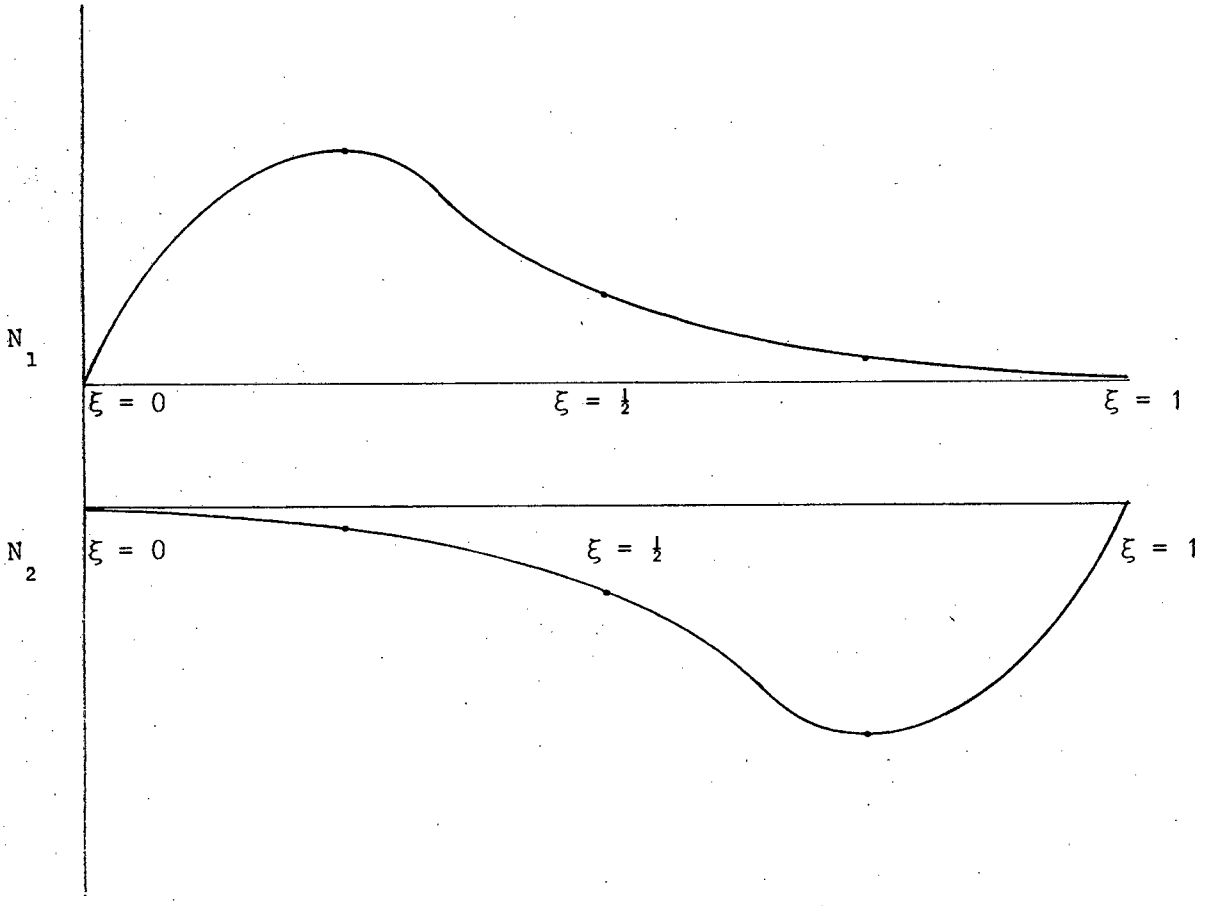

Figure G1 Shape Functions

APPENDIX H

SECTION LISTS

The following section lists form the reservoir of sections that can be used in the design process.

The sections listed are

- Pipes
- Equal angles
- Unequal angles
- Double equal angles (back to back)
- Double unequal angles (back to back)
- Channels
- T-sections.

PIPES

Index	Dimensions	Area x 10^{-6} m^2	i x 10^{-3} m	Z_e x 10^{-6} m^3	I x 10^{-6} m^4
1	12,7	56,7	3,96	0,4	0,002
2	15,9	73,1	5,08	0,45	0,003
3	19,1	89,5	6,20	0,5	0,004
4	21	121,3	6,9	0,5359	0,0057
5	21	152,7	6,7	0,6390	0,0068
6	27	156,5	8,8	0,9073	0,0122
7	27	177,8	8,7	1,0084	0,0136
8	32	187,2	10,6	1,3131	0,0209
9	34	199,2	11,2	1,4907	0,0251
10	38	226,2	12,8	1,9346	0,0368
11	42	253,8	14,3	2,4488	0,0519
12	48	290,9	16,4	3,2339	0,0781
13	51	307,9	17,3	3,6296	0,0926
14	42	325,1	14,1	3,0493	0,0646
15	60	366,3	20,6	5,1680	0,1558
16	42	394,1	13,9	3,5943	0,0762
17	48	413,6	16,1	4,4307	0,1070
18	48	453,4	16,0	4,7974	0,1159
19	42	482,5	13,7	4,2410	0,0899
20	60	522,9	20,3	7,1617	0,2159
21	76	533,3	26,1	9,5504	0,3634
22	102	625,8	35,2	15,2820	0,7763
23	60	641,3	20,1	8,5817	0,2587
24	76	732,9	25,8	12,8196	0,4878
25	76	820,0	25,7	14,1936	0,5401
26	89	866,6	30,5	18,0311	0,8060
27	102	899,2	34,9	21,5735	1,0959
28	89	1073,2	30,2	21,9350	0,9805
29	114	1252,0	39,2	33,5929	1,9198
30	127	1545,7	43,5	46,0809	2,9261
31	152	1864,8	52,5	67,4190	5,1373
32	165	2024,4	57,0	67,5158	4,7143

Continued/....

PIPES

Index	Dimensions	Area x 10^{-6} m^2	i x 10^{-3} m	Z_e x 10^{-6} m^3	I x 10^{-6} m^4
33	140	2074,3	47,7	79,6081	6,5716
34	165	2466,1	56,7	95,9252	7,9186
35	165	2709,2	56,5	104,7484	8,6470
36	165	3143,0	56,2	120,2037	9,9228
37	219	3297,4	75,8	172,7147	18,9209
38	219	4016,8	75,4	208,3019	22,8195
39	319	4211,7	75,3	217,8128	23,8614
40	unknown	5000,0	100,0	300,0000	50,0000

EQUAL ANGLES

Index	Dimensions	Area x 10^{-6} m^2	i x 10^{-3} m	Z_e x 10^{-6} m^3	I x 10^{-6} m^4
1	25x 25x 3	141,9	4,82	0,4475	0,0080
2	30x 30x 3	173,7	5,80	0,6490	0,0140
3	35x 35x 3	203,7	6,83	0,9016	0,0229
4	40x 40x 3	234,9	7,82	1,177	0,0345
5	45x 45x 3	266,3	8,81	1,486	0,0493
6	35x 35x 5	327,7	6,74	1,447	0,0356
7	40x 40x 5	378,9	7,72	1,912	0,0543
8	45x 45x 5	430,3	8,70	2,435	0,0784
9	40x 40x 6	447,9	7,69	2,257	0,0631
10	50x 50x 5	480,3	9,72	3,049	0,1096
11	45x 45x 6	509,3	8,66	2,886	0,0916
12	50x 50x 6	569,3	9,68	3,612	0,1284
13	60x 60x 5	581,9	11,7	4,447	0,1937
14	60x 60x 6	690,9	11,7	5,285	0,2279
15	50x 50x 8	741,3	9,63	4,684	0,1628
16	70x 70x 6	812,7	13,7	7,272	0,3688
17	60x 60x 8	902,9	11,6	6,890	0,2915
18	80x 80x 6	934,7	15,7	9,571	0,5582
19	70x 70x 8	1065,0	13,6	9,522	0,4749
20	60x 60x10	1107,0	11,6	8,408	0,3493
21	80x 80x 8	1227,0	15,6	12,58	0,7225
22	70x 70x10	1309,0	13,5	11,66	0,5724
23	90x 90x 8	1389,0	17,6	16,05	1,044
24	80x 80x10	1511	15,5	15,45	0,8750
25	100x100x 8	1551	19,6	19,94	1,448
26	90x 90x10	1713	17,5	19,77	1,269
27	80x 80x12	1787	15,5	18,20	1,017
28	100x100x10	1915	19,5	24,62	1,767
29	90x 90x12	2029	17,4	23,34	1,480
30	100x100x12	2271	19,4	29,12	2,067
31	120x120x10	2318	23,6	36,03	3,129
32	120x120x12	2754	23,5	42,73	3,677

Continued/...

EQUAL ANGLES

Index	Dimensions	Area x 10^{-6} m^2	i x 10^{-3} m	Z_e x 10^{-6} m^3	I x 10^{-6} m^4
33	100x100x12	2754	23,5	35,60	2,486
34	120x120x15	3393	23,3	52,43	4,449
35	150x150x12	3483	29,5	67,75	7,369
36	150x150x15	4302	29,3	83,52	8,981
37	150x150x18	5103	29,2	98,74	10,50
38	200x200x16	6179	39,4	161,7	23,41
39	200x200x20	7635	39,2	199,1	28,51
40	200x200x24	9059	39,0	235,2	33,31

UNEQUAL ANGLES

Index	Dimensions	Area x 10^{-6} m^2	i x 10^{-3} m	Z_e x 10^{-6} m^3	I x 10^{-6} m^4
1	65x50x 6	658	10,6	6,099	0,2723
2	75x50x 6	719	10,8	8,008	0,4054
3	80x60x 6	811	12,8	9,294	0,5144
4	65x50x 8	860	10,5	7,930	0,3478
5	90x65x 6	901	14,0	11,82	0,7339
6	75x50x 8	941	10,7	10,45	0,5202
7	100x75x 6	1025	16,2	14,66	1,024
8	80x60x 8	1063	12,7	12,16	0,6628
9	90x65x 8	1183	13,9	15,49	0,9487
10	100x65x 8	1267	14,0	18,85	1,268
11	100x75x 8	1347	16,0	19,29	1,330
12	90x65x10	1457	13,8	19,01	1,149
13	125x75x 8	1549	16,3	29,57	2,473
14	100x65x10	1561	13,9	23,20	1,540
15	100x75x10	1661	15,9	23,75	1,618
16	125x75x10	1913	16,1	36,50	3,020
17	100x75x12	1967	15,9	23,75	1,889
18	150x75x10	2163	16,0	51,77	5,012
19	125x75x12	2269	16,0	43,22	3,540
20	150x90x10	2315	19,50	53,29	5,331
21	150x75x12	2569	15,9	61,39	5,890
22	150x90x12	2751	19,4	63,25	6,273
23	150x75x15	3163	15,8	75,34	7,135
24	150x90x15	3390	19,3	77,70	7,611
25	unknown	4000	25,0	100,00	10,00

DOUBLE EQUAL ANGLES - Back to Back

Index	Dimensions	Area x 10^{-6} m^2	i x 10^{-3} m	Z_e x 10^{-6} m^3	I x 10^{-6} m^4
1	25x 25x 3	283,8	7,5	0,8950	0,0159
2	30x 30x 3	347,4	9,0	1,298	0,0281
3	25x 25x 5	451,8	7,3	1,415	0,0241
4	40x 40x 3	469,7	12,1	2,354	0,0689
5	45x 45x 3	532,5	13,6	2,971	0,0985
6	30x 30x 5	555,4	8,8	2,079	0,0433
7	40x 40x 5	757,7	12,0	3,824	0,108
8	45x 45x 5	860,5	13,5	4,869	0,157
9	40x 40x 6	895,7	11,9	4,513	0,126
10	50x 50x 5	960,5	15,1	6,097	0,219
11	45x 45x 6	1018	13,4	5,764	0,183
12	50x 50x 6	1138	15,0	7,225	0,257
13	60x 60x 6	1164	18,2	8,893	0,387
14	60x 60x 6	1382	18,2	10,57	0,457
15	50x 50x 8	1482	14,8	9,369	0,326
16	70x 70x 6	1625	21,3	14,54	0,738
17	60x 60x 8	1806	18,0	13,78	0,583
18	80x 80x 6	1869	24,4	19,14	1,12
19	70x 70x 8	2129	21,1	19,04	0,950
20	60x 60x10	2214	17,8	16,82	0,697
21	80x 80x 8	2453	24,3	25,15	1,44
22	70x 70x10	2617	20,9	23,32	1,14
23	90x 90x 8	2778	27,4	32,10	2,09
24	80x 80x10	3021	24,1	30,90	1,75
25	100x100x 8	3103	30,6	39,88	2,90
26	90x 90x10	3426	27,2	39,54	2,54
27	80x 80x12	3573	23,9	36,41	2,03
28	100x100x10	3831	30,4	49,23	3,53
29	90x 90x12	4058	27,0	49,69	2,96
30	100x100x12	4543	30,2	58,25	4,13
31	120x120x10	4636	36,7	72,05	6,26
32	120x120x12	5508	36,5	85,47	7,35

Continued/..

DOUBLE EQUAL ANGLES - Back to Back

Index	Dimensions	Area x 10^{-6} m^2	i x 10^{-3} m	Z_e x 10^{-6} m^3	I x 10^{-6} m^4
33	100x100x15	5581	29,8	71,21	4,97
34	120x120x15	6786	36,2	104,9	8,9
35	150x150x12	6967	46,0	135,5	14,7
36	150x150x15	8605	45,7	167,0	18,0
37	150x150x18	10210	45,4	197,5	21,0
38	200x200x16	12360	61,6	323,5	46,8
39	200x200x18	13820	61,3	361,2	52,0
40	200x200x24	18120	60,6	470,4	66,6

DOUBLE UNEQUAL ANGLES - Long Legs Back to Back

Index	Dimensions	Area x 10^{-6} m^2	i x 10^{-3} m	Z_e x 10^{-6} m^3	I x 10^{-6} m^4
1	65x50x 6	1316	20,3	12,20	0,545
2	75x50x 6	1438	21,4	16,02	0,811
3	80x60x 6	1622	25,7	18,59	1,03
4	65x50x 8	1720	20,1	15,86	0,696
5	90x65x 6	1802	28,0	23,64	1,47
6	75x50x 8	1882	21,9	20,90	1,04
7	100x75x 6	2049	31,7	29,32	2,05
8	80x60x 8	2126	26,2	24,32	1,33
9	90x65x 8	2366	28,4	30,99	1,90
10	100x65x 8	2533	27,5	37,70	2,54
11	100x75x 8	2693	32,2	38,59	2,66
12	90x65x10	2914	28,9	38,03	2,30
13	125x75x 8	3098	30,9	59,19	4,95
14	100x65x10	3121	28,0	46,40	3,08
15	100x75x10	3321	32,7	47,50	3,24
16	125x75x10	3826	31,4	73,00	6,04
17	100x75x12	3933	33,1	56,10	3,78
18	150x75x10	4326	29,8	103,5	10,0
19	125x75x12	4538	31,9	86,44	7,08
20	150x90x10	4631	36,4	106,6	10,7
21	150x75x12	5138	30,3	122,8	11,8
22	150x90x12	5503	36,9	126,5	12,5
23	150x75x15	6326	31,0	150,7	14,3
24	150x90x15	6781	37,5	155,4	15,2
25	unknown	8000	60	200,0	20,0

CHANNELS

Index	Dimensions	Area x 10^{-6} m^2	i x 10^{-3} m	Z_e x 10^{-6} m^3	I x 10^{-6} m^4
1	76x 38	853	11,2	19,38	0,737
2	100x 50	1345	14,7	41,07	2,053
3	120x 55	1699	15,9	60,72	3,643
4	178x 54	1856	15,2	96,6	8,597
5	127x 64	1898	19,0	76,31	4,845
6	140x 60	2037	17,5	86,4	6,048
7	152x 76	2282	22,3	111,1	8,445
8	160x 65	2401	18,8	115,6	9,247
9	180x 70	2797	20,1	150,4	13,54
10	200x 75	3218	21,4	191,1	19,11
11	220x 80	3744	22,9	244,6	26,91
12	240x 85	4231	24,2	299,9	35,99
13	260x 90	4828	25,6	371,1	48,24
14	280x 95	5342	27,3	448,3	62,76
15	300x100	5876	29,0	535,2	80,28
16	381x102	7019	28,9	782,8	149,1

T-SECTIONS

Index	Dimensions	Area x 10^{-6} m^2	i x 10^{-3} m	Z_e x 10^{-6} m^3	I x 10^{-6} m^4
1	133x102	1610	28,8	62,7	1,3350
2	102x152	1810	48,5	100,8	4,265
3	133x102	1900	28,3	72,5	1,524
4	102x152	2090	48,3	117,3	4,865
5	146x127	2370	35,4	114,8	2,964
6	140x203	2470	62,6	182,8	9,664
7	165x152	2570	43,0	154,7	4,754
8	171x178	2840	52,7	196,0	7,903
9	140x203	2940	61,9	182,8	11,29
10	171x178	3220	52,1	222,9	8,766
11	178x203	3420	61,2	265,6	12,80
12	171x178	3600	52,1	247,2	9,779
13	178x203	3800	60,3	299,2	13,82
14	178x203	4270	60,7	331,7	15,72
15	191x229	4740	68,8	413,4	22,44
16	210x267	5210	82,1	520,3	35,11
17	191x229	5690	68,9	490,5	26,98
18	210x267	6460	81,4	649,9	42,77
19	210x267	6920	81,4	694,5	45,88
20	210x267	7780	81,6	775,1	51,78

APPENDIX I

USERS MANUAL FOR PREPRO

I.1 Preamble

The preprocessor, PREPRO, was developed in order to provide reliable and rapid data preparation and data collection for the processor, MICRODEST.

PREPRO is designed to be a simple, unsophisticated preprocessor. The major motivation for this design strategy is to have a preprocessor that could easily be transferred or adapted for use on similar packages.

PREPRO is a modest preprocessor prototype which should evolve into a more sophisticated preprocessor as it is adapted for use in other packages. It is currently being adapted as part of an M.Sc. project of U.C.T.

I.2 Using PREPRO

PREPRO operates interactively. A potential user should first be acquainted with the overall operation of PREPRO before attempting to use it. PREPRO is menu-driven. Figure I.1 clearly illustrates the options or tasks provided by PREPRO's menu.

Listed in the main menu are major tasks which are then broken down, in a structural manner, to more manageable and definable sub-tasks. Chapter 3 in the main text deals with these tasks.

Program control always returns to the main menu. It is not possible to transfer program control from one sub-menu to another. Transferring control from NODE-DEFINE (sub-menu) to SIMPLE-SUPPORT (sub-menu) would not be possible. However, transferring program control from item to item in a sub-menu is possible.

Some preprocessing concepts that are mentioned and presented in the text may not be fully developed at this stage. This conforms to the strategy that PREPRO will evolve and be refined as it is adapted to suit the needs of the package it is serving.

To use PREPRO the user has to sequentially work his way down the main menu tasks, as shown in Figure I.1. This is due to the fact that all data is intimately related. In many cases defining data depends on prior data having been defined.

As PREPRO is an interactive preprocessor, prompting on the screen is often sufficient explanation. The following section clearly sets out and explains the features offered in PREPRO.

I.3 Task Explanation

The main tasks are listed below:-

- Job title
- Nodal data
- Super element
- Topology
- Design groups
- Restraints
- Design data
- Loading data
- Graphics
- Check and prepare.

I.3.1 Job Title

In this section a title describing the nature of the data can be defined. The maximum length of this is 200 characters, including spaces.

I.3.2 Nodal Data

This option provides the facility to input all data related by the nodes of the model. The following sub-tasks form the basis of Nodal data:-

- Node define
- Generate nodes
- Display nodes
- Edit nodes
- Graphics
- Node sets.

I.3.2.1 Node Define

The Cartesian nodal coordinates are defined individually. The node number is requested and then the accompanying X, Y, Z coordinates are furnished. Entered data is echoed on the screen instantaneously. The data has to pass the following checks to be accepted:-

- Node number has to be an integer
- Node number must be greater than zero
- Node number (n) must be in the range $0 < n \leqq N$, where N is the total number of nodes in the model
- Node number must not have been previously defined.

A facility exists in this section to re-define existing defined node or to delete or abort a nodal definition.

To cease defining nodes, one at a time, and to return to the main menu, type in EXIT and hit return.

I.3.2.2 Generate Nodes

This is an incremental node generator. The start and end nodes must be specified together with the node number increment and the number of nodes to be generated. This facility is useful if the user requires to generate nodal coordinates with specific node numbers. See Figure I.3.1 for an example.

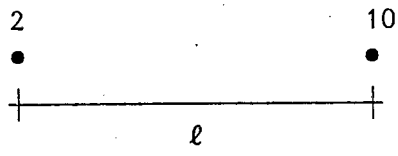

Start node = 2
End node = 10
Node increment = 3
Number of generated nodes = 3, then

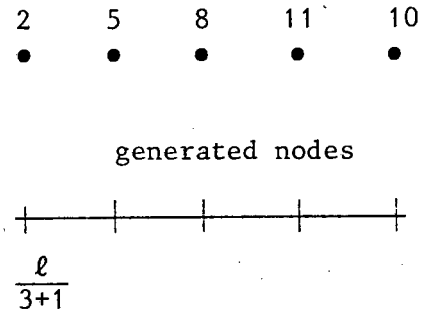

Note! Nodes are incremented from the start node.

Figure I.3.1 Illustration of Nodal Generation

I.3.2.3 Node Sets

Node sets can be defined in order to group nodes together to facilitate defining nodal loads and possibly for output.

A maximum number of 10 Node sets can be defined with a maximum of 50 nodes contained per set.

Only defined nodes can belong to a set. A node cannot be repeated within a set. However, a single node can appear in more than one set.

I.3.2.4 Display Nodes

This option prints all the defined nodes and their respective coordinates. All the undefined nodal numbers within the initially specified nodal range are also listed. An example is provided in Figure I.3.2.

```
 DISPLAY NODES
NODE       X            Y            Z
 1          0            0            0
 2           undefined
 3          7.05882352941            7.05882352941            2.35294117647
 4           undefined
 5          14.1176470588            14.1176470588            4.70588235294
 6           undefined
 7          21.1764705882            21.1764705882            7.05882352941
 8           undefined
 9          28.2352941176            28.2352941176            9.41176470588
 10          undefined
 11         35.2941176471            35.2941176471            11.7647058824
 12          undefined
NODE       X            Y            Z
 13         42.3529411765            42.3529411765            14.1176470588
 14          undefined
 15         49.4117647059            49.4117647059            16.4705882353
 16          undefined
 17          undefined
 18         60           60           20
 19          undefined
 20          undefined
    Total number of nodes..... 20
    Number of defined nodes..... 9
    Number of undefined nodes..... 11
```

Figure I.3.2 Example of Display Nodes Printout

I.3.2.5 Edit Nodes

Options currently available

- Total nodes
- Delete nodes.

Total nodes re-defines the total number of nodes in the model.

Delete nodes deletes a defined node, clears the coordinates and makes it available for re-use.

I.3.2.6 Graphics

This option will plot the nodes and number them on the screen. The screen plot may be dumped. See Figure I.3.3 for an example.

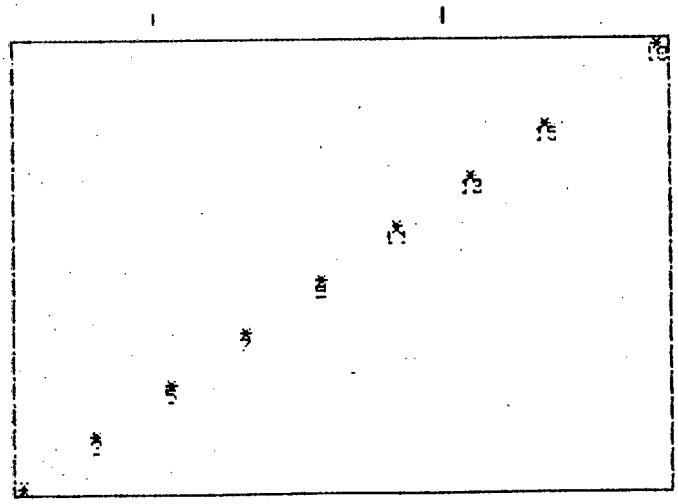

Figure I.3.3 Node Plot

I.3.3 Super Elements

A Super-element is defined as a set of identical elements generated between two points. The internal node and element numbering is arbitrary and need not be incremental. Provided in this option are the following sub-tasks

- Straight super-elements
- Circular super-elements.

These routines generate nodal coordinates and element topologies, assigning to the generated nodes and elements the lowest available number, given the start, end nodes and the number of elements in the super-element.

Provision is made to check the start and end node coordinates which can be edited if so desired.

I.3.3.1 Generating Straight Super-Elements

Data required for this option is listed below:-

- Start node number (to be previously defined)
- End node number (to be previously defined)
- Number of identical elements to be generated in the super-element.

Figure I.3.3 provides an example.

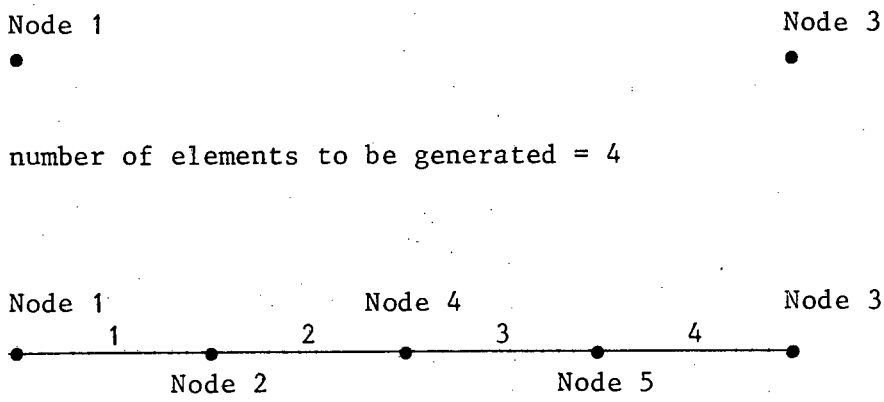

Generated straight super-element.

Figure I.3.3 Illustrating the Straight Super-Element

I.3.3.2 Generating Curved Super-Elements

This is done in exactly the same manner as the straight super-element except that an extra data item is required. The origin of the arc has to be furnished.

As a general rule, never generate a super-element of more than 180°. This type of generation works in a clockwork sense. Data required is listed below:-

- Start node number (previously defined)
- End node number (previously defined)
- Coordinates of arc origin
- Number of identical curved elements to be generated.

I.3.4 Topology

This option provides the facility to enter all data related to the elements of the model. The following tasks are available for that purpose:-

- Single elements
- Single curved elements
- Generate elements
- Generate curved elements
- Element sets
- Zoom in.

I.3.4.1 Single Elements

This routine defines the topology of a single element at a time. The element will be given the lowest available element number. Required in this option is

- the connectivities of the element.

For an element to be defined, the connectivities of the element must be within the nodal range, and have to be integers.

To leave this routine, type in EXIT and press the ENTER key twice.

I.3.4.2 Single Curved Element

Exactly the same as for the single element. (Section I.3.4.2) except that the initial nodal rotations of the element, i.e. α_i , has to be furnished. The initial nodal rotations are measured in radians. See Figure I.3.4.

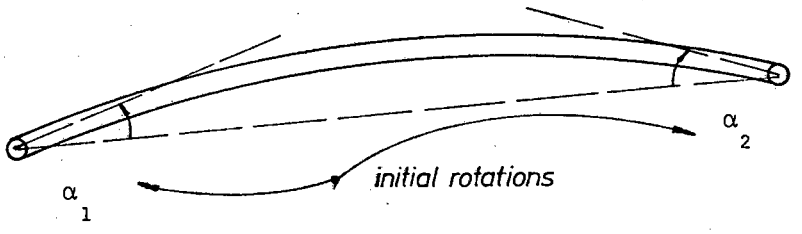

Figure I.3.4 Initial Nodal Rotations

I.3.4.3 Generate Elements

This option allows the user to generate elements from a master element, which has been previously defined. The increment in the node numbers of the generated element topology has to be given. Also required is the number of elements to be generated from the master element. The lowest available element number is given to the generated elements.

Before generating elements, the data has to pass these checks:-

- if the increment is a non-zero integer
- if the generated element is already defined
- if the nodes associated with the generated topology exist.

I.3.4.4 Generate Curved Elements

This is the same as "Generate elements". Here the initial nodal rotations are given as well. Usually it will not be necessary to use this option as the Curved Super-element option supercedes this and is much easier to use.

I.3.4.5 Edit Elements

This is a facility to delete elements. The concerned element number is given, which is then removed from the topology list.

I.3.4.6 Element Sets

Element sets can be defined in order to group elements together. This facilitates repeated reference to groups of elements. This is particularly useful when defining element loads, design groups and material data.

A maximum number of 10 element sets can be defined with a maximum of 50 elements contained per set. Only defined elements can belong to a set. An element cannot be repeated within a set. However, a single element can appear in more than one set.

I.3.4.7 Zoom In

This is a facility to zoom in on a screen plot.

I.3.5 Design Groups

In order to yield practicable designs, it is necessary to group elements into sets. In this way they can be attributed the same design section. If this is not used, then every element in the model is designed separately.

These design groups are defined using previously defined element sets.

I.3.6 Restraints

A maximum of 50 supports can be defined. The type of restraints offered are:-

Single support	-	restrained in XYZ translation
Roller X	-	unrestrained in X translation, restrained in YZ translation
Roller Y	-	unrestrained in Y translation restrained in YZ translation
Roller Z	-	unrestrained in Z translation, restrained in XY translation
Fully fixed	-	fully built in (encastre)
Fixed in X	-	restrained in X rotation and simple support
Fixed in Y	-	restrained in Y rotation and simple support
Fixed in Z	-	restrained in Z rotation and simple support.

The support can only be defined if the desired restrained node already exists. To define a support the following steps are performed.

- Enter the node to be restrained
- Select the type of restraint (soft keys)
- Enter the next node to be restrained or type in EXIT to leave this section which returns control to the main menu.

The support node is checked to see if it has been defined, if it is an integer and whether it is within the prescribed nodal range of the model.

I.3.7 Design Data

Here the design parameters are displayed, showing their default values e.g. E = 206 GPa. If necessary, they can be changed by selecting the appropriate soft key. In this way the design parameters can be changed.

I.3.7.1 Slenderness Ratios

The default value for slenderness ratio is 0.85 for all elements. This can be changed for all or specific element sets or a single element using the slenderness ratio soft key option.

To set the slenderness ratio for all elements in the model (i.e. other than the default, 0.85);

- select the "all elements" soft key
- enter the slenderness ratio.

To change the slenderness ratio for element sets

- select the "element set" soft key
- enter the slenderness ratio
- enter the element set number that is to have the new slenderness ratio
- enter the next set or leave this section by entering 0 (zero).

Similarly, to change the slenderness ratio for single elements

- select the "single element" soft key
- enter the slenderness ratio
- enter the element number
- enter the next element or leave this section by entering 0 (zero).

All slenderness ratios have to be in the following range

$$0 < \text{slenderness ratio} \leq 1.2 \ .$$

I.3.7.2 Member Cross-Section Allocation

After all the design parameters have been settled, the type of cross-sectional area has to be defined for each element. The default section for all elements is an equal angle section.

To assign sections

- select the section to be assigned to all the elements, element sets or elements using the soft keys.

Single elements - enter the element to be assigned the cross-section to exit, enter 0 (zero)

Element sets - enter the element set that will be assigned the cross-section

- to exit, enter 0 (zero)

All elements - assigns the cross-section to all elements. When this is complete, control will return to the cross-section sub-menu.

The cross-sections available are,

- pipe sections
- equal angle
- unequal angle
- double equal angle (back to back)

- double unequal angle (back to back)
- channels sections
- T-sections.

All these sections are listed in Appendix H.

I.3.8 Loading

Nine different load types are offered via the soft keys. An explanation is provided on the screen. The loads available are

Fx - point load in x direction
Fy - point load in y direction
Fz - point load in z direction
Dx - distributed load in x direction
Dy - distributed load in y direction
Dz - distributed load in z direction
M - applied moment in xz plane.

First select the type of load under consideration for that load case. Then specify the node/element or set associated with that type of load. A maximum of 5 load cases is allowed.

I.3.9 Check and Prepare

This facility checks the data for mistakes. Only if the data passes the scrutiny of this test is program control allowed to proceed to collate and store the data on external mass storage. The stored data is then used by MICRODEST. Data errors encountered in the data checking procedure can be rectified after which another checking pass can be made through the data. Data is checked to see

- if all the nodes exist
- if any two nodes have the same coordinates
- if all the elements exist
- if the element topology is unique

- if a node in a node set is not repeated
- if an element in an element set is not repeated
- if boundary conditions are present
- if all the design data is specified
- if all the load cases are present.

Diagnostic messages will appear if any data errors are encountered.

I.4 Improvements and Recommendations

To be a fully fledged preprocessor, PREPRO has to undergo a great deal of development. Listed are some areas that require attention.

- Editing facilities have to be provided for all data options. These editing facilities need to be streamlined

- PREPRO currently lacks the ability to load up data from external storage for editing purposes. This is an important feature.

- Some data preparation facilities are duplicated which is unnecessary

- Some facilities need to be perfected and completed.

APPENDIX J

OPERATING MICRODEST

MICRODEST is very simple to operate. The program will prompt for a data file once it is running.

Data changes or additions concerning analysis or design can be made via the Interactive option. MICRODEST constantly prompts the user for data and furnishes the necessary information for operation.

NOTE!

The processor developed for MICRODEST is currently being adapted to be used in a suite of programs developed under the supervision of Prof. W.S. Doyle at U.C.T.

Refinements and improvements to PREPRO and MICRODEST are thus envisaged.

THE FOLLOWING COURSES WERE COMPLETED IN
PARTIAL FULFILMENT OF THE M.Sc. (ENG) DEGREE
AT THE UNIVERSITY OF CAPE TOWN

Course		Date Credited	Credit Value
CE5B3	Structural Dynamics	1984	3
CE5B6	Frame Analysis	1984	2
CE5B10	Finite Element Analysis	1984	3
CE5B16	Finite Element Modelling of Structures	1984	4
AM343	Numerical Methods	1984	4
CE5A3	Applied Probability	1985	3
CE5G1	Properties of Concrete	1985	4
		Total	23

Course Credits : 23
Thesis Credits : 20
Total 43

Total credit requirements for the M.Sc. (Eng) Degree : 40

A brief description of the courses are given as follows:-

CE5B3 - STRUCTURAL DYNAMICS

Principles of dynamics. Natural modes of vibration. Energy methods. Forced vibrations; differential equations, normal mode and frequency response methods. Damping. Introduction to earthquake effects.

CE5B6 - FRAME ANALYSIS

The application of the force method of analysis to framed structures of straight and curved members. The stability of equilibrium of framed structures.

CE5B10 - FINITE ELEMENT ANALYSIS

Plane stress and plane strain elements, plate bending elements, shell elements, three-dimensional elements. Programming of the finite element displacement method. Techniques for equation solving.

CE5B16 - FINITE ELEMENT MODELLING OF STRUCTURES

The modelling of structures using finite element analysis methods. The application of computer aided design (CAD) techniques to finite element data preparation. Computer programming of the finite element method. Optimum solution techniques.

AM343 - NUMERICAL METHODS

The theory and practice of numerical methods is dealt with in this course. Topics include: approximate solution of nonlinear equations, interpolation, numerical integration, numerical solution of ordinary differential equations.

CE5A3 - APPLIED PROBABILITY

Topics are: random variables, distribution functions, regression and correlation, statistics of extremes, Monte Carlo simulation, reliability theory, reliability-based design.

CE5G1 - PROPERTIES OF CONCRETE

The properties and behaviour of fresh concrete, of hardened concrete, and of the constituent materials, testing and control.